Eruptive history of Mount Katmai, Alaska

Wes Hildreth* and Judy Fierstein*,†
Volcano Science Center, U.S. Geological Survey, MS 910, Menlo Park, California 94025, USA

ABSTRACT

Mount Katmai has long been recognized for its caldera collapse during the great pyroclastic eruption of 1912 (which vented 10 km away at Novarupta in the Valley of Ten Thousand Smokes), but little has previously been reported about the geology of the remote ice-clad stratovolcano itself. Over several seasons, we reconnoitered all parts of the edifice and sampled most of the lava flows exposed on its flanks and caldera rim. The precipitous inner walls of the 1912 caldera remain too unstable for systematic sampling; so we provide instead a photographic and interpretive record of the wall sequences exposed. In contrast to the several andesite-dacite stratovolcanoes nearby, products of Mount Katmai range from basalt to rhyolite. Before collapse in 1912, there were two overlapping cones with separate vent complexes and craters; their products are here divided into eight sequences of lava flows, agglutinates, and phreatomagmatic ejecta. Latest Pleistocene and Holocene eruptive units include rhyodacite and rhyolite lava flows along the south rim; a major 22.8-ka rhyolitic plinian fall and ignimbrite deposit; a dacite-andesite zoned scoria fall; a thick sheet of dacite agglutinate that filled a paleocrater and draped the west side of the edifice; unglaciated leveed dacite lava flows on the southeast slope; and the Horseshoe Island dacite dome that extruded on the caldera floor after collapse. Pre-collapse volume of the glaciated Katmai edifice was ~30 km^3, and *eruptive* volume is estimated to have been 57 ± 13 km^3. The latter figure includes ~40 ± 6 km^3 for the edifice, 5 ± 2 km^3 for off-edifice dacite pyroclastic deposits, and 12 ± 5 km^3 for the 22.8-ka rhyolitic pyroclastic deposits. To these can be added 13.5 km^3 of magma that erupted at Novarupta in 1912, all or much of which is inferred to have been withdrawn from beneath Mount Katmai. The oldest part of the edifice exposed is a basaltic cone, which gave a ^{40}Ar/^{39}Ar plateau age of 89 ± 25 ka.

The seismic record of caldera collapse includes 14 earthquakes of magnitude 6.0–7.0. By combining the times of earthquakes, the hours of downwind plinian-fall episodes from Novarupta, and the stratigraphic record of hydrothermal explosion breccia and phreatic mud layers ejected around the caldera rim and intercalated within the Novarupta pumice-fall sequence, it can be inferred that collapse began in the 11th hour of the 60-h-long eruption and continued fitfully for 3.5 days. Several big landslides and pumiceous debris flows shaken loose by the collapse-related seismicity are bracketed in time by their levels of intercalation within the Novarupta pumice-fall sequence. An intracaldera lake was ~10 m deep by 1916, drained away in 1923, and has since deepened progressively to ~250 m today.

Compositionally, products of Mount Katmai represent an ordinary medium-K arc array, both tholeiitic and calcalkaline, that extends from 51.6% to 72.3% SiO_2. Values of ^{87}Sr/^{86}Sr range from 0.70335 to 0.70372, correlating loosely with fractionation indices. The 5–6 km^3 of continuously zoned andesite-dacite magma (58%–68% SiO_2) that erupted at Novarupta in 1912 was withdrawn from beneath Mount Katmai and bears close compositional affinity with products of that edifice, not with pre-1912 products of the adjacent Trident cluster. Evidence is presented that the 7–8 km^3 of high-silica rhyolite (77% SiO_2) released in 1912 is unlikely to have been stored under Novarupta or Trident. Pre-eruptive contiguity with the andesite-dacite reservoir is suggested by (1) eruption of ~3 km^3 of rhyolite magma first, followed by mutual mingling in fluctuating proportions; (2) thermal and redox continuity of the whole zoned sequence despite the wide compositional gap; (3) Nd, Sr, O isotopic, and rare earth element (REE) affinities of the whole array; (4) compositional continuity of the nearly aphyric rhyolite with the glass (melt) phase of the phenocryst-rich dacite; and (5) phase-equilibrium experiments that indicate similar shallow pre-eruptive storage depths (3–6 km) for rhyolite, dacite, and andesite.

INTRODUCTION

Mount Katmai rises at the head of the Valley of Ten Thousand Smokes on the upper Alaska Peninsula, along the volcanic front of the Aleutian arc. Among the many andesite-dacite stratocones along the volcanic line between Cook Inlet and Becharof Lake (Fig. 1), Mount Katmai is unique in having products that extend from basalt to rhyolite. Published results of our 20 summer expeditions to the Valley of Ten Thousand Smokes and Katmai cluster of stratovolcanoes include numerous papers on the great 1912 eruption (listed in Hildreth and Fierstein, 2012), a regional volcanological map (Hildreth and Fierstein, 2003), and a series of papers that detail the structure, eruptive history, and composition of each stratovolcano (Hildreth et al., 1999, 2000, 2001, 2002, 2003a, 2004, 2007). Here, we extend that series to Mount Katmai, which underwent caldera collapse during eruption of ~13.5 km^3 of magma at Novarupta on 6–8 June 1912.

Little volcanological work had previously been undertaken on the Mount Katmai edifice. We summarized our own preliminary findings a decade ago (Hildreth and Fierstein, 2000, 2003), and we have recently recapitulated the history of reconnaissance observations dating back to 1908 (Hildreth and Fierstein, 2012).

Five andesite-dacite stratovolcanoes have erupted during the Holocene within 15 km of

*Emails: Hildreth: hildreth@usgs.gov; Fierstein: jfierstn@usgs.gov.
†Corresponding author.

Geosphere; December 2012; v. 8; no. 6; p. 1527–1567; doi:10.1130/GES00817.1; 31 figures.
Received 5 May 2012 ♦ Revision received 15 August 2012 ♦ Accepted 18 August 2012 ♦ Published online 16 November 2012

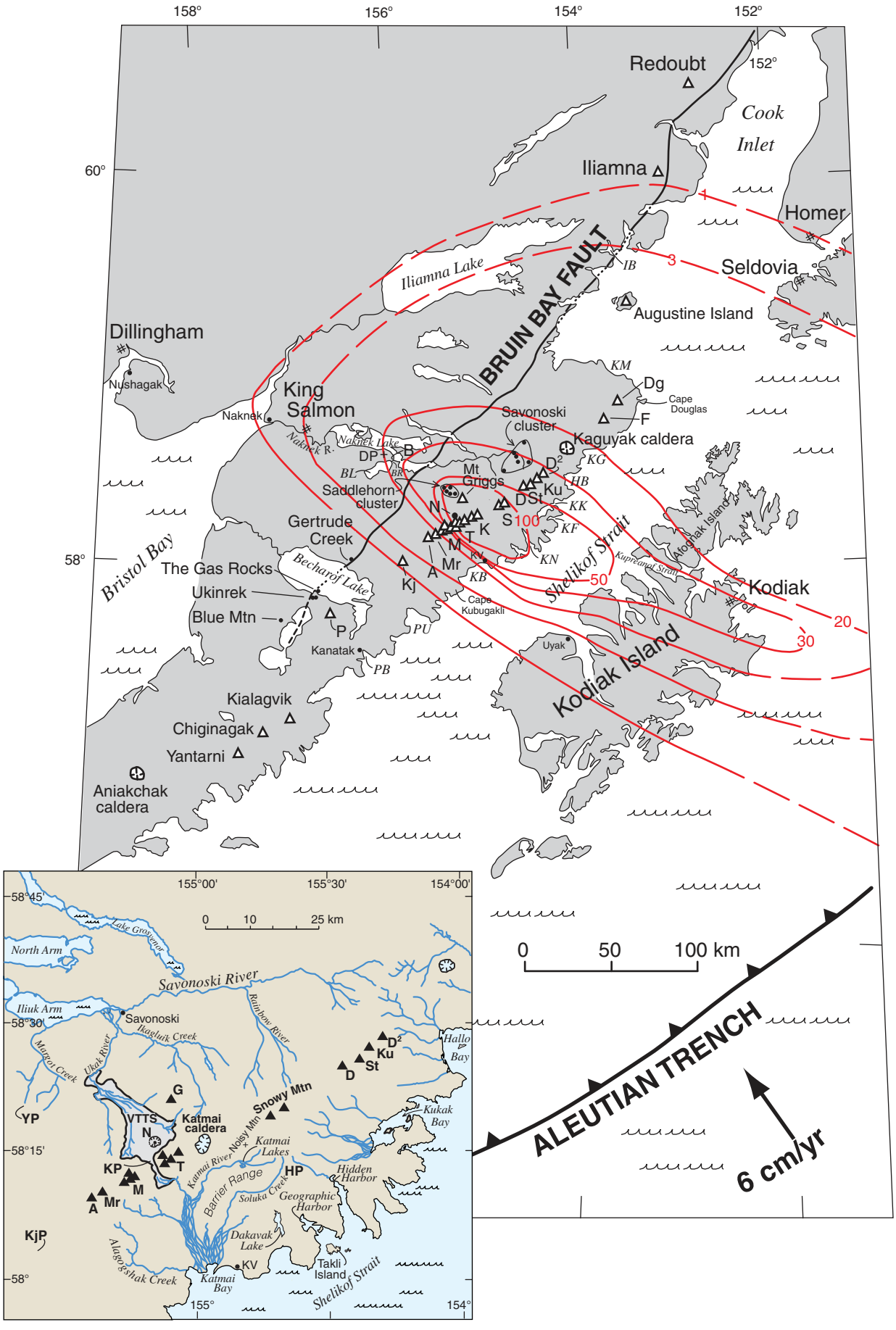
158°
156°
154°
152°
60°
58°
Redoubt
Cook Inlet
Iliamna
Homer
Seldovia
Iliamna Lake
BRUIN BAY FAULT
Augustine Island
Dillingham
Nushagak
King Salmon
Naknek
Naknek R.
Naknek Lake
Savonoski cluster
Kaguyak caldera
Cape Douglas
Saddlehorn cluster
Mt Griggs
Gertrude Creek
Becharof Lake
Bristol Bay
The Gas Rocks
Ukinrek
Blue Mtn
Kanatak
Shelikof Strait
Kodiak
Kodiak Island
Cape Kubugakli
Uyak
Kupreanof Strait
Afognak Island
Kialagvik
Chiginagak
Yantarni
Aniakchak caldera
1
3
20
30
50
100
0 50 100 km
ALEUTIAN TRENCH
6 cm/yr
155°00'
155°30'
154°00'
58°45'
58°30'
58°15'
58°
0 10 25 km
Lake Grosvenor
North Arm
Savonoski River
Iliuk Arm
Savonoski
Ikagluk Creek
Rainbow River
Margot Creek
Ulak River
Hallo Bay
Kukak Bay
Snowy Mtn
Noisy Mtn
Katmai caldera
VTTS
Katmai Lakes
Katmai River
Barrier Range
Soluka Creek
Hidden Harbor
Geographic Harbor
Dakavak Lake
Takli Island
Shelikof Strait
Katmai Bay
Alagogshak Creek
YP
KP
HP
KjP
KV

the 1912 vent at Novarupta, and all remain fumarolically active today: Mount Katmai, Trident Volcano, Mount Mageik, Mount Martin, and Mount Griggs (Fig. 2). The first four are virtually contiguous along a N65°E. trend that defines the Quaternary volcanic front, whereas rear-arc Mount Griggs (Hildreth et al., 2002, 2004) is centered 12 km behind the front. The Quaternary volcanic chain here is the most tightly spaced line of stratovolcanoes in Alaska (Fig. 1; Wood and Kienle, 1990; Miller et al., 1998). Spacing between adjacent (commonly contiguous) edifices is typically 5 km or less. This includes the Devils Desk–Kukak-Steller-Denison alignment northeast of Snowy Mountain (Fig. 1) as well as the Katmai cluster itself. The frontal volcanoes of this arc segment were constructed along the preexisting rangecrest (the Pacific–Bristol Bay drainage divide), where prevolcanic basement typically reaches elevations of 1200–1600 m, which is unusually high for basement along the Alaska Peninsula. As the volcanic summits reach 1830–2290 m and lie in a region of high precipitation, all the centers are heavily ice covered, as (to a lesser degree) is 2330-m-high Mount Griggs northwest of the frontal axis.

Access is difficult because the Katmai cluster lies entirely within the roadless wilderness of Katmai National Park. The only convenient access is by boat or amphibious aircraft from King Salmon to Brooks Camp on Naknek Lake. A daily commercial shuttle bus traverses a 37-km-long dirt road from Brooks Camp to the Overlook Cabin, a visitor center perched on a scenic knoll near the terminus of the ash-flow sheet in the Valley of Ten Thousand Smokes. The distal part of the sheet can be reached in an hour's walk by steep trail from the Overlook Cabin, but anything more than a brief visit demands camping expertise and survival equipment. Reaching Novarupta requires a day-long backpack trip, each way. The surrounding ice-clad stratovolcanoes, including Mount Katmai, should not be climbed without mountaineering skills and equipment. High winds, frequent rain and drizzle, brown bears, icy stream crossings, crevassed glaciers, and especially its remoteness make the area a true wilderness, exhilarating but risky, occasionally glorious, seldom comfortable, and never to be trifled with. Information can be obtained from the National Park Service (Box 7, King Salmon, Alaska 99613; 907-246-3305) or the King Salmon Visitor Center (907-246-4250); http://www.alaskageographic.org/static/272/king-salmon-visitor-center.

Figure 1. Map of upper Alaska Peninsula and Kodiak Island group, showing many geographic locations mentioned in text and, in red, regional isopachs for total 1912 tephra-fall deposit (thickness in cm). Triangles indicate stratovolcanoes; ovals indicate calderas. Abbreviations for volcanoes: A—Alagogshak; D—Denison; D²—Devils Desk; DG—Douglas; F—Fourpeaked; K—Katmai; Kj—Kejulik; Ku—Kukak; M—Mageik; Mr—Martin; P—Peulik; S—Snowy Mountain; St—Steller; T—Trident. Behind volcanic chain is Novarupta (N—black dot), vent site of 1912 eruption. Abbreviations for other geographic features: B—Brooks Camp; BL—Brooks Lake; BR—Brooks River; DP—Dumpling Mountain; IB—Iliamna Bay; HB—Hallo Bay; KB—Katmai Bay; KF—Kaflia Bay; KG—Kaguyak Bay; KK—Kukak Bay; KM—Kamishak Bay; KN—Kinak Bay; KV—Katmai village; PB—Portage Bay; and PU—Puale Bay (called Cold Bay in 1912). Inset map shows drainage system near Valley of Ten Thousand Smokes (VTTS, shaded); additional abbreviations here: G—Mount Griggs; HP—Hagelbarger Pass; KjP—Kejulik Pass; KP—Katmai Pass; and YP—Yori Pass.

BASEMENT ROCKS

The Katmai cluster was built on a set of rugged glaciated ridges carved from the subhorizontal to gently warped, marine siltstone and sandstone of the Jurassic Naknek Formation (Riehle et al., 1993; Detterman et al., 1996). These well-stratified rocks are intruded locally by several porphyritic granitoid stocks of Tertiary age. Although Quaternary lavas drape the basement to elevations as low as 180–550 m, the Jurassic strata crop out as high as 1340 m on Mount Griggs, 1370 m on Mount Katmai, and 1555 m in the saddle between Mounts Martin and Mageik. Because the axial volcanic chain straddles the drainage divide of the Alaska Peninsula (Fig. 2), eruptive products can flow either southeastward down the Pacific slope toward Shelikof Strait or northwestward toward the Naknek Lake system and Bristol Bay.

Permian to Jurassic sedimentary rocks that regionally underlie the Naknek Formation (itself more than 2 km thick) do not crop out in the Katmai area, but the stratigraphic framework of the Alaska Peninsula (Detterman et al., 1996) suggests that such rocks as thick as 3.5 km are concealed beneath the Katmai volcanoes.

A few remnants of Pliocene and early Quaternary volcanic rocks (Hildreth et al., 2004) cap peaks and ridges near Mount Griggs, but most such rocks have been eroded from the area surrounding the Valley of Ten Thousand Smokes. Much of the basement east of Mount Katmai and south of Snowy Mountain, however, includes altered volcanic rocks (Riehle et al., 1993) that have received little attention. Erupted from several ill-defined centers, these rocks are ordinary arc andesites and dacites, either undeformed or gently warped, variably altered hydrothermally, and presumed to be Neogene (Shew and Lanphere, 1992) but possibly also in part early Quaternary.

CONVERGENT MARGIN

The Quaternary volcanic front trends narrowly N65°E along the Katmai segment of the Aleutian arc (Fig. 1). The Mesozoic basement rocks upon which the volcanic centers are built is part of the Peninsular terrane, which is thought to have originated far to the south and to have been added to southern Alaska during the middle or late Mesozoic (Plafker et al., 1994), prior to oroclinal bending of southern Alaska. Since then, additional terranes and subduction-related accretionary complexes were added along Alaska's southern margin, such that the Aleutian trench (5–6 km below sea level) now lies 350 km southeast of the volcanic front. Eocene seafloor is currently being subducted there, nearly orthogonally, at a convergence rate of ~6 cm/yr. The inclined seismic zone is well defined and 20–30 km thick (Kienle et al., 1983). It dips only ~10° NNW for some 300 km, then steepens to ~45° beneath the present-day arc, and persists to depths as great as 200 km; its top lies ~100 km beneath the Katmai volcanic cluster. Although the arc alignment shifted modestly during the Tertiary (Wilson, 1985; Riehle et al., 1993), the Aleutian arc was well established along the Alaska Peninsula by the middle Eocene, soon after onset of northwestward motion of the Pacific plate beneath southern Alaska (Plafker et al., 1994).

Crustal structure in the Katmai region is poorly known and the nature of the basement under the subhorizontal Mesozoic section remains particularly uncertain. Alaska Peninsula crust is thought to be 30–36 km thick farther to the northeast (Moore et al., 1991), as well as near the peninsula's southwest extremity (Fliedner and Klemperer, 2000). Although the lower crust under the forearc and arc may be especially mafic, having atypically high seismic velocities for normal continental crust (Fliedner and Klemperer, 2000), the many Tertiary granitoid plutons in the Katmai region show that the sub-arc crust is now essentially continental. Gabbroic xenoliths containing Paleozoic and Proterozoic zircons were ejected by Redoubt Volcano (Fig. 1), suggesting that more ancient basement rocks are concealed within or beneath

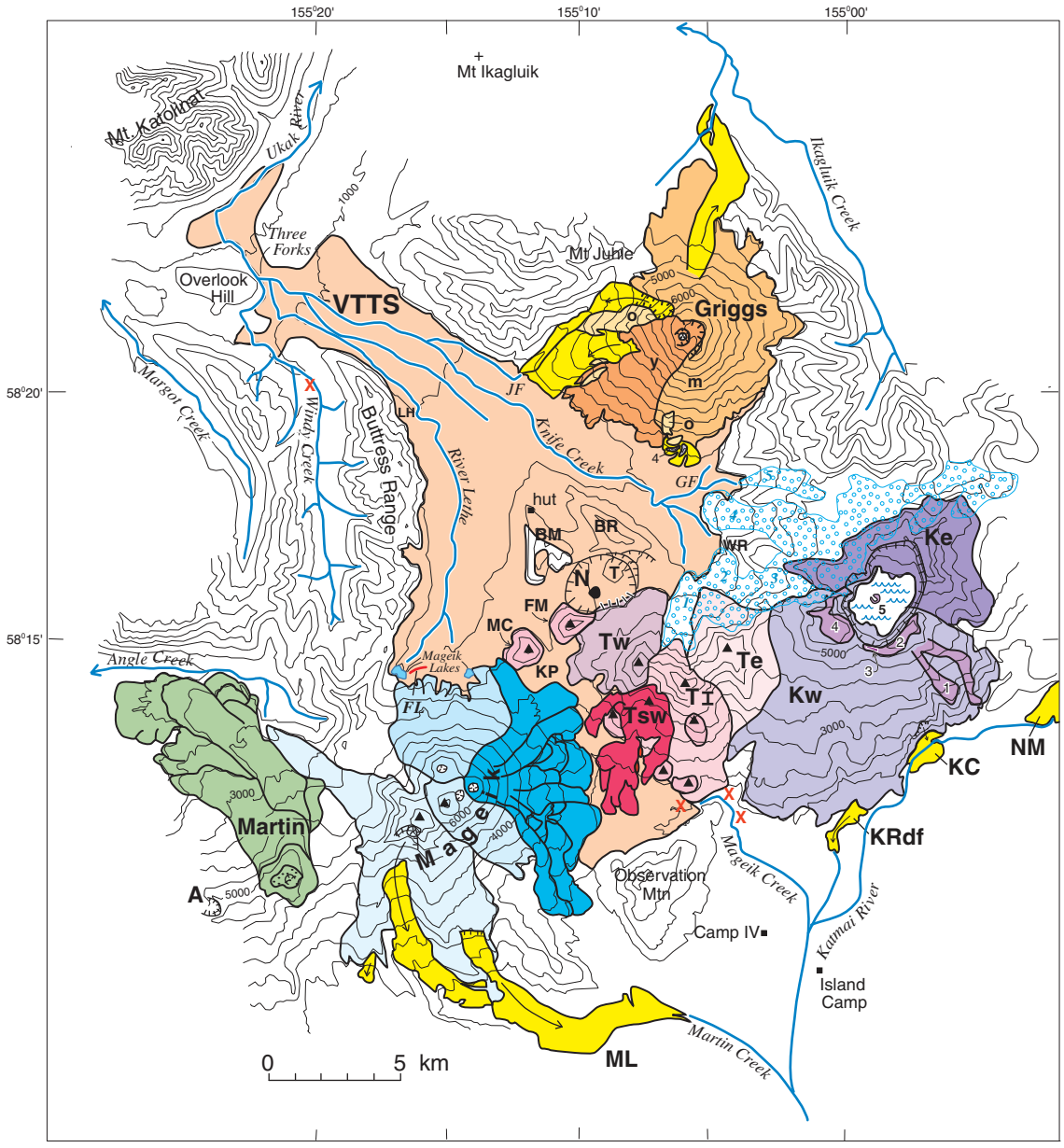

Figure 2. Simplified geologic map of Valley of Ten Thousand Smokes (VTTS) and volcanoes of the Katmai cluster. Contour interval 500 feet. From hachured vent depression around Novarupta lava dome (N—black), 1912 ignimbrite (tan) extends northwest 20 km along VTTS as well as across Katmai Pass for 10 km down Mageik Creek on Pacific slope. Knife Creek Glaciers (blue pattern) are numbered 1–5; other glaciers are omitted for clarity. Alagogshak volcano (A), long extinct, is indicated only by its eroded crater. Mount Mageik consists of four overlapping centers (in shades of blue); only the youngest and easternmost center (for which individual lava flows are indicated) is Holocene. Mount Martin, entirely Holocene, consists of small fragmental summit cone and several overlapping coulees. Trident group consists of three Pleistocene cones, East Trident (Te), Trident I (T_I), and West Trident (Tw), as well as historical Southwest Trident (Tsw) lavas and fragmental cone of 1953–1974; several peripheral Pleistocene lava domes, comagmatic with Trident, include Mount Cerberus (MC) and Falling Mountain (FM). Mount Katmai consists of two overlapping centers, Northeast Katmai (K_e) and Southwest Katmai (K_w), both truncated by 1912 collapse of hachured Katmai caldera, which is now partly filled by lake. Five youngest eruptive units of Mount Katmai are numbered (1–5) and discussed individually in text: 1—leveed dacite lava flows; 2—south-rim rhyodacite lavas; 3—zoned scoria fall atop unit 2; 4—dacite agglutinate sheet on caldera rim and correlative scoria-flow deposit at Knife Creek; and 5—Horseshoe Island dacite dome. Remnants of 22.5-ka plinian rhyodacite pumice-fall deposits (and ignimbrite) in Windy and Mageik Creeks (sites indicated by red X) are related to most evolved lava of unit 2. Products of Mount Griggs are subdivided by age into older (o—middle Pleistocene), middle (m—late Pleistocene), and younger (y—postglacial) exposures. Holocene debris-avalanche and debris-flow deposits are in bright yellow; those emplaced in 1912 are labeled: KC—Katmai Canyon landslide; KRdf—Katmai River pumiceous debris flow; ML—Mageik Landslide; NM—Noisy Mountain landslide. Uncolored basement rocks are Jurassic Naknek Formation or Tertiary porphyritic intrusions. Miscellaneous features: BM—Baked Mountain; BR—Broken Mountain; FL—site of Fissure Lake; GF—Griggs Fork of Knife Creek; JF—Juhle Fork of Knife Creek; T—Turtle; WR—Whiskey Ridge; *hut*—Baked Mountain Hut, research shelter; *Island Camp* and *Camp IV* were way stations between Katmai Bay and VTTS for 1916–1919 expeditions.

the Peninsular terrane (Bacon et al., 2012), but whether such rocks are present southeast of the Bruin Bay fault (Fig. 1) is unknown.

Crustal earthquakes, generally shallower than 10 km, are abundant beneath the Katmai volcanoes (except Mount Griggs). As many as 1000 local earthquakes each year are recorded here by Alaska Volcano Observatory (http://www.avo.alaska.edu/), nearly all of them smaller than magnitude 2.5 (Jolly and McNutt, 1999; Moran, 2003; Jolly et al., 2007; Murphy et al., 2010; Prejean et al., 2008).

MOUNT KATMAI EDIFICE

Overview

Centered 10 km east of Novarupta and adjacent to Trident (Fig. 2), Mount Katmai is a compound stratovolcano that consisted of two contiguous cones, both beheaded by the caldera collapse of 1912 (Fig. 3). Separate foci of hydrothermal alteration are exposed on the caldera walls, and abutting stacks of lava flows and ejecta dip against each other from discrete northeast and southwest centers, here called NE Katmai and SW Katmai. A coastal survey in 1908 (Griggs, 1922, p. 270–275) sketched four summits (Fig. 4), three of which were lost in 1912. The westernmost of the four survived and forms the twin peaks 6128 and 6200 (Fig. 5), which rise above the western edge of a marginally preserved remnant of a pre-1912 filled crater of the southwest cone. The eastern margin of that crater may have included the main summit, former peak 7500, whereas two other pre-1912 summits (peaks 7360 and 7260; Fig. 4) belonged to the northeast cone and were probably high points on the crater rim, now wholly destroyed.

The steep-walled caldera (Fig. 5) has an area of ~4 km^2 at its floor and ~8.8 km^2 at the rim. Its internal volume is today ~4 km^3, and the foundered superstructure amounted to an additional 1.1–1.5 km^3, giving a collapsed volume of ~5.5 km^3. A postcollapse dacite dome and numerous fumaroles on the caldera floor (Griggs, 1922; Fenner, 1930) were by 1929 covered by rising lakewater, which is today deeper than 200 m and ~1 km^3 in volume.

Eruptive products of Mount Katmai range from basalt to rhyolite (51.6%–72.3% SiO_2), an array wider than that of any other stratovolcano in Alaska and surpassed only by the Novarupta pyroclastic eruption of 1912 (50.4%–77.8% SiO_2). Andesitic lava flows and breccias are major components of both subedifices of Mount Katmai, and products more mafic than 55% SiO_2 are limited. Silicic lavas (63%–72% SiO_2) are also common, dominating the youngest products of both cones. No lava domes are recognized in the caldera walls, though a few thick silicic lava flows truncated by the walls could have extended from summit domes obliterated by the 1912 collapse. The most silicic materials identified on the northeast cone are dacite lava flows (66% SiO_2), as thick as 60 m where they cap the North Ridge (Fig. 5). The southwest cone likewise has many dacites but further produced several rhyodacitic to rhyolitic lava flows (68%–72% SiO_2) that armor its upper southern slopes and cap much of the south to southeast rim. The most evolved of the south-rim lavas yielded a $^{40}Ar/^{39}Ar$ age of 22.5 ± 1.6 ka, but a zoned dacite-andesite scoria fall and a few of the rhyodacite lavas overlie it (Hildreth and Fierstein, 2003).

Pre-collapse volume of NE Katmai was ~10 km^3 in 1912 and of SW Katmai ~20 km^3. Rough estimates of *eruptive* volumes from the glaciated cones are 15 ± 3 km^3 and 42 ± 10 km^3, respectively. The latter figure includes 25 ± 5 km^3 for the edifice itself, 5 ± 2 km^3 for off-edifice dacite pyroclastic deposits, and 12 ± 5 km^3 for 22.8-ka rhyolite plinian and ignimbrite deposits. To these can be added the 13.5 km^3 of magma that erupted in 1912, all or much of which is inferred to have been withdrawn from beneath Mount Katmai.

Figure 5A provides, for reference, a simplified outline map of the caldera that indicates locations of topographic features cited and the azimuths or sectors encompassed by most of the panoramic photographs that follow.

Caldera Wall Exposures

We describe and interpret the eruptive units on the caldera walls by starting with the oldest components, exposed on the northeast wall, and proceeding counterclockwise to the southeast wall, where some of the youngest units occur. For reference to figures, we often describe features relative to four conspicuous low points on the caldera rim (Fig. 5A). These are the East Notch and West Notch (both at elevations of 4900 ± 50 ft), the South Notch (at ~5000 ft), and the North Notch (at ~5900 ft). Because topographic maps here are contoured only in feet, we cite elevations accordingly, and because the contour interval is 100 feet, many elevations cited are only approximate. The lake level, still rising slowly in recent decades, now stands at ~4100 ft (1250 m asl), some 750 ft (230 m) below the East Notch, low point on the rim.

Northeast Wall

The northeast wall (Fig. 6) provides a section through a steep mafic stratocone (52%–55% SiO_2) that forms the principal and earliest component of the NE Katmai edifice. Where best exposed, high on the inside rim, its fragmental deposits include sequences of ash-rich, cross-bedded, pyroclastic-density-current (pdc) deposits; dark-gray, flow-breccia sheets; and thin oxidized scoria falls interbedded with agglutinate (Fig. 6A). Summit 6715 and the 1-km-long, knife-edged rim south of it (Fig. 7) expose a stack of as many as 100 fragmental layers that dip outward at 25°–30° and form the wall down to lake level. Intercalated with these proximal ejecta are fountain-fed mafic lava flows, which near the rim are subordinate and typically only 0.5–2 m thick but thicken downslope and eventually exceed the fragmental proportion down on the eastern apron. Several vertical dikes, each 1–2 m thick (Fig. 6) and probably once radial to a central vent (that foundered with the caldera), cut the stack just north and south of the summit; although the set of dikes is best exposed on the inside wall, at least two dikes also crop out on the outer slope of the edifice. Greatest vertical exposure of the mafic cone is ~800 m, between the summit and lake surface.

Along the east wall south of the summit, strata of the mafic cone dip 25°–30°S and continue below the East Notch where they disappear beneath lake level (Fig. 8). North of peak 6715, the mafic strata dip ~30°N, but where the north wall swings westward their apparent dip is 15°–20°W. The strata extend through an erosional fin prominent in the North Notch (Fig. 6) and gradually descend for ~2.5 km southwest where their upper surface drops below lake level on a promontory ~800 m west of the northern intracaldera glacier (as seen in Figs. 9 and 10).

Although the cone strata include thin sheets of proximal agglutinate and spatter-fed lava flows that thicken downslope on the outboard apron, on the caldera walls they are principally fragmental. Many layers exposed on the wall appear to be phreatomagmatic, including coarse chaotic breccia in sheets 5–10 m thick along with stratified intervals of poorly sorted finer breccia and lithic-rich ash beds 10–100 cm thick. High in the section, in the North Notch and on summit peak 6715, scoria-rich fall layers are interbedded with 20 or more thin sheets of lava, each 0.5–2 m thick. Red and black scoria-fall layers are most conspicuous between lava flows on the steeply outward-dipping east slope of the summit ridge (Fig. 7). Repeated phreatomagmatic activity in building the cone suggests wet crater fill, snow and ice, or perhaps a small crater lake. Sporadic exhaustion of the water source allowed transitions to open-vent eruptions of scoria and spatter, especially toward the end of cone growth. The lower half of the northeast wall between the northern intracaldera glacier and the East Notch is so

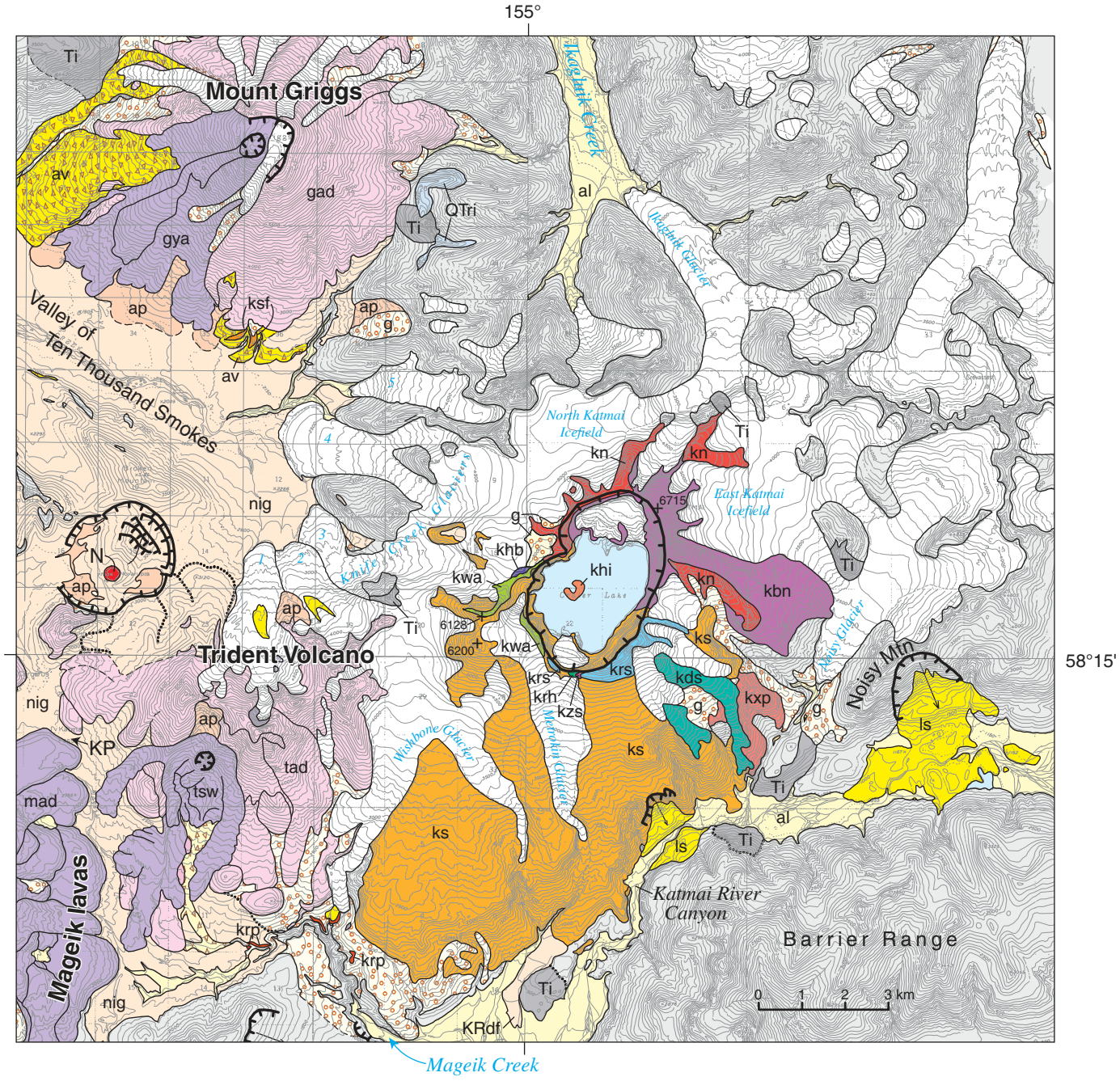

Figure 3 (*Continued on facing page*). Simplified geologic map of Mount Katmai, emphasizing its position relative to Trident Volcano and Novarupta. Map units are identified on accompanying list and discussed in text. Glaciers white; Knife Creek Glaciers numbered 1–5. Abbreviations: KP—Katmai Pass; N—Novarupta rhyolite dome; KRdf—Katmai River pumiceous debris-flow deposit of June 1912. Twin peaks on caldera's west rim are 6128 and 6200; peak 6715 on northeast rim is highest point remaining after caldera collapse. Map modified from regional map of Hildreth and Fierstein (2003).

LIST OF MAP UNITS

khi	Dacite lava of Horsehoe Island (1912) (now submerged ~200 m below lake level)
khb	Hydrothermal explosion breccia of Katmai caldera rim (1912)
kds	Dacite lava flows of southeast slope (Holocene)
kwa	Dacite agglutinate of west rim (early Holocene or late Pleistocene)
ksf	Dacite scoria flow deposit of Knife Creek (early Holocene or late Pleistocene)
kzs	Zoned scoria-fall deposit on south rim (early Holocene or late Plestocene)
krs	Pyroxene-rhyodacite lava flows capping south rim (late Pleistocene)
krh	Hornblende-bearing rhyolite lava flow of south rim notch (late Pleistocene)
krp	Plinian pumice-fall and ignimbrite deposits of hornblende-bearing rhyodacite (late Pleistocene)
ks	Andesite-to-rhyodacite lavas and pyroclastic deposits of Southwest Katmai (late Pleistocene)
kxp	Andesite crystal-poor lavas of southeast slope (late Pleistocene)
kn	Andesite-dacite lava flows and pyroclastic deposits of Northeast Katmai (late Pleistocene)
kbn	Basaltic and andesitic lava flows and pyroclastic deposits of Northeast Katmai (late Pleistocene)
nig	Valley-filling Novarupta ignimbrite of June 6-7, 1912
ap	Pumiceous alluvium of 1912 Novarupta pyroclastic debris (1912 and younger)
al	Alluvium (Holocene)
ls	Landslide deposits (6-7 June, 1912)
av	avalanche deposits (Holocene and Pleistocene)
g	glacial till (Holocene and late Pleistocene)
gya	Andesite lavas of Mount Griggs (late or middle Holocene)
gad	Andesite and dacite lavas of Mount Griggs (early Holocene and Pleistocene)
tsw	Andesite-dacite lava flows and ejecta of Southwest Trident (1953-1974)
tad	Andesite-dacite lava flows and pyroclastics of Trident Volcano (late Pleistocene)
mad	Andesite-dacite lava flows and proximal ejecta of Mount Mageik (Holocene)
QTri	Rhyolite ignimbrite of Ikagluik Creek (early Quaternary or Pliocene)
Ti	Tertiary intrusive rocks (Pliocene and Miocene)
bu	Basement rocks, undivided (Mesozoic and Tertiary)

Figure 3 (*Continued*).

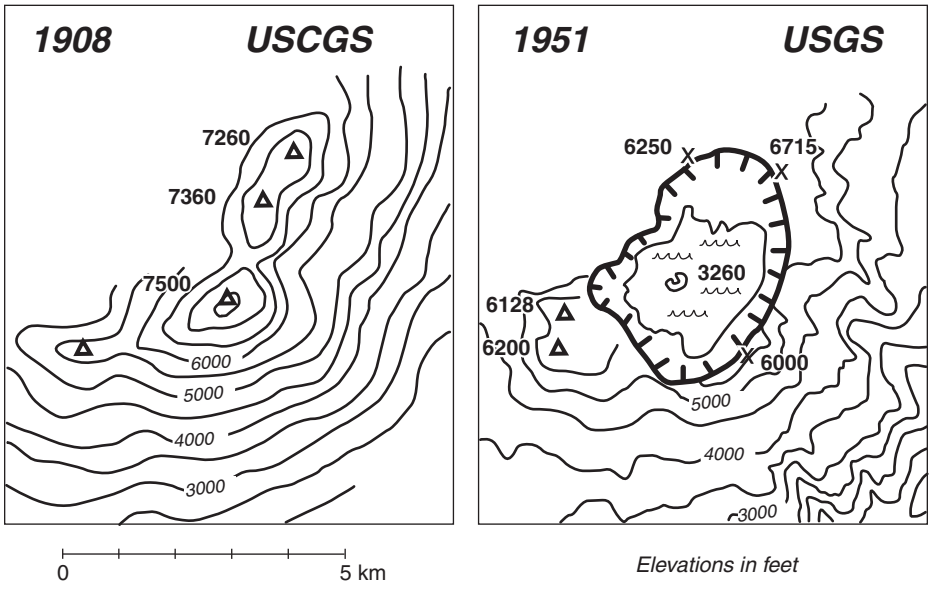

Figure 4. Mount Katmai before and after the caldera collapse of 1912. Left panel is adapted from Coast Survey Chart 8555 (Griggs, 1922; Fenner, 1923); summit elevations were triangulated from the coast 25–42 km south of Mount Katmai, and contours were apparently sketched visually with little additional control. Right panel is adapted (for the same area at the same scale) from U.S. Geological Survey quadrangles Mt. Katmai A-3, A-4, B-3, and B-4 (1:63,360 series, 1951), which were prepared by photogrammetric methods from aerial photographs taken in 1951. Elevations in feet. Horseshoe Island dacite dome is on sublacustrine caldera floor at an elevation of ~3260 feet, now covered by as much as 820 feet (250 m) of sediment and still-deepening lakewater.

severely acid altered (Fig. 6) that primary facies are hard to distinguish.

The mafic cone is overlain unconformably by glaciated remnants of andesite-dacite lava flows (unit **kn**) that appear to have issued from high on the (now collapsed) NE Katmai cone. The most extensive are along the north rim (Figs. 6 and 9; see next section), but others are near the East Notch (Figs. 7 and 8) and at the northeast toe of the NE Katmai cone (Fig. 3). The last is a set of pyroxene-plagioclase andesite lava flows (59.7% SiO_2), glacially scoured but still locally blocky and vesicular, that rests on distal strata of the mafic cone and is eroded into a divergent pair of glacier-bordered ridges (Fig. 3), each ~1.5 km long. The basal andesite flow gave a K-Ar age of 70 ± 13 ka, and a lava flow (52.6% SiO_2) of the mafic cone at the North Notch gave a $^{40}Ar/^{39}Ar$ plateau age of 89 ± 25 ka (Hildreth et al., 2003b).

Near the East Notch (Fig. 8), a southeast-dipping sequence of andesitic lava flows and fragmental strata (**kn**) drapes the south and southeast slopes of the mafic cone (Figs. 6 and 7). Probably roughly time-correlative with andesites of the north rim just mentioned, the sequence is as thick as 200 m outboard, but, owing to incision by the glacial trough that heads on the notch, it is only 80–100 m thick on the caldera wall below the notch (Fig. 6), where it overlies altered mafic strata (**kbn**) and is overlain by dacite lava flows of the southeast wall (Fig. 8). On the north side of the notch, a stack of poorly sorted andesitic pyroclastic strata at least 70 m thick is exposed that includes 10-m-thick sheets of coarse massive breccia (proximal vulcanian block beds?) and stratified lapilli falls in layers 10–50 cm thick, dominated alternately by pumice or dense (originally glassy) clasts. Many or all of these deposits were emplaced phreatomagmatically and later hydrothermally altered, though fresh interiors of glassy blocks have 58%–59% SiO_2. Overlying this section, and at least 100 m thick, is a package of several andesite lava flows (59%–61% SiO_2) with intercalated sheets of altered autobreccia that dip as steeply as 30°SE from Crag 6400 (Figs. 3, 6, and 7). The flows extend 2.5 km southeastward as a glaciated cleaver ~100 m high that distally overlies outboard apron lavas of the mafic cone.

North Wall

Northwest-dipping strata of the mafic summit cone form much of the north wall for 2 km west of the North Notch (Fig. 9). They make up the black fin that stands in the notch like a gunsight, and they exhibit a consistent westerly apparent dip of ~15° as far as a steep discontinuity just west of the northern intracaldera glacier, where all but the basal 50 m of the exposed mafic section ends abruptly. High on the wall, the ~300-m-thick mafic section is truncated by an undulating erosional unconformity (Fig. 9) that is overlain by glacially ravaged remnants of andesite-dacite lava flows and breccias that dip north and northwest from vents that foundered inside the caldera in 1912. Orientations of these flows and stratigraphic relations with the SW Katmai cone on the northwest rim (Figs. 10 and 11) indicate that their vents were on the NE Katmai cone, close to that of the preceding mafic cone. The intermediate strata above the unconformity are much less altered than the mafic strata below (Fig. 9).

The ice-sculpted, intermediate-lava remnants on the north rim are labeled in Figure 9. (1) The truncated face of the North Ridge, which towers as high as 6450 ft (erroneously shown as 6100 ft on topographic maps), consists of a stack of pyroxene-dacite lava flows (66% SiO_2) and thick autobreccias (Fig. 9A). The North Ridge extends 1.7 km northward as a sharp cleaver (Fig. 5) on which are exposed four plagioclase-rich flows that each locally exceed 50 m in thickness. Proximally, several thinner lava flows, partly brecciated and 10–30 m thick, augment the ridge-forming stack at the caldera wall (Fig. 9A). Distally, only 1.7 km outside the rim, the basal flow rests on Jurassic siltstone at 4400 ft elevation. (2) A remnant of the North Ridge dacite stack is preserved on the caldera rim 300 m farther west, shown in Figure 9 as "Two-tip knob," consisting of about eight sheets of altered dacite breccia and massive lava (65.6% SiO_2), each 3–10 m thick, that rest atop mafic strata of the north wall. (3) The North Pyramid is cut from a stack of andesite (60% SiO_2) lavas, autobreccia, and scoria falls that caps a thick section of ballistic-fall and surge deposits (Fig. 9B). The pyramid rises ~175 m above the unconformity and ~110 m above the rim. Its lower half consists of ~30 layers, each 1–5 m thick, including oxidized lithic-rich scoria falls, coarse breccias, and poorly sorted, cross-bedded, ash-rich intervals (Fig. 9C)—probably largely of phreatomagmatic origin. The upper half consists of 15 layers that dip 25–30°NNW and include several massive lava flows 10–15 m thick along with intercalated flow breccias and a few coarse breccia layers that were probably emplaced explosively. (4) The NNW Buttress, western end of the high northern wall, is a continuation of the andesite stack exposed on the North Pyramid, but the stack thickens to ~225 m before being abruptly truncated by a 200-m-high west-facing scarp (Figs. 9 and 10).

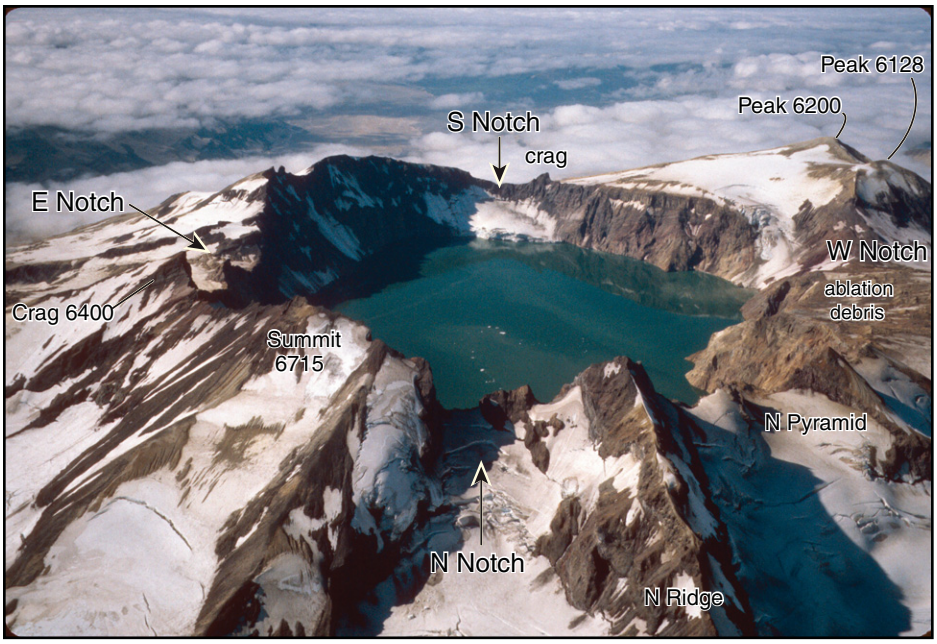

Figure 5. Katmai caldera, 4 × 3 km across at rim, collapsed fitfully on 7–10 June 1912. Aerial view toward southwest. Sunlit southwest wall of caldera and twin peaks 6200 and 6128 at head of ice slope are all part of SW Katmai edifice, as is southeast wall, in shadow. Knife-edged rim in left foreground includes present-day summit (Fig. 6) and is part of NE Katmai edifice, as are northwall crags at lower right. Thick dacite lava flow caps North Ridge cleaver in right foreground; that ridge and andesitic pyramid to its right are labeled in Fig. 9. Low southwest rim (right, middle) is covered by wasting ice and ablation debris. Lake is now 200–250 m deep, its surface ~800 m below summit and ~600 m below southeast rim. Radial dips of volcanic strata are conspicuous in topography. Several extracaldera radial glaciers persist despite loss of mountain's summit in 1912. Icefield at upper right, which mantles slope of twin peaks had by 1929 engendered narrow intracaldera ice tongue on west wall. Slump-block bench (at south shore of lake) progressively accumulated an intracaldera glacier that reached lake level by 1976.

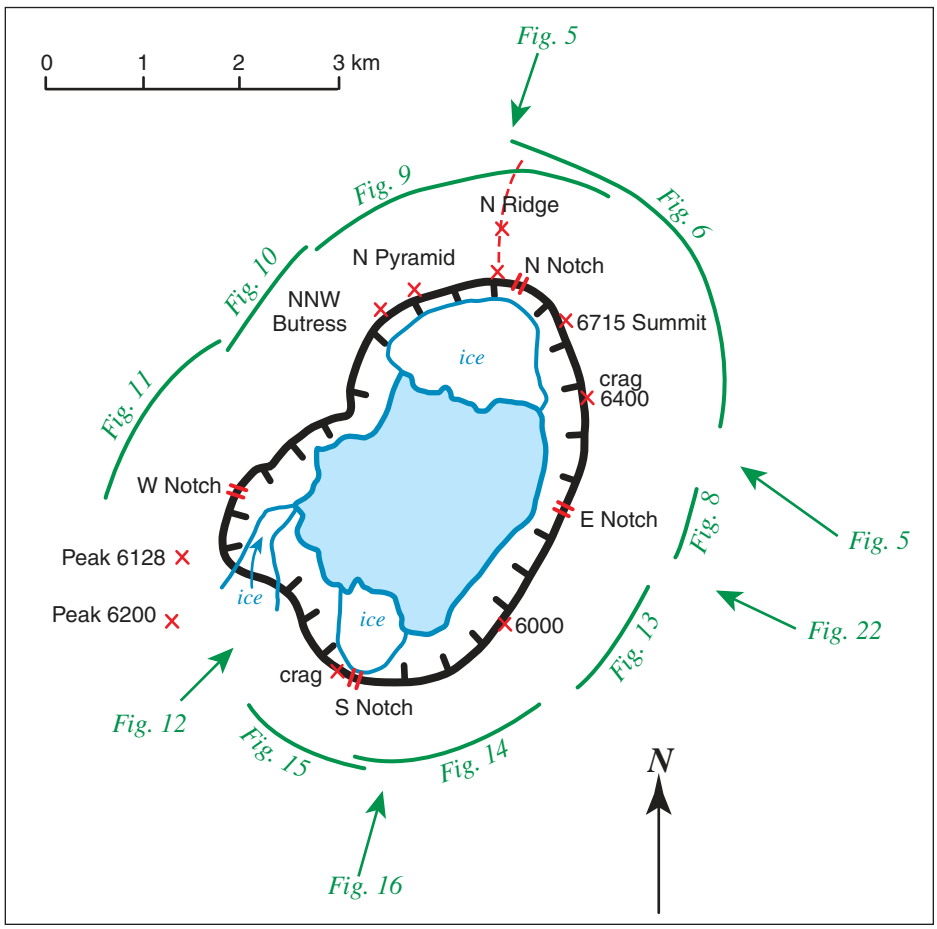

Figure 5A. Reference outline map of Katmai caldera, showing locations of topographic features mentioned in text or figures as well as the azimuths or sectors encompassed by the photo-figures that follow. For example, aspect of Figure 5 across caldera toward SSW is indicated by arrow at top of outline map.

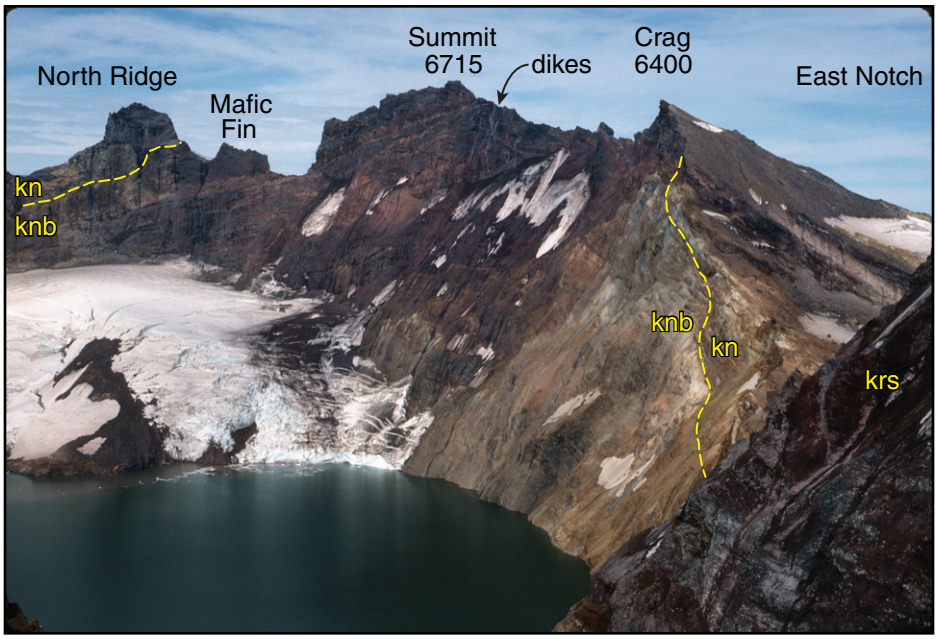

Figure 6. North and northeast wall of Katmai caldera viewed from southeast rim. Slump-block bench at foot of north wall progressively accumulated an intracaldera glacier that now reaches lake level. Hydrothermally altered wall at East Notch (right) is one of several such internal zones that supplied acid-altered ejecta during caldera collapse (see Fig. 25). Northwest-dipping mafic strata of true summit (peak 6715 on central skyline) are cut by vertical dike complex. Southeast-dipping altered strata above East Notch (at right) are part of same edifice; upper third of section consists of andesitic lavas and breccias that culminate in Crag 6400 and overlie strata of mafic cone. Tower on left skyline rim above glacier is head of North Ridge dacite lava flow prominent in Figure 5. To its right, basaltic fin stands like gunsight in North Notch. At lower right are rhyodacite lavas and oxidized breccias of upper southeast wall (see Fig. 13).

Figure 6A. North face of true summit (peak 6715) of Mount Katmai on northeast rim of caldera. Aerial view toward southwest, displaying ~80 m relief. Ash-rich cross-bedded surge deposit at lower right is truncated by northeast-dipping sequence of proximal fall deposits that include red scoria falls and agglutinated spatter and sandwich coarse gray breccia, which is probably proximal autobreccia. On right skyline 20 km away, ice-clad Mount Mageik rises beyond twin peaks of Mount Katmai's west rim (seen in Fig. 5).

Lower flows of the stack continue for an additional 1.5 km southwest along the caldera rim; a 100-m-thick rim flow extends 500 m beyond the base of the buttress, then thins to 25 m before pinching out atop products of SW Katmai (Fig. 10). Two thick lava flows of pyroxene andesite sampled on the buttress scarp have 58%–59% SiO_2, and flows on the glaciated 5400-ft shelf that extends 800 m farther southwest have 61%–62%. Because the NNW Buttress stack dips 25°NW and the shelf lavas ~10°W, they all appear to have issued from NE Katmai, like all the other north-rim eruptive units.

Northwest Wall

Abrupt truncation of the NNW Buttress, thinning of its shelf-forming andesite stack farther southwest, and the generally lower rim along the northwest wall of the caldera probably all reflect erosion by an edifice-mantling Pleistocene ice cap that flowed preferentially toward the valley that in 1912 became the Valley of Ten Thousand Smokes. For 2 km southwest from the base of the NNW Buttress, the caldera rim gets gradually lower (Figs. 10 and 11), from ~5400 ft to ~4900 ft at the West Notch. This segment of the wall consists of four principal components. (1) Andesitic lava flows (61%–62% SiO_2) and breccias erupted from SW Katmai form most of the stratified 300-m-high wall. The package dips generally away from the caldera (to N and NW), but along the wall it displays an apparent-dip component of ~10° to the northeast,

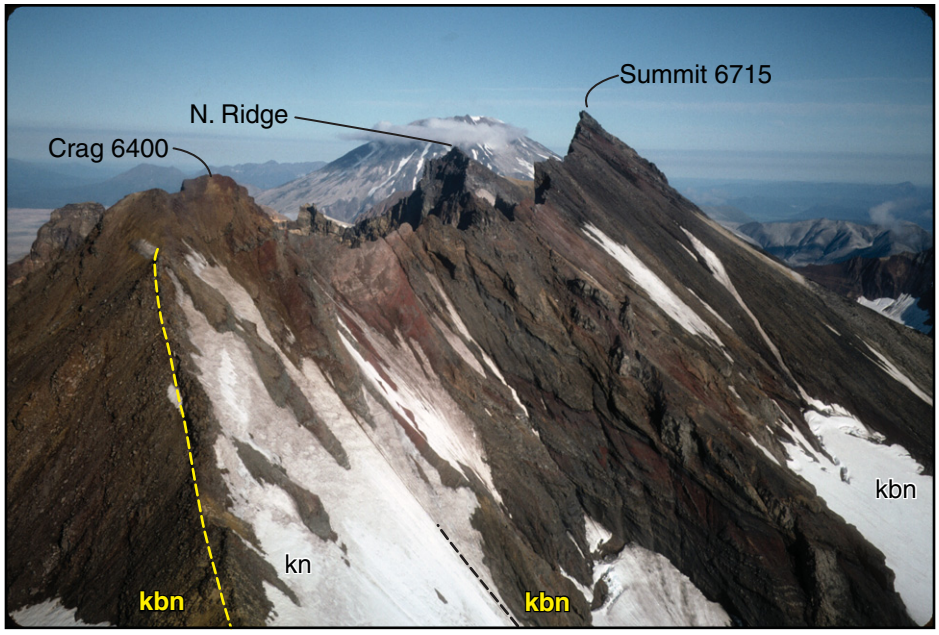

Figure 7. Aerial view of eastern flank of NE Katmai looking northwestward. Foreground relief is ~400 m. Steeply dipping lavas and red scoria layers are mafic (kbn; 52%–55% SiO_2), whereas younger products draping peak 6400 at left are andesitic (kn; 58%–61% SiO_2). For intracaldera view of steep inner wall of these crags, see Figure 6. Andesitic stack (kn) is also seen in background of Figure 13. Beyond sharp caldera rim rises andesitic cone of Mount Griggs, 15 km from camera.

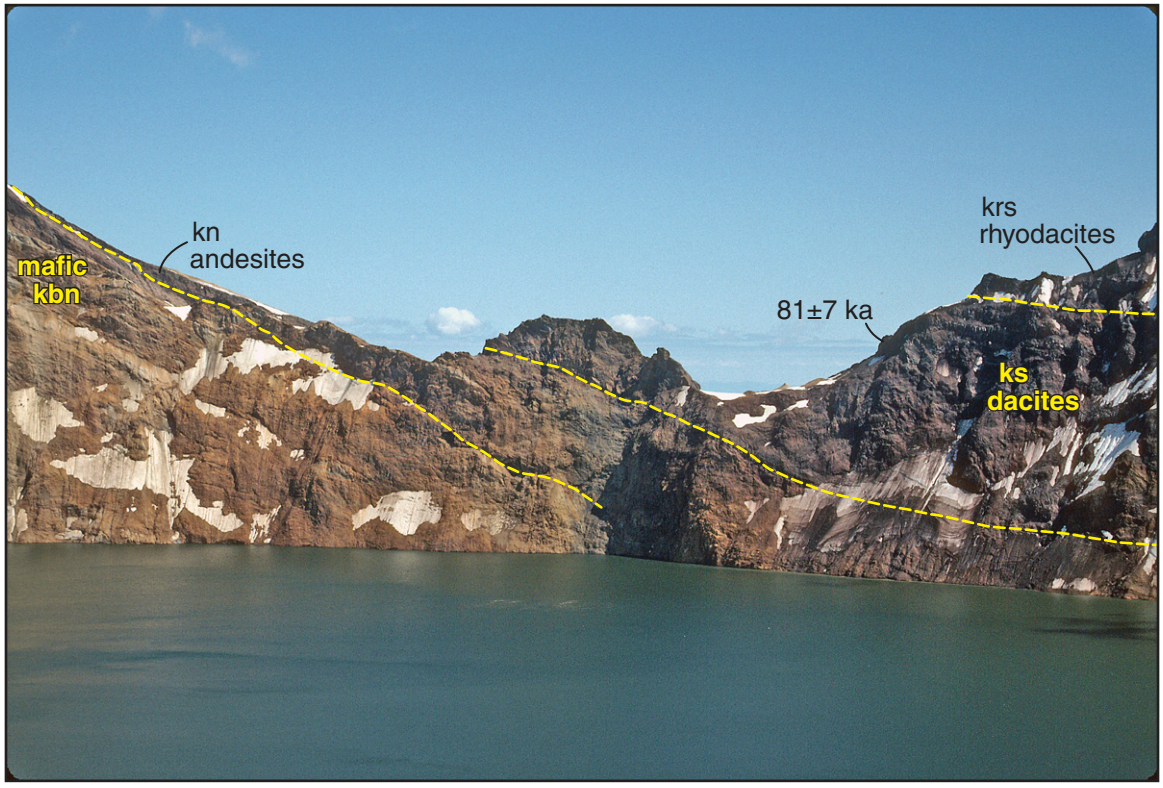

Figure 8. East Notch, low point on caldera rim. At left, strata of NE Katmai edifice dip 25°S; lower half of section is from mafic cone, upper half is andesite-dacite fragmental strata of Crag 6400 that drape the mafic cone (see Fig. 6). At right is sequence of dacite lava flows from SW Katmai edifice that dips 25°SE (away from the camera), and abuts the older sequence unconformably on wall below notch. At center of notch, 50-m-high knob is dacite lava flow and breccia (64.4% SiO_2) that extends north (to left) over strata of the NE Katmai edifice.

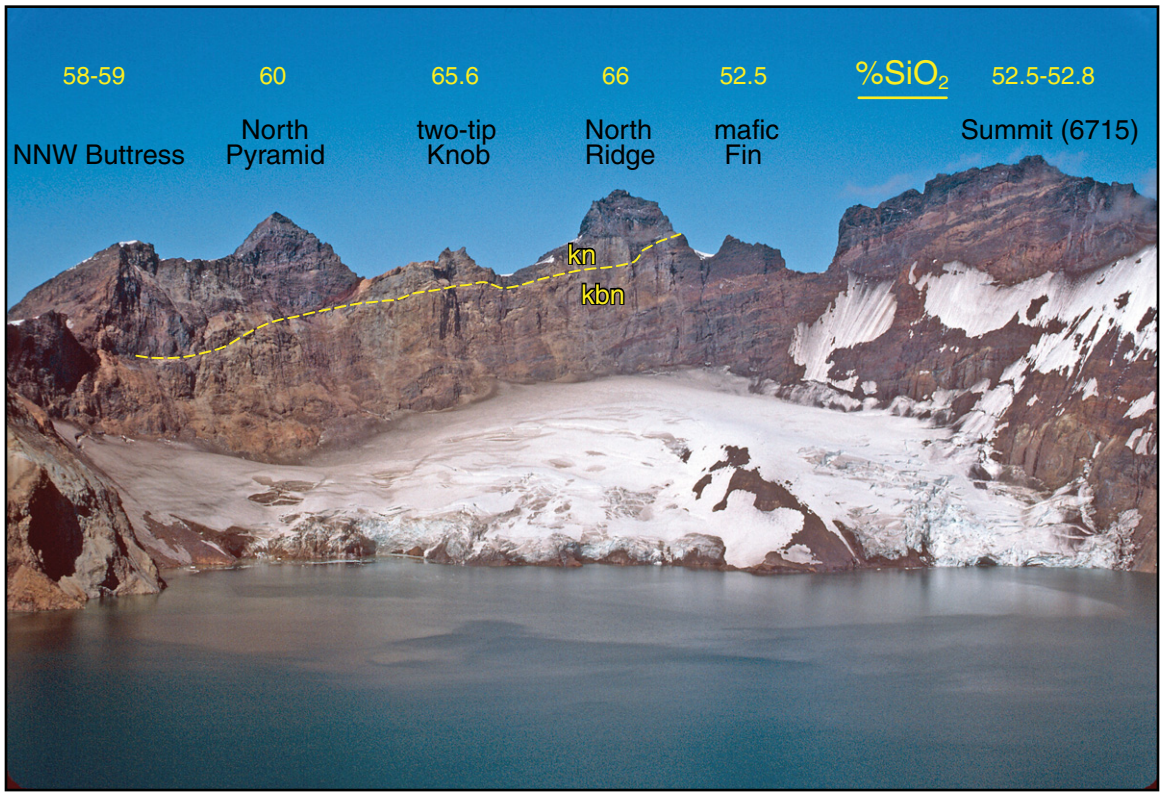

Figure 9. North wall of Katmai caldera (345° to 040°), illustrating consistent NW dip of lava flows and ejecta that built NE Katmai edifice. Thin mafic strata, pale colored owing to hydrothermal alteration of edifice interior (principally of fragmental layers), are separated by an erosional unconformity from overlying stacks of dacite and andesite lava flows that dip N and NW. Unconformity descends westward from ~6100 ft elevation below North Ridge to ~5500 ft below North Pyramid to ~5000 ft at far left. Labeled prominences on rim are seen from above in Figure 5. Slump-block bench in foreground was ice-free in 1917 and was first observed to have accumulated a small ice shelf in 1929; by 1976, glacier was >50 m thick and had descended to lake level.

thinning, descending, and then terminating near the intracaldera glacier. At the base of the promontory 800 m west of that glacier, the package overlies a tapering wedge of mafic strata from NE Katmai that here descends beneath lake level. (2) A strikingly white 100-m-thick package of severely acid-altered lavas, breccias, tuffs, and sediments, virtually horizontal, extends for ~900 m along the wall (Figs. 10 and 10A), separating the first and third components. (3) The 5400-ft shelf that extends 800 m southwest from the toe of the NNW Buttress consists of several andesitic lava flows (58%–62% SiO_2) and stratified flow breccias that issued from NE Katmai and pinch out westward atop the altered white package (Fig. 10). (4) A stratified sheet of dacite agglutinate (unit **kwa**), here 10–25 m thick, rims the caldera west of that pinch-out (Fig. 11), resting on the lower package and, farther west, steeply draping peak 6128. All four components of the northwest wall were covered by thick glacial ice prior to 1912. Incomplete wasting of the glacier beheaded by caldera collapse has left this sector of the caldera rim covered by muddy heterolithologic glacial diamict, tilted seracs, disrupted Novarupta pumice falls, and hydrothermal breccia ejected during fitful caldera subsidence (as detailed in a later section, below).

The lower package, which makes up the 300-m-high wall between the lake and the rim agglutinate, consists here of subequal proportions of lava flows and fragmental deposits that appear to include both lava-flow autobreccias and explosively emplaced phreatomagmatic breccias. The package thins northeastward to ~150 m at the promontory beneath the white altered section (Fig. 11), but at least 200 m more is concealed below lake level. Much of the stack is moderately altered hydrothermally, especially the fragmental strata. Caldera-wall lava flows were not sampled here, but several correlative flows exposed in windows through the ice 1–2 km west of the rim are all plagioclase-rich pyroxene andesites with 61%–62% SiO_2. Within the wall embayment below the West Notch (Fig. 11) and for 800 m farther northeast, the upper half of the wall (beneath the rim agglutinate) is unconsolidated lithic breccia, massive or crudely stratified, poorly sorted, some of it block rich, much of it ash dominant with sparse blocks, and most of it oxidized red or yellow-brown. Apparently lacking a juvenile component, it may represent debris that filled a pre-1912 crater, only a fraction of which survived caldera collapse. Beneath this section, the lower half of the wall is a stack of lava flows and autobreccia sheets.

The acid-altered white package (Fig. 10), 80–110 m thick, includes massive lava and related autobreccia, stratified pyroclastic breccias, and an inaccessible upper section, 25–30 m thick, of horizontally stratified tuff and ashy sediment, thin to thick bedded (Fig. 10A). Lower breccias are coarse and clast supported, but higher layers are thinner, ash dominant, and locally exhibit low-angle cross-bedding and stringers of coarse lithics. The breccias and tuffs appear to bank northeast against a steep wall that truncates lava flows (mafic below and

Figure 9A. East face of North Ridge seen from North Notch on caldera rim. Visible section is ~100 m high, consisting of lava flows of plagioclase-rich pyroxene dacite (66%–67% SiO_2) separated by thin breccia sheets, here mostly autobreccias. Geologist at top of talus at left, where caldera wall cuts stack of lavas at ~70°. For perspective of location, see Figure 9.

Figure 9B. Near view of North Pyramid, which rises ~100 m above caldera-rim notch at right. For perspective of location, see Figure 9. Below rim, oxidized sequence includes phreatomagmatic surge and breccia sheets but is dominated by lithic-rich scoria falls and thin layers of agglutinated andesitic spatter. Above rim, two andesite lava flows (58%–60% SiO_2), 20 m and 40 m thick, sandwich another oxidized fragmental section.

Figure 9C. Southeast foot of North Pyramid, at west (left) side of caldera rim notch seen in Figure 9B. Exposure in image, ~35 m high, displays upward transition from explosively emplaced surge (altered), fall, and agglutinate deposits to effusive andesitic lava flows. Thin lavas are present in middle pyroclastic section, and thin fall units separate the thick lava flows above. At left rear is NNW Buttress (Fig. 9).

andesitic above) of NE Katmai. The altered breccias overlie the lava-flow stack from SW Katmai, which also appears to terminate eastward against the same steep wall of NE Katmai strata (Fig. 10). The altered section is overlain by 60–90 m of gray-brown brecciated andesite that extends to the rim. We speculate that the acid-altered material filled a depression eroded between the two centers, rather than a paleocrater. Massive white lava (K-2694) sampled on the rim of the promontory is pyrite bearing, is pale blue-gray inside large blocks, and has sulfur crystals in sparse vugs. Chemical analysis shows it strongly depleted in Na, Ca, and Mg, relatively enriched in Al, Fe, S, and H_2O, and probably originally andesitic.

Southwest Wall

From the West Notch to the South Notch, the 2.2-km-long southwest wall (Figs. 5 and 12) is rimmed almost continuously by stratified dacite agglutinate unit **kwa** (discussed at length in section below titled Youngest Eruptive Units). The cliff-forming, variably welded sheet is elsewhere 10–25 m thick, but midway along the southwest rim it thickens inward to more than 70 m, evidently a marginal remnant of the fill of a pre-1912 crater, within which the agglutinate might have been very much thicker before the old crater was destroyed by caldera collapse. If the 1912 dacite dome on the caldera floor reflected the principal vent site for the old crater as well, then the rim radius of the paleocrater could have been 1000 ± 200 m.

Andesite-dacite lava flows and breccias that make up the upper two-thirds of the 300-m-high wall below the agglutinate rim (Fig. 12) erupted at SW Katmai and dip 20–25°SW, away from the caldera and opposite to the inward dip of the agglutinate. Massive lavas and fragmental layers alternate on scales of 5–20 m, but one lava flow is ~50 m thick. We managed to collect only two samples representing this stack; both are pyroxene dacites (66.5%–67.5% SiO_2), and one gave a K-Ar age of 47 ± 13 ka.

This relatively fresh dacite stack unconformably overlies a hydrothermally altered sequence of strata, largely fragmental, exposed for 100 m above lake level on two promontories just south of the narrow ice tongue that descends the southwest wall (Figs. 5, 11, and 12). This lower sequence appears to be continuous across the wall reentrant below the West Notch with the 300-m sequence that dominates the northwest wall. If so, the main dacite sequence on the southwest wall is entirely younger than that of the northwest wall, though both are elements of SW Katmai.

Southeast Wall

The southeast rim extends 2.5 km between the South and East Notches, and its high points reach nearly 600 m above the lake surface. All three sequences to be described here are thought to have erupted from SW Katmai. Although strata exposed in the 60° wall dip outward at 25°–30°, the southeast wall experiences more frequent rock fall than anywhere else in the caldera, in part because the upper third of the section includes a large proportion of unconsolidated autobreccia that separates numerous lava flows, thick and thin (Fig. 13).

Flows exposed along the rim are pervasively glassy and 15–30 m thick (Fig. 13). All flows but one are plagioclase-rich pyroxene rhyodacites (unit **krs**; 67%–69% SiO_2), rich in mafic enclaves (54.5%–59% SiO_2). Rim lavas flowed down ~30° slopes and developed numerous sheets and lenses of glassy autobreccia. Beneath the thick rim flows, however, a stack of thinner rhyodacite flows forms most of the upper third of the wall. Gray massive zones of flows are 2–20 m thick, but layers of brick-red autobreccia and scoria between them are 1–20 m thick and make up half of the 150-m sequence (Fig. 13). Some of the thinner massive layers appear to be agglutinate or thin fountain-fed lava flows. In any section through the sequence, at least 10 massive flow units can be counted.

Beneath these, the middle third of the wall consists largely of massive lava flows with a

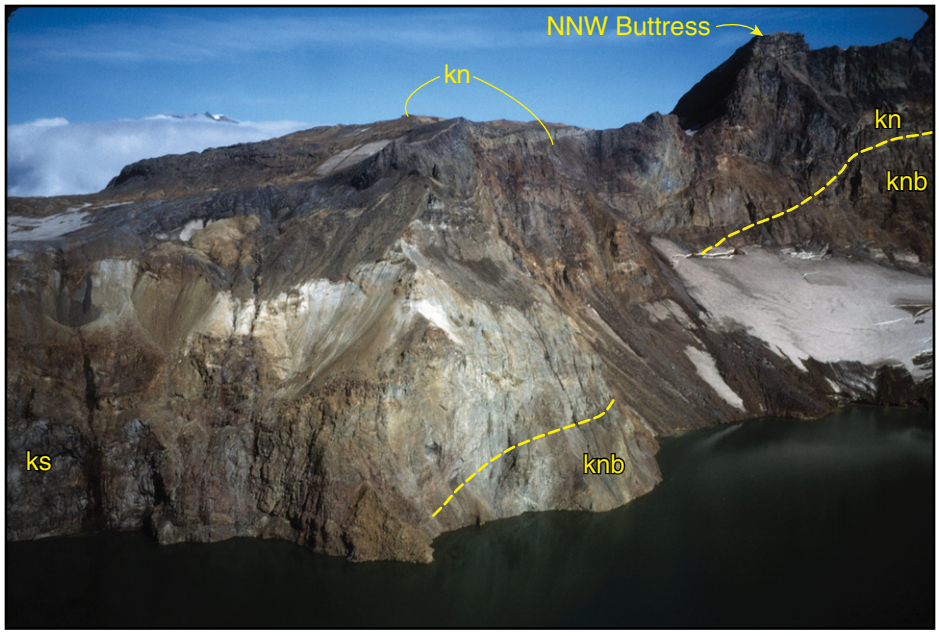

Figure 10. Promontory on northwest wall of caldera, illustrating interfingering of strata from NE and SW Katmai. Northern intracaldera glacier at right (see Fig. 9). NNW Buttress at upper right and 5400-ft andesite shelf on skyline to its left; these are both products of NE Katmai (kn), as is dark-gray brecciated rim section, which thins from 110 m to ~25 m before pinching out beneath ice and diamict at left. Wall at lower left is andesite stack (ks) erupted from SW Katmai and banked against older lavas of NE Katmai mafic cone (knb), which dip beneath lake level at base of promontory. Upper half of wall at right consists of andesite-dacite lava flows of NE Katmai (kn) that unconformably overlie products of the mafic cone (see Fig. 9). Strikingly white, mid-wall section, 80–110 m thick, consists of acid-altered lava flows and breccias, except for top 30 m, which consists of finer-grained tuffaceous strata (see Fig. 10A).

lesser fraction of breccias. Where some of these flows extend to the East Notch (Fig. 8), samples are plagioclase-rich pyroxene dacite with 65%–66% SiO_2. The floor and south wall of the East Notch and a prominent knob within the notch (Fig. 8) consist of such dacite (both platy lava and stratified breccia), glacially scoured and overlain by the glassy rim rhyodacites on a 25° southeast-dipping erosional unconformity. A dacite lava flow on the south wall of the East Notch gave a $^{40}Ar/^{39}Ar$ plateau age of 81 ± 7 ka.

The lower third of the southeast wall consists of thicker flows with only a modest proportion of interflow rubble, and the flows are apparently more altered than the fresh dacites and rhyodacites above. We were not able to sample the lower section (nor the 200-m section below lake level), but plausibly correlative flows on the outer southeast slope and massive blocks ejected to the rim during caldera collapse are all pyroxene andesites (58%–62% SiO_2) with fewer phenocrysts than the dacites.

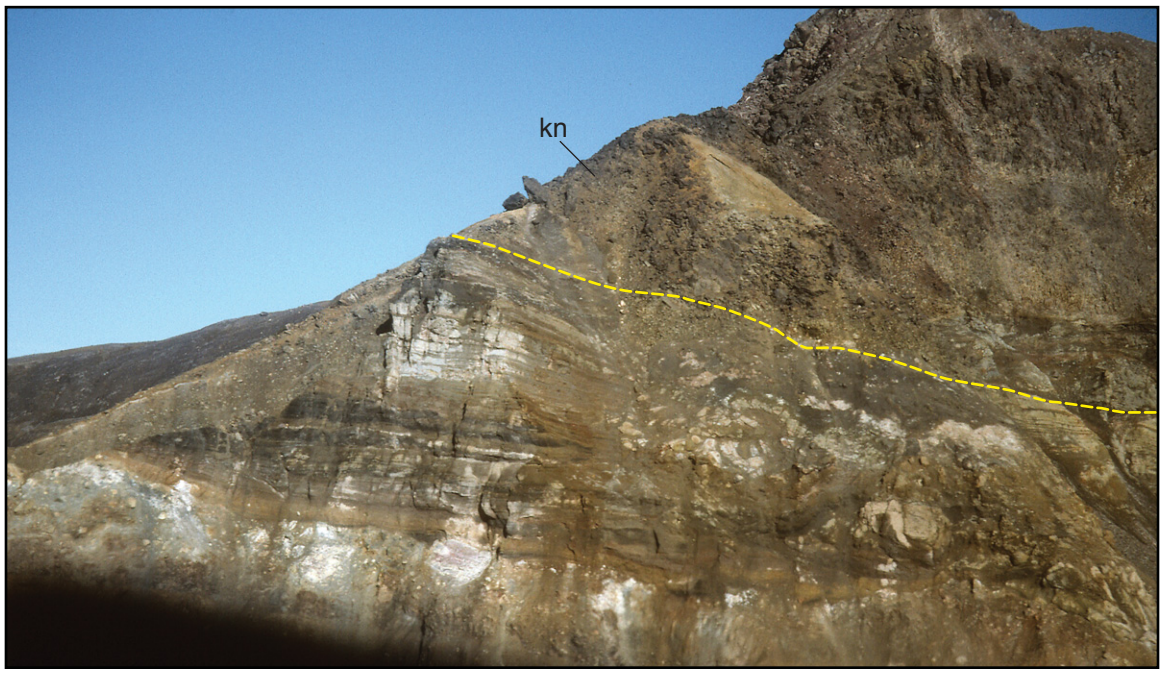

Figure 10A. Aerial close-up of stratified upper 30 m of white altered section seen in Figure 10. Overlying it, brown andesite breccia (kn) extends 70 m to skyline.

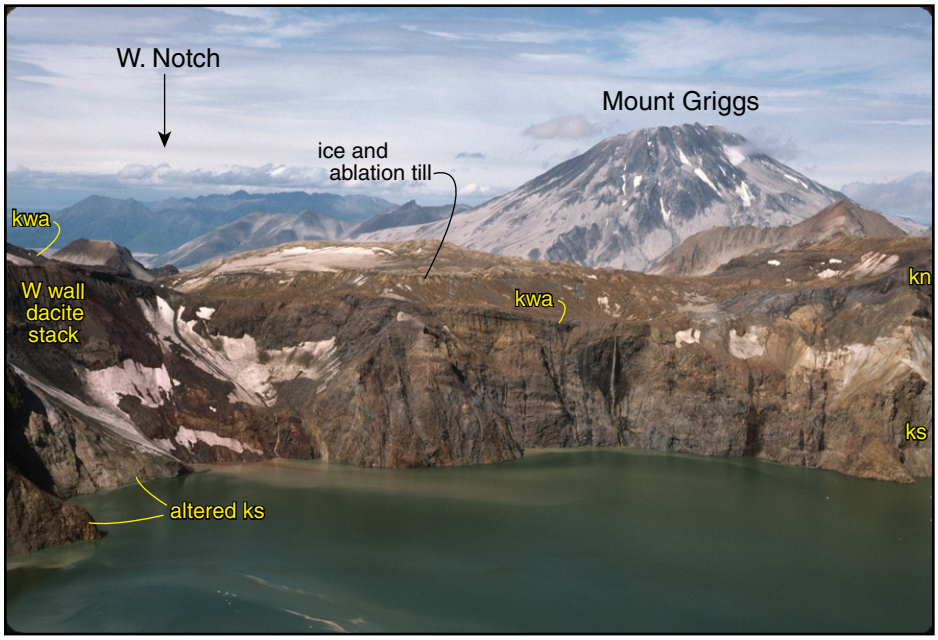

Figure 11. Northwest wall of caldera (280° to 330° sector), from West Notch at left to acid-altered white promontory (Fig. 10) at right. Andesitic lava flows (61%–62% SiO_2) and breccia forming stratified 300-m-high wall (ks) dip away from viewer (to N and NW) but along the wall display an apparent-dip component of ~10° to the right (to NE). Erupted from SW Katmai, they dip beneath andesite lava flows of NE Katmai edifice that form west-dipping, dark-gray rim and higher shelf at right (kn). Latter flows thin westward and pinch out atop white, acid-altered section (~110 m thick), which separates oppositely dipping packages of flows from different centers. At lower left, two promontories expose a west-dipping stack of altered lava flows and breccias that appears to be continuous with the northwest wall sequence; exposed for ~100 m above lake level, the altered stack unconformably underlies the main dacite lava sequence that dominates the southwest wall (Fig. 12). Dacitic sheet of agglutinate (kwa) rims caldera wall from center to left. Muddy deposit mantling shelf behind northwest rim consists of caldera-collapse phreatic ejecta and ablation diamict left by beheaded glacier that has receded as far as 500 m from rim since 1912. Mount Griggs, highest peak in the Katmai area, rises to ~2330 m, 11 km beyond the caldera rim.

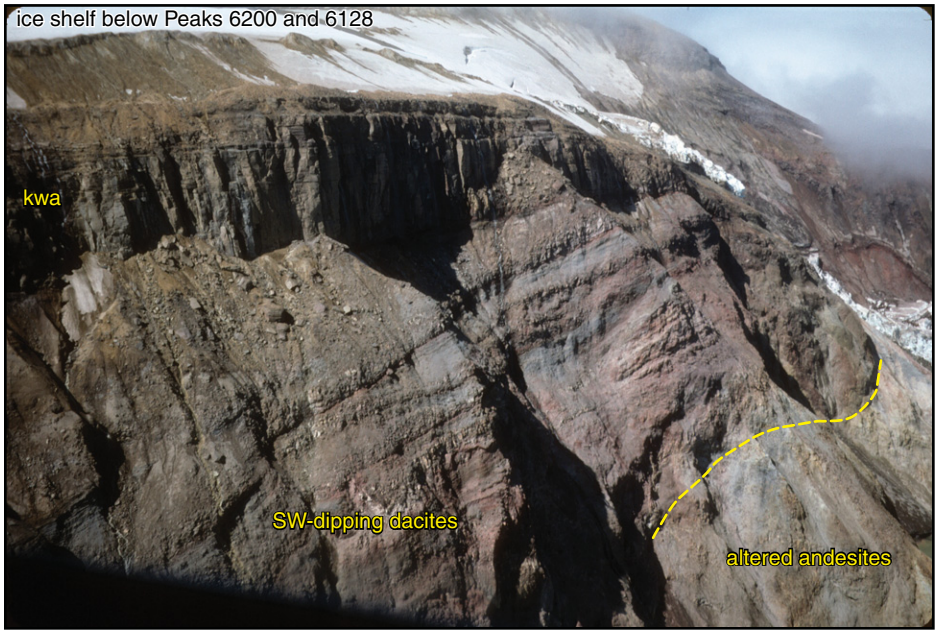

Figure 12. Southwestern inner wall of Katmai caldera from helicopter. Bench-forming rim cliff is stratified dense dacite agglutinate (kwa) that dips gently inboard where it filled a precaldera crater. Upper cliff of agglutinate is 8 m high, main lower cliff >60 m high. Stack of dacitic lavas on lower wall is ~300 m thick, dips ~25°SW (opposite to the agglutinate), and is part of SW Katmai edifice that enclosed the paleocrater. Beneath an unconformity at lower right is a paler, older andesite sequence, altered hydrothermally and containing a large proportion of fragmental material, that is apparently continuous with main sequence of adjacent northwestern wall (as shown in Fig. 11). Narrow glacier at right extends from ice shelf on rim to lakeshore (for wider view, see Fig. 5).

Figure 13. Upper ~150 m of southeast wall at its highest point (~6000 ft). Rim flow is glassy rhyodacite (unit krs; 68.8% SiO_2), 20–30 m thick, effusive but widely brecciated, and dips 30°SE. Beneath it, several gray rhyodacite layers are 2–20 m thick and separated by oxidized flow breccias and scoria falls. Some are flow-foliated, fountain-fed lavas and agglutinate sheets. Rim is mantled by tan Novarupta pumice falls and sprinkled with blocks ejected by hydrothermal explosions during caldera collapse. Beyond East Notch at far left, stack of andesites (kn) dips SE from Crag 6400 and overlies altered strata of mafic cone (kbn; see also Figs. 6, 7, and 8). Geologist on rim in foreground.

In a general way, it thus appears that the 600-m southeast-wall stack records a secular progression from andesite to dacite to rhyodacite in products of SW Katmai. A single flow of hornblende-pyroxene-plagioclase rhyolite (72% SiO_2) that crops out on the South Notch rim, intercalated with the rhyodacites, is the most evolved unit found at Mount Katmai (unit **krh**; Fig. 14). It yielded a $^{40}Ar/^{39}Ar$ plateau age of 22.5 ± 1.6 ka. As a mid-wall dacite is dated at 81 ± 7 ka, the upper half of the sequence exposed on the south side of Mount Katmai erupted within a span of ~60 kyr. The unsampled andesitic sequence low on the inner southeast wall is older, but no potentially correlative flows exposed on the outer southeast flank have been dated.

A welded scoria fall deposit (unit **kzs**), zoned upward from dacite to andesite, is sandwiched between the rhyolite lava flow at the South Notch and an overlying rhyodacite lava (Fig. 14). This unit and the rhyolite (unit **krh**) are discussed further in the section titled Youngest Eruptive Units.

Just west of the South Notch, a 50-m-high black crag (Fig. 15) is a continuation of the rim-capping rhyodacite sequence, which here also extends an additional 60 m below the rim. The 110-m-thick, stratified pile of shattered vitrophyre includes both autobreccias and pyroclastic breccias, and extends upward into the crag, which has within it three zones of massive rhyodacite vitrophyre, each 3–10 m thick. Lavas and breccias alike are plagioclase-rich pyroxene rhyodacites (67%–69% SiO_2) that carry abundant mafic enclaves (1–15 cm). Just northwest

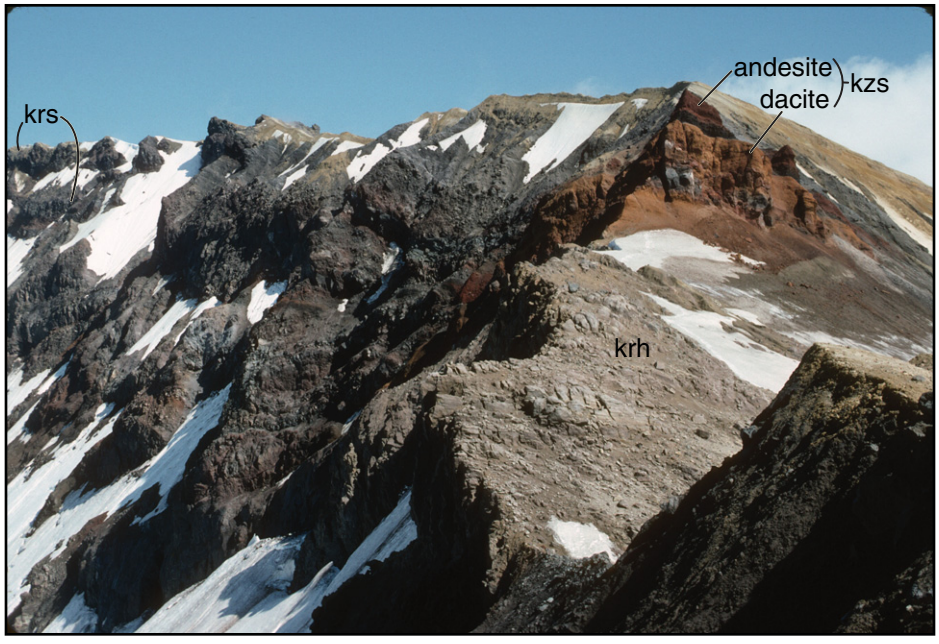

Figure 14. South Notch and southeast rim of Katmai caldera, viewed eastward. Saddle in foreground is floored by pale-gray rhyolite lava flow (unit krh), compositionally most evolved unit at Mount Katmai (72% SiO_2); it gave a $^{40}Ar/^{39}Ar$ plateau age of 22.5 ± 1.6 ka. Rhyolite is overlain by 35-m-thick zoned fall sequence (unit kzs)—orange agglutinated dacite pumice fall, which changes upward into andesite scoria fall, first black, then brick red. Tan deposit on skyline is Novarupta pumice fall of 1912, here ~10 m thick. Upper third of black and red wall at left is rhyodacite lava and breccia (unit krs), uppermost part of which banks against and overlies zoned scoria-fall deposit; beneath rhyodacites, middle third of wall is stack of dacite lava flows, one of which gave a $^{40}Ar/^{39}Ar$ plateau age of 81 ± 7 ka. Rhyodacite section ~1 km farther northeast is seen in Figure 13. All units dip south (to right, outward from rim).

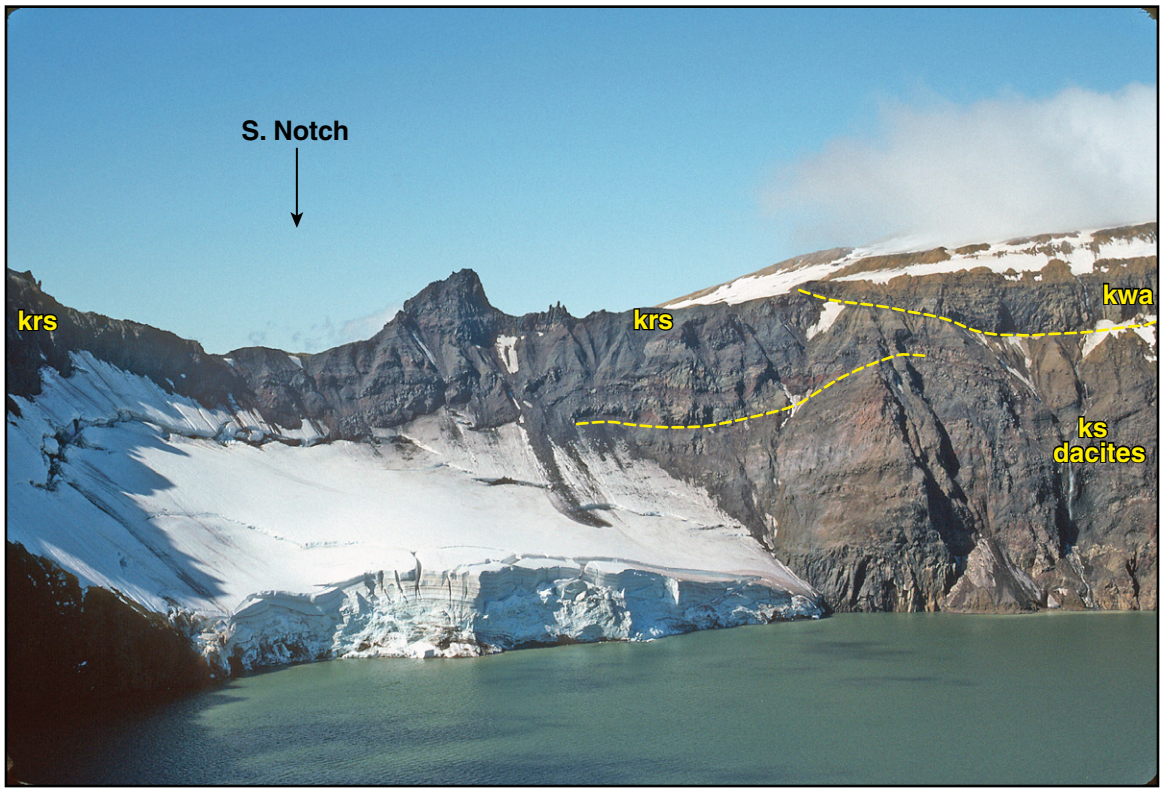

Figure 15. South Notch and southern intracaldera glacier. 50-m-high black crag on rim is part of glassy rhyodacite lava sequence (krs) that appears to be horizontal and extends 2.5 km farther to left, along southeast rim of caldera (Figs. 13 and 14). Above right end of glacier, rhyodacite stack banks unconformably against dacite sequence of southwest wall (ks), which here displays gentle apparent dip to left. Both sequences actually dip outward, away from the viewer. Wall at right is ~360 m high; its top ~60 m is sheet of dacite agglutinate (kwa; Fig. 12), which overlaps both wall sequences. All units exposed are elements of SW Katmai.

of the crag, the fragmental rhyodacite sequence overlaps the southwest-dipping stack of dacite lava flows of the southwest wall, and both are overlain there by the dacite agglutinate sheet (unit **kwa**; Fig. 15).

Outer Slopes of Mount Katmai

Although Mount Katmai is centered on the regional drainage divide, the edifice is strikingly asymmetrical. Around its northern half, lava flows extend no farther than 2.5 km from the caldera rim, but the southern apron extends as far as 7.5 km while descending 1500 m to Katmai River and Mageik Creek (Fig. 3). The abbreviated northern flanks reflect confinement by high rugged ridges of Jurassic basement rocks as well as erosion by icefields and valley-filling glaciers that remain vigorous today and were certainly more so throughout most of Mount Katmai's ~90-kyr-long Pleistocene history. The extracaldera flanks and aprons of Mount Katmai will now be described, starting again with the mafic summit cone and proceeding counterclockwise.

East Slope

To the east, the mafic apron lavas (52%–55% SiO_2) of the peak 6715 (Figs. 3 and 7; unit **kbn**) thicken with radial lessening of slope and dip only ~15° where they disappear under the East Katmai Icefield, only 1 km from the caldera rim. To the ESE, the apron extends 4 km to Noisy Glacier, where it runs out onto Jurassic basement or abuts glacial ice. Glassy outcrops with pervasive 15–25 cm chunk joints are widespread, and distal exposures locally preserve horizontal columns and rosettes indicative of emplacement against ice.

North Slope

The north flank is quite abrupt (Fig. 3), consisting of just a few short cleavers that were carved by glaciers that had headed on the pre-1912 edifice. The cleavers consist of stacks of andesite and dacite lava flows (59%–66% SiO_2), each 10–60 m thick, along with subordinate autobreccias. All appear to have erupted from NE Katmai after termination of mafic cone growth. Due north, the stacks disappear beneath the North Katmai Icefield, but to the northeast they overlie flank lavas of the mafic cone and lap distally onto Jurassic basement and a small granitoid intrusion (Fig. 3). The mafic cone yielded a $^{40}Ar/^{39}Ar$ plateau age of 89 ± 25 ka, and the basal andesite flow overlying it on the northeast cleaver gave a K-Ar age of 70 ± 13 ka.

West Slope

The west side of Mount Katmai also has limited exposure, owing again to both ice cover and confinement by ridges of basement rocks and by the adjacent East Trident edifice (142 ± 15 ka), but also owing to especially thick 1912 fallout from Novarupta. Exposures are limited to the northwest slopes of peaks 6128 and 6200 and to three windows through the ice at the heads of Knife Creek Glaciers #3 and #4 (Fig. 3).

The three windows expose one, two, and four andesite lava flows, respectively, and they range in elevation from 4100 to 5100 ft, exactly the range of the inside wall of the caldera nearby. All are plagioclase-rich pyroxene andesite with 61%–62% SiO_2, and all carry abundant mafic enclaves, 1–15 cm across, one of which was analyzed and contains 54.5% SiO_2.

Peak 6128, northern summit of the twin peaks at the west side of Mount Katmai, rises 280 m higher than the nearby caldera rim and ~600 m above the lake surface (Fig. 5). Peak 6200 stands 600 m south of peak 6128. Neither peak exposes any near-vent facies, both are capped by thick andesitic lava flows that dip ~30° outboard (from N around to W), and both are heavily mantled with 1912 fallout. They are topographic eminences left by severe erosion of a much larger volcano, not themselves constructional edifices. Peak 6200 is exposed only near its summit and down the north face of its steep WNW ridge. A set of four flows of plagioclase-rich pyroxene andesite (~60% SiO_2), each 10–20 m thick, caps the summit and dips 30–35°W. The uppermost flow is block jointed, flow foliated, and carries sparse mafic enclaves. The otherwise gray flows tend to be pinkish or purplish gray where vesicular or fractured and thus permeable to oxidizing steam. Beneath this summit stack, the lower two-thirds of the 300-m-high face is predominantly glassy black breccia with several thin lava flows intercalated.

The steep north face of peak 6128 (Fig. 5) exposes ~14 lava flows, most of which have massive zones 8–20 m thick, separated by interflow rubble; one flow at the top and another near the base are 30–40 m thick. The top flow is glassy block-jointed, plagioclase-rich pyroxene andesite (57.1% SiO_2) with sparse mafic enclaves (1–10 cm across). The lowest flow exposed on the north face is pyroxene dacite (66.5% SiO_2) that gave a K-Ar age of 47 ± 13 ka.

The outward-dipping stack of lava flows that makes up most of the caldera's southwest wall is probably continuous with the outward-dipping stacks exposed on peaks 6128 and 6200. The eastward-sloping, ice-covered bench separating the twin peaks from the caldera rim (Fig. 5) crosscuts this sequence and was evidently eroded by glacial action after 47 ± 13 ka but apparently before formation of the paleocrater for which evidence is preserved at the 1912 caldera rim (Fig. 12). We infer the paleocrater to have formed during plinian eruption of unit **krp** at 22.8 ka; see section below titled Youngest Eruptive Units. The summit ridge and NE slope of peak 6128 are draped by dacite agglutinate unit **kwa**, which thickens abruptly into the edge of the paleocrater at the caldera rim (Fig. 12), only 800 m east of that summit.

Southwest Slope

South of peak 6200, a broad, slightly beveled, dipslope (Fig. 16) of eight or more andesite lava flows extends 7 km to Mageik Creek and Katmai River. The upper 3 km of the slope is covered by ice and 1912 pumice, but below the 3500-ft contour, glacial scour of the 7° slope has eroded a stair-step set of beveled flows 15–25 m thick, locally blocky or flow foliated, that expose both vesicular vitrophyre and platy interior facies. At its lower end, the slope terminates in a scarp 500 m high (Fig. 16) that is dominated by three glassy flows, each 100–200 m thick (Fig. 17). The thick flows are columnar or chunk-jointed vitrophyre virtually throughout, having evidently ponded against valley-filling ice at the toe of the volcano, where Jurassic basement is widely exposed at the base of the stack (Fig. 3). All 15 samples taken in this quarter, whether from thick flows or thin, are plagioclase-rich pyroxene andesites (57.5%–59% SiO_2), with or without traces of olivine.

South Slope

From the caldera rim, the south slope descends 1600 m, extending 4–6 km to the lower gorge of Katmai River canyon. The proximal kilometer is capped by the south-rim rhyodacite lavas (unit **krs**), but the dozen or so flows exposed farther downslope are pyroxene andesites (57.5%–59.8% SiO_2; n = 12), much like those to the southwest, with the exception of a 100-m-thick flow of pyroxene dacite (65.7% SiO_2) on the gorge rim at the snout of Metrokin Glacier (Fig. 3). The west wall of Katmai River gorge exposes two columnar to chunk-jointed, pervasively glassy, andesite lava flows, each 120–150 m thick, that clearly banked against a valley glacier. They are underlain and overlain by compositionally similar flows, 20–30 m thick, that expose convolute platy interiors as well as vesicular vitrophyric margins. The basal flow (59.2% SiO_2), which rests on Jurassic basement just outside the canyon mouth, gave a K-Ar age of 39 ± 12 ka.

The 300-m-high head scarp of the Katmai River landslide (Fig. 18) exposes a stack of ~10 andesite flows, each 10–50 m (rarely 80 m) thick; all examined are plagioclase-rich pyroxene andesites (some with minor olivine), and two flows analyzed both contain 59.2% SiO_2. A glaciated buttress 600 m north of the scarp rim (upslope at elevations 3000–3650 ft) also exposes ~10 similar andesite flows. Just east of

Figure 16. Mount Katmai beheaded. View northward from alluvial floodplain 15 km south of caldera rim in 1989. Photo site on Mageik Creek alluvial fan, where mouth of Mageik Creek canyon lies at extreme left. Peak 6200 on left skyline (also seen in Fig. 5). Rhyodacite crag (unit krs) in South Notch, at center, is same as viewed from north in Fig. 15. Low point visible on rim is at 5000 ft (1525 m) elevation; camera at ~250 ft (75 m) asl. Upper slopes are mantled by snow, ice, and 1912 Novarupta pumice-fall deposits. Middle slope is stair-step set of benches eroded on stack of andesite lava flows, each 15–25 m thick. Lower black scarp, ~550 m high, consists of a few andesite lava flows, 50–150 m thick, that rest on Jurassic basement and were emplaced against valley-filling glacial ice in late Pleistocene.

Figure 17. Thick andesitic ice-contact lava flows at south base of Mount Katmai, viewed northward from surface of Katmai River debris-flow deposit in 1989. Geologist stands on deposit surface, which locally retains overlying patches of 1912 Layer H and veneer of alluvial gravels. Falls-forming lava flow is chunk-jointed vitrophyre ~200 m thick and basally columnar, consisting of pyroxene andesite with 59.0% SiO_2. Middle flow, also ~200 m thick, is largely glassy pyroxene andesite but has thin platy interior and contains 58.7% SiO_2. Skyline flow is also pyroxene andesite with 57.6% SiO_2, ~100 m thick, and likewise retains thick glassy zones despite glacial erosion of its plateau surface. Canyon leading to waterfall drains southeast tongue of Wishbone Glacier (Fig. 3). As recorded by Griggs (1922, p. 123), who camped here in 1919 with his wife (Laura Amelia Tressel), they called the waterfall "David's Falls" for their son (David Tressel Griggs, 1911–1974), who became an experimental geophysicist after joining his father's final trip to the Valley of Ten Thousand Smokes in 1930.

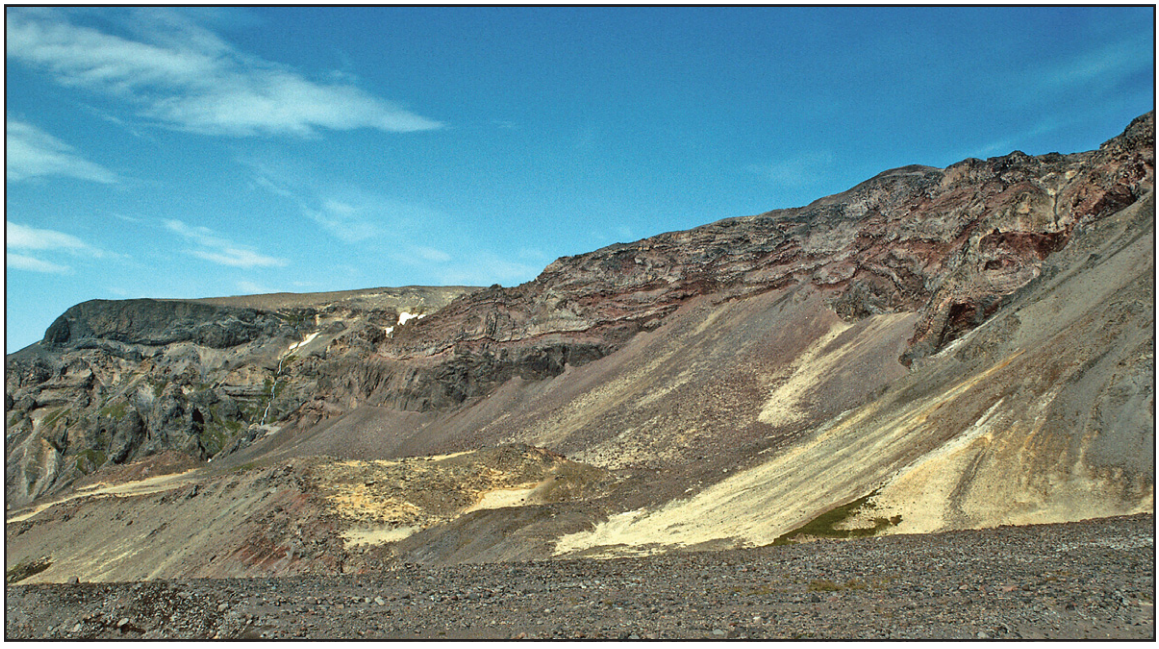

Figure 18. Stack of ~10 andesitic lava flows representative of south and southeast flanks of Mount Katmai, exposed in headwall scarp of Katmai River landslide, which was triggered by earthquakes during caldera collapse on night of 6/7 June 1912. Gray interior zones of flows are 10–50 m thick, separated by brick-red scoriaceous interflow breccia zones that add up to a third of the section. Flows were emplaced down ~20° slope, probably over snow, enhancing autobrecciation and allowing some to drape over eroded or collapsed ledges of their predecessors. Lowest flow near center of image and rim flow at upper left are both ~80 m thick. Top flow at right and lowest flow at right each contain 58.2% SiO_2; thick skyline flow at left has 56.5%.

the slide mass, the head-scarp stack overlies a glassy ice-contact andesite flow at least 150 m thick that extends beneath the canyon floor.

No remnants of lava flows from Mount Katmai are preserved on the opposite side of Katmai River. This might simply reflect glacial and fluvial erosion, but the many 50- to 150-m-thick glassy columnar andesite flows around the southern foot of Mount Katmai suggest that thick glacial ice could have generally prevented them from crossing the valley.

Southeast Slope

The southeast flank of Mount Katmai, extending from the landslide to Noisy River, is incised by four rugged gulches that drain small glaciers higher on the edifice. Jurassic basement floors three of the gulches and is exposed to an elevation as high as 3250 ft, halfway up to the caldera rim. Oldest Katmai lavas in this sector are a set of several glaciated flows of phenocryst-poor andesite (Fig. 3; unit **kxp**; 57.1%–58.1% SiO_2) that crop out for ~2 km along the middle two gulches, from as high as 3900 ft to as low as 1100 ft along Noisy River. Individual ledge-forming flows are 20–50 m thick, and the whole set may be as thick as 200 m. Most exposures are glassy and columnar or chunk jointed, disintegrating into screes of small glassy angular blocks. The rocks are nearly aphyric, containing less than 1% phenocrysts of plagioclase and clinopyroxene, few larger than 0.5 mm. Although the crystal-poor flows are seen to rest exclusively on Jurassic basement, they contain common angular xenoliths of plagioclase-rich pyroxene andesite, which were evidently entrained, either at the vent or high on the edifice.

Just west of the phenocryst-poor andesites is a set of ~10 plagioclase-rich andesite lava flows (Fig. 3; unit **ks**) that wall the two southwesterly gulches, from as high as 3900 ft to as low as 900 ft at Katmai River. Individual flows are 25–50 m thick and are eroded into a stair-step stack of ledges separated by rubbly autobreccias. Most are glassy and hackly or chunk jointed, but some thicker ones are spectacularly columnar jointed, notably the 50–70-m-thick flows at the bottom of the pile. Nearly all are plagioclase-rich pyroxene andesites (59.7%–62.1% SiO_2), with or without sparse olivine, but the 50-m-thick basal flow that rests on Jurassic siltstone at the confluence of Noisy and Katmai Rivers has only 56% SiO_2 and substantial olivine.

The northernmost of the four gulches extends all the way to the East Notch on the caldera rim. High on the edifice this gulch is bounded by narrow cleavers that consist of lava flows younger than those just described lower on the southeast flank. North of the gulch, the cleaver extends 2.5 km southeast, overlies only the mafic cone and its apron, and consists of three flows of pyroxene andesite (Fig. 3; unit **kn**; 59%–61% SiO_2) and intercalated breccia sheets that all issued from the NE Katmai edifice. South of the gulch, the other cleaver (unit **ks**) issues from the SW Katmai edifice, also extends 2.5 km southeast, overlies the set of crystal-poor andesites at its steeply eroded terminus, and consists of two flows of glassy plagioclase-rich pyroxene dacite (65%–66% SiO_2), each of which thickens downslope to ~100 m. Near the caldera rim, the dacite cleaver is overlain by flows of rim-capping rhyodacite unit **krs**.

Only 500 m south of the latter cleaver, an unglaciated set of leveed dacite lava flows drapes the southeast slope, overlying both the phenocryst-poor and phenocryst-rich andesite sequences that dominate the lower slopes. These postglacial dacites (unit **kds**) are described below in the section titled Youngest Eruptive Units.

Summary of Cone Sequences

Separate vent areas, ~2 km apart, built discrete NE and SW Katmai cones and produced several eruptive sequences that overlapped spatially and temporally. The oldest component appears to be (1) the mafic cone (89 ± 25 ka) that supports the present-day true summit on the northeast rim (Figs. 6 and 7). Where the mafic strata dip to lake level at the promontory on the northwest wall (Fig. 10), they are overlain by (2) an andesitic sequence that came from SW Katmai and forms most of that 300-m wall (Fig. 11). After a depression at the conjunction of those oppositely dipping sequences collected ~150 m of heterolithologic fill, and after that fill (3) was hydrothermally altered (Fig. 10), a 300-m sequence (4a) of north-dipping andesites and dacites from NE Katmai overran all three earlier packages and was later eroded into the rugged features that cap the north wall (Fig. 9). An andesite lava flow of that sequence resting directly on strata of the mafic cone yielded an age of 70 ± 13 ka. Probable correlatives (4b), predominantly andesitic, fragmental, and altered, overlie the southeast slope of the mafic cone and dip south and southeast beneath the East Notch (Figs. 7 and 8). At the East Notch, a stack of dacite lava flows (5) from SW Katmai that forms the middle section of the southeast wall abuts and unconformably overlaps the sequence (4b) from NE Katmai (Fig. 8). One of those dacite flows gave an age of 81 ± 7 ka. An undated stack of lava flows (0) at the base of the southeast wall and below lake level probably correlates with phenocryst-poor and phenocryst-rich andesite flows that dominate the outer southeast slopes of the mountain. Although older than 81 ± 7 ka, age relations of these stacks of flows with the mafic cone (89 ± 25 ka) have not been established, so they are arbitrarily grouped as sequence (0).

The northwest wall sequence (2) dips beneath lake level just west of the West Notch and is overlain unconformably by a radially outward-dipping stack of andesite-dacite flows (6), 300 m thick on the caldera wall and as thick as 500 m on the twin peaks. A dacite flow low on peak 6128 gave an age of 47 ± 13 ka, and an andesite flow on the distal apron extending from peak 6200 to Katmai River gave an age of 39 ± 12 ka. Overlying both this sequence (6) and the mid-wall dacites of the southeast wall (5) is a set of rhyolite and rhyodacite lava flows and breccias (7) that caps the south and southeast caldera rim; one flow gave an age of 22.5 ± 1.6 ka. The rhyodacites (unit **krs**) and a few contemporaneous and younger units are described below in the section titled Youngest Eruptive Units.

A modest fraction of the caldera-wall strata near the East and West Notches are poorly sorted fragmental deposits containing angular lithic blocks, some very coarse, in an ash-rich matrix. Similar sequences also appear high on the north wall, on the northwest promontory, and at the base of the southwest wall. Most such material was apparently expelled by phreatomagmatic (and phreatic?) eruptions and emplaced as surges along with (vulcanian?) ballistic showers. It can be speculated that paleocraters contained wet rubble, reworked pyroclastic fill, and (probably much of the time) snow, ice, or lakes. Such water-rich fill would first have to be expelled before open-vent eruptions could produce the many andesite-dacite lava flows, the mafic cone, the agglutinates, or the south-rim rhyodacites. As attending clouds of fine ash would typically have been widely dispersed over the surrounding glaciated terrain, the only ash-dominant strata (poor in coarse clasts) exposed on the caldera walls are atop the acid-altered white section on the northwest promontory (Fig. 10).

Near Katmai River, Mageik Creek, and Noisy River, many lava flows relatively low in the Mount Katmai pile are 50–150 m thick, pervasively glassy, and widely columnar; several display sets of slender curving columns, some of which are subhorizontal. Such features, which occur in both andesites and dacites of SW Katmai and even in a few mafic lavas of NE Katmai, indicate ponding of many Katmai lavas against ice near paleocanyon floors. More proximal interaction of flowing lava with ice may account for the high fraction of glassy breccia in the south-rim rhyodacite pile and on the outer slopes of the twin peaks. Widespread

"chunk jointing," where extensive glassy surfaces form mosaics of angular quasi-cubic joint polygons, typically 5–20 cm across and neither blocky nor columnar, is also taken as evidence of ice contact.

YOUNGEST ERUPTIVE UNITS

South Rim Rhyodacites and Rhyolite (Units krs and krh)

Exposed along the south and southeast rim of Katmai caldera are beheaded remnants (Fig. 13) of at least four plagioclase-rich, pyroxene-rhyodacite lava flows (67%–72% SiO_2) and associated breccias (unit **krs**), all part of the SW Katmai edifice. The westernmost of these flows make up the 50-m-high crag in the South Notch (Fig. 15). For 2 km east of that notch, rhyodacite lavas cap most of the southeast rim, extending as far as the East Notch. All but the most silicic rhyodacites contain plentiful enclaves (1–20 cm) of chilled andesite (54.5%–59% SiO_2). On the caldera wall, the rhyodacites are as thick as 150 m and overlie a thick sequence of dacitic lava flows; outside the caldera (where largely covered by ice and 1912 fallout), the rhyodacites extend only ~1 km downslope. The most evolved flow among them (72% SiO_2), the only one lacking conspicuous mafic enclaves, gave a late Pleistocene $^{40}Ar/^{39}Ar$ plateau age of 22.5 ± 1.6 ka. This rhyolitic flow (unit **krh**) floors the South Notch and is intercalated within the stack of enclave-rich rhyodacite lavas and breccias (Fig. 14). The flow is ~50 m thick, flow foliated, pale gray or locally pinkish gray, glacially striated, and cut by the caldera rim; it contains rare andesitic blebs as big as 1 cm.

Late Pleistocene Plinian Fall and Ignimbrite (Unit krp)

A plinian pumice-fall deposit, 5–7 m thick, and overlying nonwelded ignimbrite are locally preserved beneath glacial deposits along Mageik and Windy Creeks, respectively 7–9 km southwest and 21 km northwest of the caldera rim. A west-bank scarp at Windy Creek locally exposes 5 m of fallout beneath 8 m of ignimbrite (Fig. 19). At six exposures along a 3-km-long reach of Mageik Creek, the plinian fall deposit is as thick as 7 m (Fig. 20), and the overlying ignimbrite is as thick as 75 m (though typically eroded much thinner). Most pumice is white, but sparse medium-gray pumice is compositionally indistinguishable. The pumice contains 8–12 wt% crystals, including plagioclase > orthopyroxene > hornblende > Fe-Ti

Figure 19. Rhyolitic plinian pumice-fall and ignimbrite deposit (unit krp) on west bank of Windy Creek, 21 km northwest of caldera rim. Upper geologist is at contact between 5-m plinian (fall) exposure and 8-m-thick nonwelded ignimbrite (ig), which is overlain by fluvial, then glacial, deposits. Base of plinian lies below stream level and, because frozen, was not excavated. Fluvial gravel layer 30 cm thick is intercalated within plinian deposit at shoulder level of lower geologist. Dark clods are not clasts in ignimbrite but turf sloughed from rim above till.

oxides. It is chemically similar to the most evolved south-rim rhyolite lava (unit **krh**) just mentioned. Together, the lava and pumice are unique among products of the Katmai volcanic cluster in having 71%–72.3% SiO_2 and nearly unique in containing hornblende microphenocrysts. At Mageik Creek, pumice-fall clasts are predominantly lapilli, and 15–30 cm clasts are not uncommon; at Windy Creek, most plinian pumice is smaller than 3 cm, and the largest are 5–6 cm across. Lithic fragments in the plinian deposit at Mageik Creek are largely crystal-rich rhyodacite and dacite (66%–68% SiO_2), as big as 8 cm, along with minor fractions of basaltic scoria (50.7% SiO_2), crystal-poor and crystal-rich andesite, hydrothermally altered lavas, and Jurassic siltstone/sandstone. Similar lithics are commonly as big as 8–11 cm in the ignimbrite, which carries abundant pumice 10–25 cm and some 25–45 cm across. At Windy Creek, ignimbrite pumice is generally smaller and the largest lithics are 2–4 cm, mostly the crystal-rich varieties.

The rhyolite pyroclastic sequence is evidently of late Pleistocene age, overlain only by glacial till and stream deposits at both sites. The base is frozen and not exposed at Windy Creek, while at Mageik Creek the fall deposit rests on stream gravels, till, or locally on poorly indurated laminated mudstone—possibly an ice-marginal pond deposit. At both locations, the pyroclastic section is cut by clastic dikes, 3–20 cm thick, perhaps induced by seismicity or by the stress of overriding ice. Organic material at the base of the plinian pumice fall in Mageik Creek yields an age of 19,240 ± 70 ^{14}C years B.P., equivalent to a calendar age of 22.8 ka, which is similar to the $^{40}Ar/^{39}Ar$ plateau age of the rhyolite lava flow on the south rim of the caldera (22.5 ± 1.6 ka). As the plinian fall remnants are 5–7 m thick, the eruption may well have been as great or greater in volume than that of 1912. Rhyolitic ash-fall layers possibly correlative with this major late Pleistocene eruption have been reported as far away as Kodiak Island and the Seward Peninsula. Survival of only sparse remnants of thick ash-flow deposits as far as 21 km from Mount Katmai suggests that emplacement took place largely over glacial ice. We infer that this large eruption was responsible for formation of the paleocrater marginally preserved atop the SW Katmai edifice and later partly filled by unconsolidated breccia and the dacite agglutinate unit **kwa** (Fig. 12). No other pre-1912 eruptive unit seems voluminous enough to be associated with a crater 1–2 km wide.

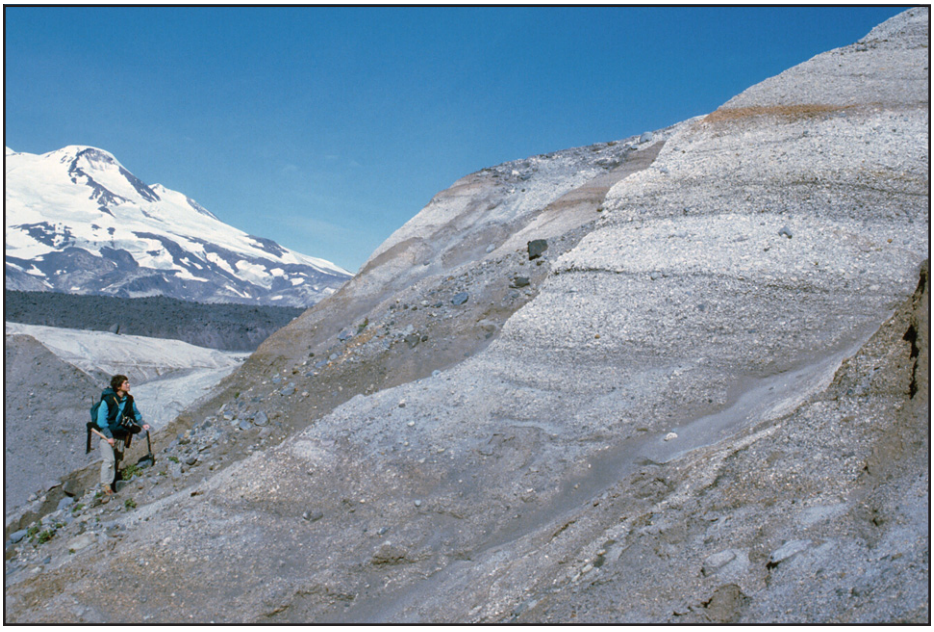

Figure 20. Rhyolitic plinian pumice-fall deposit (unit krp) on north bank of Mageik Creek, 9 km southwest of caldera rim. Here 7 m thick, fall sequence is capped (above image) by thin ignimbrite and then glacial deposits, but ignimbrite better preserved nearby is as thick as 75 m. Bedding in fall deposit indicates fluctuations in discharge rate and column height, as does fluvial intercalation illustrated in Figure 19. Organic layer at base of plinian deposit gave ^{14}C age calibrated to 22.8 ka. Ice-clad Mount Mageik stratovolcano and black 1953 dacite lava flow from Trident Volcano at left background.

Zoned Scoria Fall (Unit kzs)

Although the rhyodacites (unit **krs**) are generally the rim-forming unit on the south and southeast wall of the caldera, they do not represent a simple compositional climax for Mount Katmai nor a direct precursor to the 1912 rhyolite, because the most evolved of the lavas is directly overlain by a 35-m-thick remnant of stratified dacite-andesite scoria fall (unit **kzs**), which is in turn overlain by more rhyodacite breccia. On the caldera rim just east of the South Notch (Fig. 14), the plagioclase-rich pyroxene-dacite (65.1%–65.4% SiO_2) scoria fall, 20–25 m thick, rests directly on the rhyolite lava flow (unit **krh**). Most of the dacite section is tack welded and oxidized orange, but, within the middle ~7 m, bombs are flattened into dense black fiamme. The fall deposit grades abruptly upward from dacite to plagioclase-rich, pyroxene-andesite scoria (57.8% SiO_2), similarly crudely stratified, mostly tack welded, and ~12 m thick. The lower third of the andesite section is black, the rest oxidized brick red. Andesite scoria bombs are as big as 50 cm and dacite bombs as big as 40 cm, but the sequence is dominantly scoria lapilli. Lithics are sparse (1%–2%) but include angular fragments of the underlying rhyolite and rhyodacite lavas, as big as 25 cm. The section dips outboard at 15–20°SE. More than half (probably a lot more) of the original strombolian scoria deposit collapsed into the caldera in 1912.

Dacite Agglutinate of West Rim (Unit kwa)

SW Katmai produced a stratified sheet of scoriaceous to agglutinated, plagioclase-rich pyroxene-dacite fall (64.5%–65.8% SiO_2), which widely caps the west rim of the caldera, drapes peak 6128, and thickens into a pre-1912 crater (largely obliterated in 1912), where it reaches a maximum preserved thickness of more than 70 m on the caldera's inner southwest wall (Fig. 12). Glacier covered until 1912, this variably welded, stratified fall unit is now well exposed, still mantles steep topography, and represents one of the youngest pre-1912 eruptive units identified at Mount Katmai. On the very summit of peak 6128, the sheet is 2.5 m thick, grades from tack welded to densely welded with flattened scoria bombs, and consists of >95% scoriae (mostly 1–10 cm across but as big as 40 cm). Lithic fragments (1–15 cm), which make up 1%–5% of the deposit, are chiefly devitrified andesite. The sheet dips 15–20°W down the west ridge of peak 6128 and is preserved for ~500 m west of the summit. The sheet also dips northeastward off the peak as steeply as 35° before leveling off near the West Notch (Fig. 21) and then extending 2 km farther along the northwest rim of the

Figure 21. Shelf of densely agglutinated stratified dacite fallout (unit kwa), thinning from ~20 m to ~10 m against foot of peak 6128, viewed southwestward from West Notch on caldera rim. Agglutinate sheet continues beneath talus up slope at left and over and beyond summit of peak. Overhang beneath ledge exposes 1–2 m-thick nonwelded base of dacite scoria fall. In foreground, dense agglutinate drapes rim of apparent paleocrater and overlies nonindurated, poorly stratified, poorly sorted fill, at least 50 m thick. At upper right, lowest of andesite-dacite lava flows dipping 30°N on north slope of peak 6128, an eroded outboard element of SW Katmai, gave a K-Ar age of 47 ± 13 ka. For scale, note geologists and packs at lower right.

caldera (Fig. 11). Along that rim, the sheet has a nonwelded basal black scoria layer 1–2 m thick that grades up into a reddish-brown weakly welded zone ~3 m thick that contains more abundant lithics and a few lithic-rich nonwelded partings; this is capped by dense agglutinate, 10–15 m thick, with black fiamme. Between the West Notch and peak 6128, the fallout sheet is 10–20 m thick, displays abrupt transitions in welding intensity among its many layers, and includes two thin ash-rich flow units. Just south of the West Notch, adjacent to the narrow icefall, the agglutinate and some thin lava flows drape into the caldera-wall embayment (Fig 11), which exposes thick massive diamict that may be a marginal remnant of the fill of the pre-1912 paleocrater.

The same agglutinate extends for 1.1 km along the southwest rim of the caldera, where it crops out as a pair of conformably stratified cliffs separated only by a narrow bench or cleft eroded from a nonwelded to tack-welded, scoria-fall layer 2–3 m thick. The strongly agglutinated lower sequence is >60 m thick and the similarly dense upper sequence ~8 m thick (Fig. 12). Layers in both cliffs are 10–50 cm thick, dip 5°–15° lakeward, and are banked into the upper part of a paleocrater wall steeper than 50°, which is here cut into southwest-dipping dacite lavas. The whole agglutinate section represents a continuous eruption and consists of dacite scoria lapilli and bombs, many of which are flattened at least 3:1. Various layers also contain 5%–10% lithic fragments of andesite or dacite as big as 25 cm, many of them devitrified or altered. Most scoria clasts and fiamme are glassy and black, but many less intensely welded layers and lithic-richer layers are oxidized reddish brown. The southwest rim agglutinate was overlain by an ice cliff when first seen in 1916–1919, but the collapse-truncated glacier has since receded ~100 m from the rim (Figs. 5 and 12), leaving atop the agglutinate a chaotic sheet of ablation diamict mixed with 1912 Novarupta pumice and hydrothermal explosion debris ejected from the collapsing caldera.

The agglutinate sheet was widely shaved glacially but is extensively preserved, even on the steep terrain of peak 6128 and in the West Notch where it was overrun by pre-1912 ice that flowed westward from Mount Katmai into the Knife Creek valley. Survival at the surface in such settings suggests that the undated agglutinate may be no older than ~10 ka.

Leveed Dacite Lava Flows (Unit kds)

SW Katmai also produced a branching pair of postglacial lava tongues of blocky dacite (unit **kds**) that flowed ~3.5 km down the southeast slope (Fig. 3), almost to the floor of Katmai River canyon. Several blocky to rubbly superimposed flow lobes form a stair-step sequence confined laterally by 10-m-high scoriaceous levees capped by spires and crags. They issued at a site marked by a glassy rubbly vent dome at 4700–5200 ft elevation, now partly lapped by ice, only 500 m outside the caldera and 250 m lower than its rim. The longer of the two tongues descends steeply to a crumbling flow front at an elevation of ~1500 ft near Noisy River. On middle and lower slopes, they overlie both the crystal-poor and crystal-rich andesite lava-flow sequences described above in the section titled Southeast Slope. All seven samples taken are olivine-free, plagioclase-rich, pyroxene dacite (63.8%–64.3% SiO_2). These leveed flows are unique on Mount Katmai in retaining near-primary surfaces—glassy, blocky, and scoriaceous—along with thin rubbly basal zones. Absence of columns or ice-contact features at lower end of each tongue suggests that Katmai River glacier had thinned greatly or completely retreated from Katmai Canyon by the time the lava flows were emplaced. Apparently the youngest pre-1912 eruptive unit on Mount Katmai, this dacite also stands out in being atypically rich in Zr, compared to other intermediate products of the volcano (see Fig. 29).

Horseshoe Island Dacite Dome

The Horseshoe Island dome on the floor of Katmai caldera was emplaced later than the collapse of 7–9 June 1912 but before the caldera interior was first seen in 1916 (p. 72 of Griggs, 1922). Sampled, photographed, and chemically analyzed by Fenner (1930, 1950), the lava dome had a volume <0.002 km^3 and consisted of platy to blocky plagioclase-rich pyroxene dacite (66% SiO_2). It was ~350 m in diameter, had ~20 m of visible relief, and enclosed a steep-walled central lagoon, ~75 m wide and ~20 m deep (figs. 15 and 16 of Fenner, 1930), that had been explosively reamed through the dome. The only juvenile magmatic product erupted at Mount Katmai in 1912, the Horseshoe Island, was covered by the deepening caldera lake by 1929.

Off-Edifice Pyroclastic Deposits Erupted at Mount Katmai

Four silicic pyroclastic deposits not present on Mount Katmai itself are preserved around its periphery. Three have been correlated with

relatively young units on the edifice. (1) In upper Knife Creek at the foot of Mount Griggs (Hildreth et al., 2002), glacially scoured, sintered remnants of a black dacitic scoria-flow deposit (unit **ksf** of Hildreth and Fierstein, 2003), 4–10 m thick, are present 8 km northwest of the caldera rim. Preservation only 50 m above the valley floor suggests ice-marginal deposition following shrinkage of extensive late Pleistocene glaciers into modest valley-confined tongues. The black scoriae are similar compositionally (64%–65% SiO_2) to those in the agglutinated scoria-fall deposit (unit **kwa**) that drapes the west rim of the caldera. These latest Pleistocene or early Holocene units were correlated by microprobe analysis of glass and Fe-Ti oxides (Fierstein, 2007).

(2) Fines-poor debris flows and hyperconcentrated sandflow deposits rich in dacitic pumice and crystals exposed in the lower Valley of Ten Thousand Smokes, ~23 km from the caldera rim, have been described as the "Lethe Assemblage" (Pinney and Beget, 1991; Hildreth et al., 2000). Although as thick as 25–30 m, the deposit displays no evidence for a break in deposition, implying rapid emplacement after a single eruptive event. As no correlative ignimbrite or fallout is recognized nearby, we envisage an eruption where proximal ejecta were remobilized syneruptively by snowmelt on ice-covered slopes near source, transported as slurries down a valley glacier, and ponded in an ice-marginal lowland depression (unit **kla** of Hildreth and Fierstein, 2003). Whole-pumice data (63.7%–65.5% SiO_2) and microprobe analyses of glass and Fe-Ti oxides suggest correlation with either the west-rim agglutinate (unit **kwa**) or the dacite phase of unit **kzs** on the south rim (Fierstein, 2007). The deposit has not been dated directly, but Fierstein (2007) summarized diverse evidence favoring emplacement between ~12,000 and 16,000 ^{14}C years B.P., during end-Pleistocene deglaciation.

(3) The voluminous rhyolitic plinian pumice fall and ignimbrite (unit **krp**) that erupted from Mount Katmai ~22.8 ka was discussed above.

(4) Remnants of an undated rhyolitic ignimbrite (76.6% SiO_2) as thick as 100 m cap a divide 6–8 km north of the caldera rim (unit **QTri** of Hildreth and Fierstein, 2003). The sheet is nonwelded but indurated by silicification and rests on Jurassic basement. Its pumice clasts are crystal poor, but its matrix contains abundant plagioclase and quartz phenocrysts and sparse biotite, hornblende, and Fe-Ti oxides. Abundant lithic clasts are principally andesites and basement siltstone and/or sandstone. Remnants of lava flows similarly situated on ridge tops 8–14 km farther northwest gave ages of 2.3–3.0 Ma (Hildreth and Fierstein, 2003; Hildreth et al., 2004). The ignimbrite is clearly far older than the present edifice of Mount Katmai, but the Katmai cluster is the only place in the region where high-silica rhyolite is known to have erupted.

PRE-1912 GROWTH OF MOUNT KATMAI: SUMMARY

Mount Katmai started up around 90–100 ka, its eruptive products accumulating atop subhorizontal Jurassic marine sedimentary rocks on the drainage divide of the Alaska Peninsula. The nearby Trident, Griggs, and Snowy Mountain volcanoes became active long before Mount Katmai, and activity at Mageik volcano began about the same time as at Katmai (ages in Hildreth et al., 2003b). Nearly all vent facies at Mount Katmai were destroyed by the caldera collapse of 1912, but eight or more distinguishable sequences of eruptive products dip radially away from two separate central-vent areas, which built interfingering cones designated as NE Katmai and SW Katmai. A small peripheral vent produced postglacial extracaldera unit **kds**, and the scoria-cone fragment of unit **kzs** on the south rim may represent another such vent. All the principal sequences of flows and fragmental deposits, however, each 100–800 m thick, appear to have issued from the pair of central vents, which were centered only ~2 km apart.

NE Katmai began with a steep mafic cone, dated at 89 ± 25 ka, that has >800 m of relief on the caldera wall and includes virtually the only Quaternary basalt in the Katmai region. The mafic edifice is overlain by glacially ravaged andesite-dacite sequences on its southeast and northwest sides, the latter dated at 70 ± 13 ka. A mafic dike swarm on the rim just south of peak 6715 suggests that the main vent lay only a short distance inboard.

Eruptive products of SW Katmai form the NW, SW, and SE walls of the caldera. A midwall dacite sequence on the SE wall gave an age of 81 ± 7 ka, and the thick andesite sequence of the NW wall is sandwiched by the two dated sequences from NE Katmai (just mentioned). The lowest third of the SE wall, and likely correlative andesitic lavas on the outer SE flank, are undated and may or may not be as old as the mafic cone of NE Katmai. Thick sequences of extracaldera andesite-dacite lavas from SW Katmai, forming peak 6128 to the west and the southern apron at Katmai River, yielded ages of 47 ± 13 ka and 39 ± 12 ka, respectively. These are overlain on the south rim by a thick rhyodacite-rhyolite sequence (**krs-krh**), dated at 22.5 ± 1.6 ka, that is probably related to a 10-km^3-scale rhyolitic plinian eruption, which may have enlarged a crater (as wide as 2 km) atop SW Katmai. That crater was filled in part by heterolithologic rubble and in part by agglutinated dacite fall (unit **kwa**), inferred to have been plinian or subplinian, that is undated but probably in the range 16–10 ka. The western margin of the filled crater survived the 1912 caldera collapse, and the postcollapse Horseshoe Island dacite dome may reflect roughly where the central vent of SW Katmai had been located.

The volume of NE Katmai may have been ~15 km^3 and of SW Katmai ~25 km^3—both rough estimates much reduced by glaciation and caldera collapse. To SW Katmai can be added 5 ± 2 km^3 for off-edifice dacite pyroclastic deposits and 12 ± 5 km^3 for the 22.8-ka rhyolitic plinian deposits.

Ice-contact chilling, buttressing, and thickening of lava flows have been common throughout the eruptive history of Mount Katmai, as they would be for an effusive eruption today. Alternating with open-vent strombolian and effusive episodes, repeated intervals of phreatomagmatism have been favored by intracrater snow and ice, as they would by the caldera lake today. The modest central-vent activity that progressively built the basalt-to-dacite stratocone pair gave way after ~23 ka to production of more silicic magma and more explosive eruptions, culminating with the caldera-forming eruption of 1912.

CALDERA COLLAPSE DURING NOVARUPTA ERUPTION OF JUNE 1912

Collapse of the summit of Mount Katmai during the 1912 eruption at Novarupta was one of the few caldera-forming events of the scientific age. About 13.5 km^3 of magma was released at Novarupta, all or much of it withdrawn from beneath Mount Katmai, 10 km away. About half of this was distributed as fallout and half was emplaced as ignimbrite in what then became the Valley of Ten Thousand Smokes (Fig. 22). The complex eruptive sequence, timing, mechanisms, and products have been accounted in progressively greater detail by Curtis (1968), Hildreth (1983, 1987), Fierstein and Hildreth (1992), Fierstein et al. (1997), Hildreth and Fierstein (2000, 2012), Houghton et al. (2004), and Fierstein and Wilson (2005). The fallout sequence is divided into eight Layers (A through H) that represent three discrete plinian Episodes (I–III), as simplified in Figure 23. Thick layers were deposited on Mount Katmai, which lay directly downwind of Novarupta.

Owing to syneruptive and summer-long ash clouds, lack of nearby observers, and the obstructed perspectives of remote observers, however, no one witnessed the collapse. During summer investigations of 1912 and 1913, Mount Katmai was obscured in cloud; so the first record

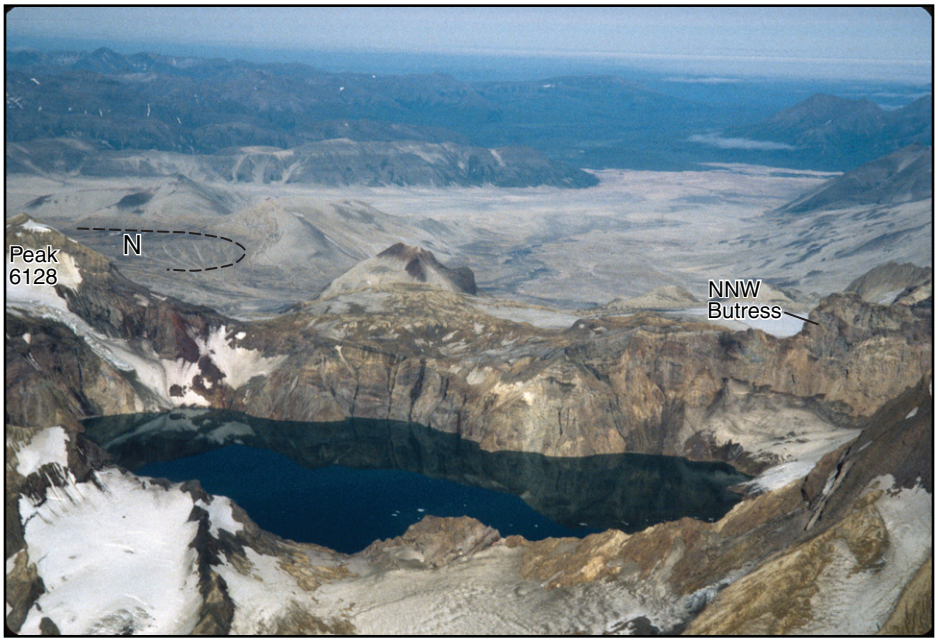

Figure 22. Valley of Ten Thousand Smokes (VTTS) viewed from air above Katmai caldera. Northwest rim beyond lake extends from peak 6128 at left to NNW Buttress at right (270° to 340° sector). Ignimbrite-filled valley terminates in distance, 29 km from center of caldera. Compositionally zoned ignimbrite erupted on 6 June 1912 from Novarupta depression (N), concurrent with plinian eruption that blanketed region with pumiceous fallout. Vent depression, 10 km west of caldera, is outlined by arcuate scarp to right of peak 6128 and is floored by proximal fall deposits, some appearing dark colored in image. Narrow intracaldera glacier draping west wall (at left) and glacier that mantles slump-block bench at base of north wall (at right) both originated in 1920s. Isolated snow slope just right of narrow glacial tongue marks descent route from West Notch taken by Yori, Fenner, and Motyka. East Notch on caldera rim is in foreground.

of its beheaded summit is a photograph taken in July 1915 (p. 100 of Griggs, 1922). Nonetheless, study of circum-caldera hydrothermal explosion deposits intercalated with Novarupta pumice-fall layers (Hildreth, 1991) and analysis of the seismic record for June 1912 (Abe, 1992) together permitted a fairly good reconstruction of the fitful collapse sequence (Hildreth and Fierstein, 2000), as summarized in Figure 23.

Seismicity Accompanying the 1912 Eruption

There were no seismic instruments within 1000 km of Katmai in 1912. Abe (1992), however, studied the records of ~40 seismological stations worldwide and was able to assign magnitudes to 50 earthquakes associated with the eruption. Thirty-three of the 50 shocks had surface-wave magnitudes (M_S) greater than 5.5, and 14 were in the range M_S 6.0 to 7.0. A plot of M_S versus cumulative frequency for the sequence (fig. 8 of Abe, 1992) shows a deficiency of recorded events smaller than M_S 5.5 and suggests that there could actually have been as many as 100 Katmai earthquakes with M_S ≥5.0. If so, about half either failed to register on 1912 instruments or did not meet Abe's selection criteria.

Many earthquakes were said to have been felt locally for at least five days prior to the eruption (Martin, 1913; Fenner, 1925), but none of them were recorded instrumentally. Similarly, following the eruption, although shocks were felt (at a village 60 km southwest of the caldera) on 50 of the next 70 days (Martin, 1913, p. 158), Abe's search detected only two Katmai earthquakes later than 10 June and none after 17 June. Since the detection threshold of the nearest station utilized (at Victoria, B.C.) was about M_S 5.0 (Abe, 1992), the absence of an instrumental record of the precursory and posteruptive felt seismicity suggests that all such earthquakes were of lesser magnitude. Because large events so dominate the total energy released, an additional 50 earthquakes of M_S~5.0 would add only 0.22% to the cumulative energy of the 1912 seismic sequence.

Figure 23 shows the sequence of earthquakes evaluated by Abe in relation to our analysis of the eruptive sequence. The first of the 50 instrumentally recorded earthquakes (M_S 5.4) took place at 0508 (local time) on 6 June, ~8 h before the plinian eruption began. Seven additional shocks (M_S 4.8–5.5) were recorded during the next 7.5 h, prior to the first sighting of the plinian column at ~1300. During the opening 10 h of the eruption, eight more shocks (M_S 4.8–5.6) were recorded, culminating in the 11th hour with the first major seismic event (M_S 6.5) at 2356 on 6 June. This event may have signaled the first strong pulse of caldera collapse, which was probably associated with ejection of the first phreatic mud layer from Mount Katmai (intercalated in the Novarupta fallout between Layers B_2 and B_3; Fig. 23). Moreover, the debris avalanches described by Griggs (1922) at Katmai Canyon, Noisy Mountain, and Martin Creek ("Mageik Landslide") all broke loose about this hour, as each deposit is draped directly by all or part of Layer B but not by the preceding Layer A (Fig. 23). About 8.5 km^3 of magma had by then been discharged at Novarupta (Fierstein and Hildreth, 1992); so, if our correlation is correct, it indicates an average magma discharge rate of ~5×10^8 kg/s (8.5 $km^3 \times 2400$ kg/$m^3 \times 11$ h^{-1}) for the initial 11 h leading up to the onset of major collapse-related seismicity.

Soon after the event at 2356, three more major shocks took place early on 7 June (M_S 6.3 at 0035, M_S 6.1 at 0223, and M_S 6.5 at 0825). The seismic energy released during this 8.5 h interval amounted to 10.2% of the total. After 0825 there was a 6.5 h interval marked by four earthquakes of M_S ≥5.1 but none greater than M_S 5.6. This interval of lesser seismic-energy release ended with a M_S 5.8 event at 1457, beginning a 6 h series of earthquakes of magnitudes 5.8, 5.7, 5.8, 5.9, 5.4, 5.8, 5.7, 6.0, 5.8, and 6.3 (at 2049), culminating with a 7.0 at 2136. This powerful event was followed an hour later by a magnitude 6.8 earthquake (at 2248 on 7 June) and by events of M_S 6.2 at 0029 and 6.6 at 0300 (8 June). The five big earthquakes between 2049 and 0300 on the night of 7–8 June account for 61.3% of the cumulative seismic energy released by the 11-day series, the M_S 7.0 shock alone representing 37.4% of the total seismic energy (see figs. 6 and 7 of Hildreth and Fierstein, 2000). Much of the structural collapse of Mount Katmai probably took place during these hours.

Surprisingly quiet by contrast, a 28-h seismic respite (interrupted by modest shocks of M_S 5.4 at 2057, 5.1 at 2045, and 5.6 at 2241) ensued from 0300 on 8 June until 0714 on

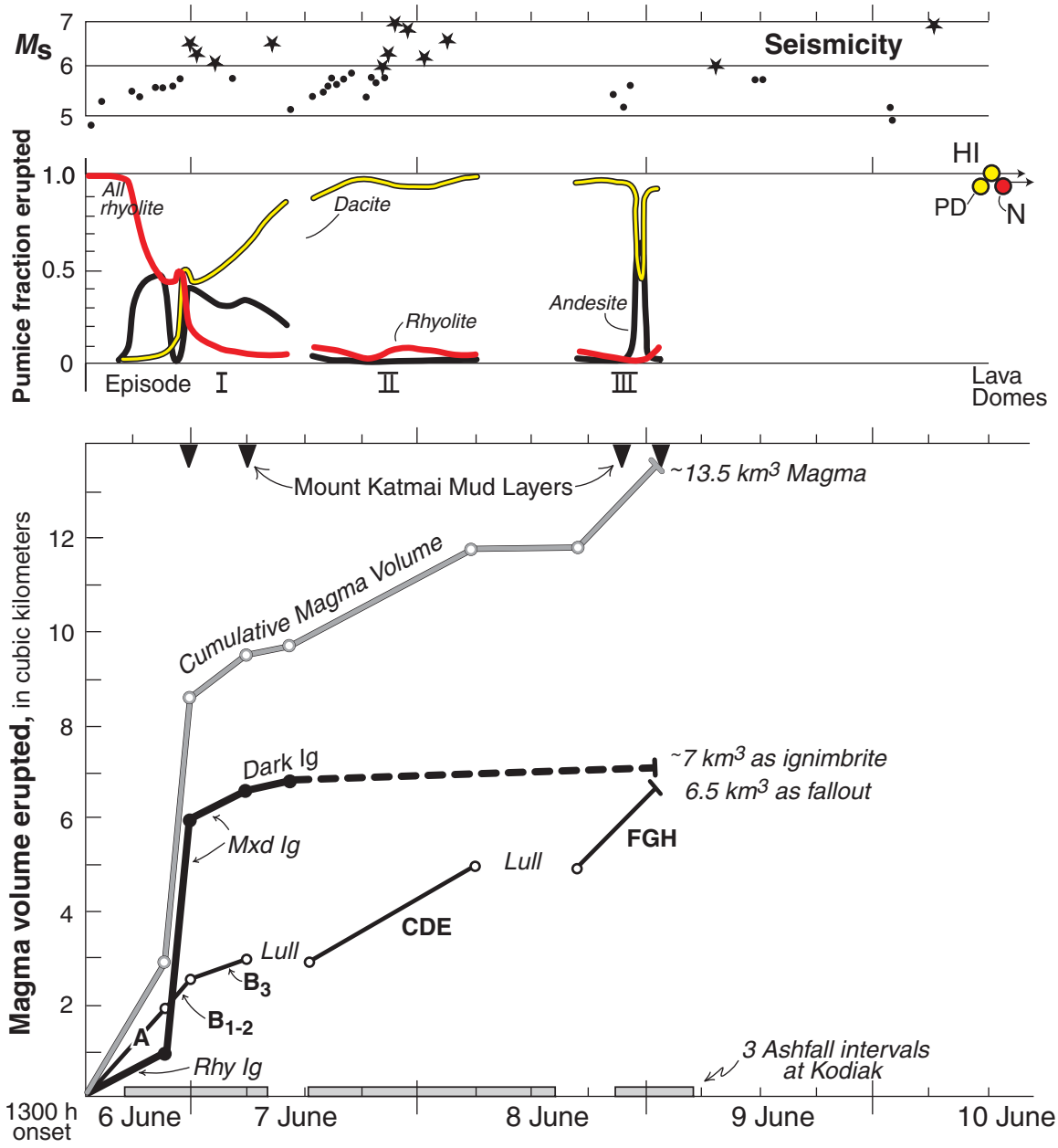

Figure 23. Eruptive sequence of June 1912, showing estimated timing and magma volumes of eruptive units, magnitudes (M_s) of earthquakes accompanying caldera collapse, stratigraphic positions of main mud layers ejected from collapsing caldera, intervals of ashfall at Kodiak village (160 km downwind), and fluctuating proportions of rhyolite, dacite, and andesite pumice that erupted concurrently. *Rhy Ig*—all-rhyolite ignimbrite; *Mxd Ig*—compositionally heterogeneous main ash-flow sequence; *Dark Ig*—late ash-flow packages rich in andesite and dacite pumice. Fall units A and B represent Episode I. Segment CDE is Episode II; segment FGH is Episode III. Mount Katmai mud layers are sheets of lithic ejecta expelled by hydrothermal explosions. Three lava domes were emplaced at unknown times after Episode III: *PD*—"Phantom dome," dacite plug explosively destroyed and distributed around Novarupta vent to produce block bed that overlies Layer H; *HI*—Horseshoe Island dacite dome on caldera floor; *N*—Novarupta dome, ~95% rhyolite but streaked with andesite and dacite. Stars emphasize earthquakes of magnitude 6.0 or greater.

9 June, when the "lull" was broken by another M_S 6.0 event. This was followed by another extended interval of relatively low seismic-energy release, 23 h long and marked by only four recorded earthquakes (M_S 4.8–5.7), that ended with a magnitude 6.9 shock at 0606 on 10 June. This earthquake, second largest of the entire series, took place 24–30 h after the main eruptive activity ceased.

Additional (unlocated) adjustments in the vent, caldera, caldera-fill, or magma-storage and plumbing systems continued for more than two months, as recorded by a magnitude 6.1 earthquake at 2104 on 11 June, a magnitude 6.2 earthquake at 0128 on 17 June, and an abundance of felt seismicity (not recorded instrumentally) that persisted at least through mid-August (Martin, 1913).

Comparison with Other Seismically Recorded Caldera Collapses

Figure 6 and Table 2 of Hildreth and Fierstein (2000) summarize comparative volcanological and seismological data for three caldera-forming eruptions and their host edifices. Although the volume collapsed and the volume of magma erupted at Katmai were each only about twice as large as at Mount Pinatubo (Philippines) in 1991 (Newhall and Punongbayan, 1996), the cumulative seismic energy released at Katmai was 250 times greater (Mori et al., 1996). No fewer than 24 Katmai earthquakes were as large or larger than the greatest shock at Pinatubo (magnitude 5.7). Likewise, during the 1968 caldera subsidence at Isla Fernandina (Galápagos), which was similar to Pinatubo in collapse volume, more than 600 earthquakes were assigned magnitudes (Filson et al., 1973), but none was larger than M_S 5.2, and the total seismic energy released was 800 times smaller than at Katmai. What factors can explain such discrepancies?

In attempting to account for the far greater seismic energy released during the collapse at Mount Katmai, factors to consider include the structure and strength of the precaldera volcanic edifice, the location, depth, and configuration of the magma reservoir, the conduit geometry and flux of magma removal, and perhaps the viscosity and volatile content of the magmas. At Fernandina, as at Mount Katmai, magma was withdrawn from beneath the collapsing edifice rather than erupting through it, but the Fernandina magma was basaltic and the edifice a basaltic shield (Simkin and Howard, 1970). At Pinatubo, however, the climactic eruption issued from vents at the site of caldera collapse, expelled predominantly dacitic magma, and took place at a long-lived andesite-dacite stratovolcano (and dome complex) somewhat larger than Mount Katmai and marked by numerous ignimbrite-forming eruptions in the past ~35 kyr (Newhall et al., 1996).

Because the volumes of collapse differ by at most a factor of three, and as the bulk densities of collapsed material are unlikely to differ substantially, we speculate that the following factors were implicated in producing the seismic-energy discrepancy. (1) In contrast to Pinatubo and Fernandina, both of which had older calderas, Mount Katmai lacked preexisting caldera faults and shear zones, requiring that all breakage be new. Many earthquakes may have taken place on older faults at Pinatubo and Fernandina. (2) Subsidence may have been buffered at Pinatubo by buoyant viscous magma vesiculating and rushing upward to escape at fissure vents surrounding or within the foundering block. To the extent that the cauldron block was broken up and the subsidence piecemeal, such cushioning might have been still more effective in limiting the seismic energy generated. At Katmai (and Fernandina), because the magma was withdrawn from below, no such subsidence-opposing magma flow took place. At neither Katmai nor Fernandina was there a magmatic ring dike serving to lessen friction around the subsiding cauldron block. (3) At Katmai, ~8.5 km^3 of magma had erupted before the first cluster of large earthquakes ($M_S > 6$) 11–13 h into the eruption, and nearly 12 km^3 had been released by the time of the second major cluster 32–38 h after the eruption started (Fig. 23). The strength of the previously unfaulted Katmai edifice may have permitted greater stress accumulation during withdrawal of magmatic support, resulting in individually greater stepwise vertical dislocations of the ultimately collapsing block(s) and, accordingly, fewer but larger earthquakes than at the pre-cut Pinatubo and Fernandina edifices. Moreover, the horizontally layered Mesozoic siltstones and sandstones, at least 5 km thick beneath Mount Katmai (Determan et al., 1996), could have contributed to greater average stress drops for each event by initially bending (with inter-bed slip, phonebook-like) before finally breaking. (4) The high-silica rhyolite magma that dominated the 1912 eruption, probably as viscous as crystal-rich Pinatubo dacite, certainly more so than Fernandina basalt, and proportionately more retentive of the excess volume contributed by vesiculation, may have played a role in slowing magma transfer within the plumbing system and slowing withdrawal of support, thereby contributing to the stress accumulation and overstepping that resulted in larger individual dislocations.

As discussed by Abe (1992), the total moment estimated from the collapse geometry of Katmai caldera can be approximated as $M_O = \mu\Delta V$. Taking ΔV = 5.0–5.5 km^3 as the caldera volume displaced, and taking μ, the shear modulus for shallow events, to be 3×10^{10} N/m^2 (Abe, 1992), then $\Sigma M_O = 1.5–1.65 \times 10^{20}$ Nm, a satisfactory approximation to the cumulative seismic moment, 1.4×10^{20} Nm, estimated from the magnitudes of the 50 Katmai earthquakes evaluated by Abe. There is thus no need to invoke major additional release of seismic energy or large displacements elsewhere in the plumbing system or at Novarupta. The cumulative seismic moment for the Fernandina collapse was roughly equivalent to that of a single earthquake of M 5.9, the Pinatubo seismic sequence to one of M 6.2, and the 1912 sequence at Katmai to one of M 7.4.

Hydrothermal Explosion Breccia and Phreatically Ejected Mud Layers

On and near the caldera rim at Mount Katmai, several layers of massive, poorly sorted, unconsolidated "mud," studded with Katmai-derived lithic fragments, were ejected by phreatic-hydrothermal explosions during caldera collapse and intercalated within the sequence of widespread plinian fallout layers from Novarupta (Hildreth, 1991). No juvenile material has been recognized in the Katmai-derived mud layers, which thin from 10 to 200 cm near the rim to ≤1 cm at radial distances of 5–8 km from the rim. With distance from the caldera, the average size of the largest lithic fragments in the mud layers declines to <1 cm from >50 cm at the caldera rim (Fig. 24). In contrast, lithics (and pumice) in the pumiceous plinian layers (A through G) coarsen toward Novarupta, away from Mount Katmai (Fig. 24). We refer to "mud layers" because under conditions prevailing at Mount Katmai these fines-rich deposits are always wet (or frozen), even gooey, and contain a hydrothermal clay component that imparts a faintly sulfurous odor. They are best exposed on the southern slopes of Trident and Mount Katmai, but a few intact remnants have been identified on and adjacent to the glaciers west of the caldera. Abundant crystals and centimeter-scale lithics occur within the dominant muddy matrix, and sparser large lithics (as big as 17 cm, as far as 5.8 km from the rim) were probably emplaced ballistically (Hildreth, 1991). The several mud layers identified are interpreted as a series of explosive ejection events released by unloading the hydrothermal system inside the cone during stepwise caldera collapse.

The first (and most voluminous) of the Katmai-derived mud layers lies between Novarupta plinian Layers B_2 and B_3, providing the earliest evidence for onset of caldera collapse. The chronology of fallout reported at Kodiak (Martin,

1913) and of seismicity reevaluated by Abe (1992) supports correlation of this stratigraphic horizon with the first major syneruptive earthquake (M_S 6.5), at 2356 h on 6 June, 11 h into the eruption (Fig. 23). By that time, ~8.5 km^3 of magma had vented at Novarupta.

Two mud layers at the B_2–B_3 contact are each a few centimeters thick on lower southern slopes (where the upper one contains accretionary lapilli), but they thicken and merge into a common layer 0.5–2 m thick where it overlies a breccia sheet (described next) on the west rim. This mud layer is 65–85 cm thick on a 4,600-ft shelf ~2.5 km west of the rim. Another thin mud layer is locally present at the contact between Layers B_3 and C, and as many as eight mud layers (each 3–30 cm thick) are intercalated within the dacite pumice-fall sequence (C through G) near the caldera rim. The thickest of these is within Layer F—30–80 cm on the south rim, 14–45 cm near the west rim, and 6 cm on the 4600-ft western shelf. At least three more mud layers, rich in sand and granules, are intercalated around the rim near the top of Layer G and within what appears to be an anomalously thick (~3 m) accumulation of fine-grained Layer H. Capping the 1912 section, this near-rim fines-rich accumulation is apparently composite, consisting in part of Novarupta-derived vitric ash (normal Layer H), in part of contributions from continuing phreatic outbursts, and in part of deposits from dust clouds attending caldera collapse and continuing slumps and rock falls. No fall layer has been identified that might correlate with eruption of the Horseshoe Island dacite dome on the caldera floor.

A wedge of coarse yellow-brown breccia as thick as 12 m is widespread on the caldera's northwest rim (Fig. 25). It directly underlies the B_2/B_3 mud layer, which is here 0.5–2 m thick. Confined to a 20-degree sector, the thick breccia was deposited atop ~1.5 m of plinian fall (Layers A through B_2), which in turn rests on glacial ice that has since wasted in situ owing to beheading of the adjacent accumulation area by caldera collapse (Fig. 26). Intact fallout sections have nonetheless survived disruption atop a few unmelted seracs. The breccia sheet thins westward across hummocky ablating ice and disappears ~800 m from the rim where the glacial ice is mobile. The breccia deposit is unconsolidated, poorly sorted, and unstratified, but it fines upward from >10 m of coarse clast-supported breccia (with <10% sandy-muddy matrix) through ~0.5 m of matrix-supported breccia into 0.5–2 m of blue-gray lithic-poor mud, which is overlain by Novarupta Layers C through H. The coarse zone thins to <1 m within 250 m northwest of the rim, but the associated mud layer extends radially as far as 8 km.

Fragments in the breccia are angular to subrounded, as large as ~1 m, and include ~10% fresh (basaltic, andesitic, and dacitic) Katmai lavas. Most clasts, however, are hydrothermally altered lavas and tuffs, some of which contain disseminated sulfides. Identified by X-ray diffraction in the few clasts sampled were smectite, gypsum, albite, pyrite, hematite, magnetite, cristobalite, and chalcedony. Oxidized fracture films and rinds on both (internally) fresh and gray-to-black sulfide-bearing clasts attest to hot emplacement and subsequent steam alteration. A few hydrothermally altered blocks developed prismatic joints after emplacement of the breccia. Neither nonvolcanic nor juvenile clasts have been observed in it. The few fresh basaltic blocks (51.6%–52.8% SiO_2) found strewn on the northwest rim have no exposed equivalent recognized at SW Katmai; they were evidently excavated from unexposed depths or from the NE edifice, where such mafic material is plentiful.

Expelled blocks are also abundant along the southwest rim, mixed chaotically with pumice and glacial ablation debris, but a coherent breccia layer like that on the northwest rim was not found. Along the high southeast rim, lenses 30–150 cm thick between pumice Layers F and G consist of lithic ejecta as coarse as 50 cm, including blocks variously glassy, lithoidal, or hydrothermally altered and pyrite-bearing. Also on that rim, a few scattered ejected blocks are several meters across.

Several kilometer-scale zones of hydrothermal alteration on the caldera walls extend beneath present lake level, had pre-collapse vertical dimensions greater than 500 m, and are an obvious source for the hydrothermal explosion breccia. Depressurization of an active hydrothermal system within the Katmai edifice where it was disrupted abruptly along caldera faults caused explosive ejection of a small fraction of the collapsing mass. The mud layers and rim breccias add up to <0.001 km^3 of ejected material, which is less than 200 ppm of the subsided volume of Mount Katmai.

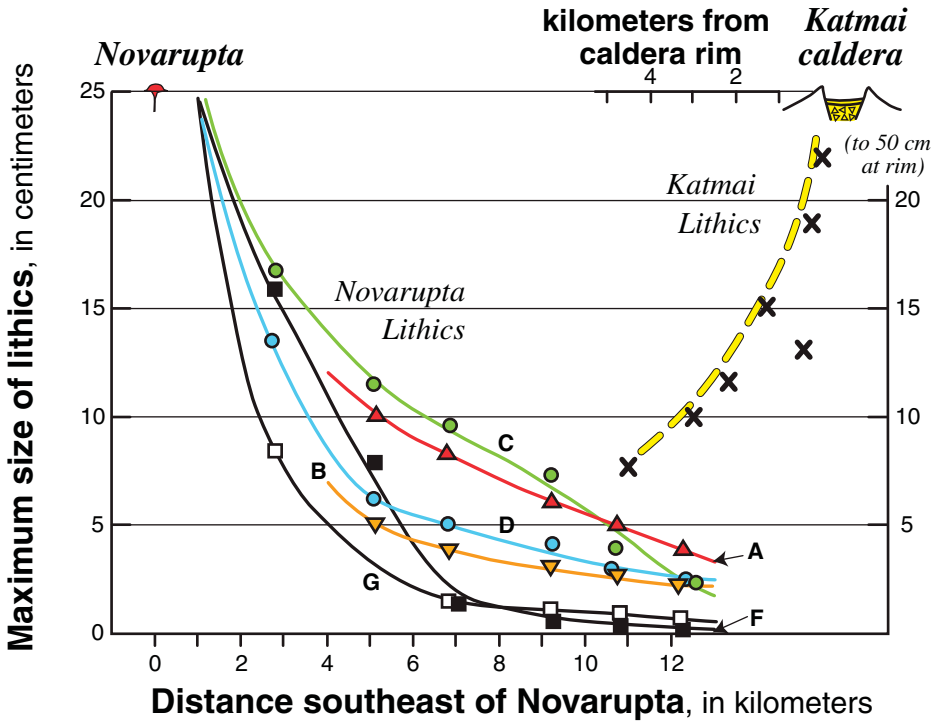

Figure 24. Variation with distance from source of *average* maximum sizes of lithic fragments expelled concurrently from vents at Novarupta and Mount Katmai. The hydrothermal mud layers that contain Katmai-derived lithics were expelled during caldera collapse and intercalated within sequence of Novarupta-derived pumice-fall layers (A–G). "Maximum size of lithics" is average of three axes of five largest lithic clasts at each station. Katmai data are largely from south and southwest slopes of Mount Katmai edifice. Some lithic blocks scattered on the caldera rim are larger than 1 m.

Syneruptive Landslides and Debris Flows

Seismicity attending caldera subsidence triggered collapse of at least three substantial extracaldera landslide masses (Figs. 2 and 3), in

Figure 25. Hydrothermal explosion breccia as thick as 12 m on northwest rim of Katmai caldera. Ice axe is 81 cm long. Derived from altered zones inside Mount Katmai edifice, material was ejected at onset of caldera collapse, thought to coincide with first major seismic event (M 6.5) in 11th hour of eruption. Deposit rests on 1.5 m of Novarupta plinian pumice fall (Fig. 26; Layers A through B_2), which in turn rested on glacial ice, which has since melted.

addition to many minor slumps and rock falls. Numerous pumice-rich debris flows during and soon after the eruptive sequence may likewise have been shaken loose from fallout deposited on steep snowy slopes by the severe earthquakes that continued at least as late as 10 June.

The *Mageik Landslide*, described at length by Griggs (1920, 1922), broke loose from a glacially eroded stack of dacite lava flows on the south side of Mount Mageik (Fig. 2), leaving behind a 120-m-high scarp with a rim at the 3000-ft level. The rugged deposit extends ~6 km down the valley of Martin Creek to an elevation of 650 ft and consists predominantly of angular blocks of fresh dacite, along with sparse chunks of basement sandstone. It has millions of dacite blocks larger than 1 m, slabs as long as 20 m, and hummocks as high as 20 m. It locally left 30-m-high superelevated trimlines and impounded drainages along its steep margins. About 800 m wide proximally, the deposit spread out to ~1.5 km medially and covers ~6 km^2. Griggs (1920) estimated an area of 10 km^2, but this included parts of pre-1912 avalanche deposits mapped separately by Hildreth and Fierstein (2003). Although thickness (5–30 m) is hard to average, the volume is probably in the range 0.05 to 0.1 km^3. The avalanche took place during eruptive Episode I, on the night of 6/7 June, because the deposit is overlain by only the upper part of Layer B and later fall units (Hildreth et al., 2000).

The *Katmai Canyon landslide deposit* likewise broke loose on the night of 6/7 June, after deposition of Layers A and part of Layer B. It is overlain directly by Layers B_3 through H. Near the south toe of Mount Katmai, the headwall scarp extends ~500 m above the canyon floor, exposing a stack of andesite lavas with scoriaceous interlayers (Fig. 18). The chaotic 0.08-km^3 slide mass covered ~1.2 km^2, was as thick as 125 m, and consists entirely of shattered debris from the Katmai edifice. The deposit blocked the narrow gorge of Katmai Canyon, impounding a 5-km-long lake, which breached by 1915 (Griggs, 1922).

The *Noisy Mountain landslide deposit* in upper Katmai Canyon (Fig. 3) is avalanche debris consisting of late Tertiary or early Quaternary andesite from Noisy Mountain, on the south slope of which the headwall scarp extends as high as 900 m above the valley floor. The 6.5-km^2 deposit is studded with numerous barren hummocks 10–20 m high (Griggs, 1922, p. 128) and a few shattered megablocks as wide as 30–80 m. Like the others, large parts of this avalanche broke loose during the first night of the eruption, as the lowest fall unit overlying it is the upper part of Layer B_2, even though Layer A is 30 cm thick directly adjacent to the landslide deposit. Griggs (1922) noted that, when they camped there in 1917, rock falls large and small continued on the scarp every few minutes, inspiring the name Noisy Mountain.

The slopes of Mount Katmai and the upper Valley of Ten Thousand Smokes almost always remain snow covered in early June. Deposition of warm pumice falls and hot ignimbrite on snow and ice thus inevitably led, on 6–9 June 1912, to rapid remobilization of eruption products by melt water, principally as ashy mudflows and pumice-rich slurries.

The *Katmai River debris-flow deposit* at the south toe of Mount Katmai (Fig. 27) was recognized by Griggs (1922) to be a secondary pumiceous diamict emplaced at low temperature atop the stratified dacite fallout that concluded the plinian eruption, but several subsequent observers interpreted it as a hot pyroclastic-flow deposit, which it resembles (fig. 7 of Hildreth, 1983). The deposit is an unstratified sheet of poorly sorted 1912 ash and pumice lapilli. As thick as 18 m, the sheet slopes ~3°S and today covers an area of ~0.75 km^2, but before erosion

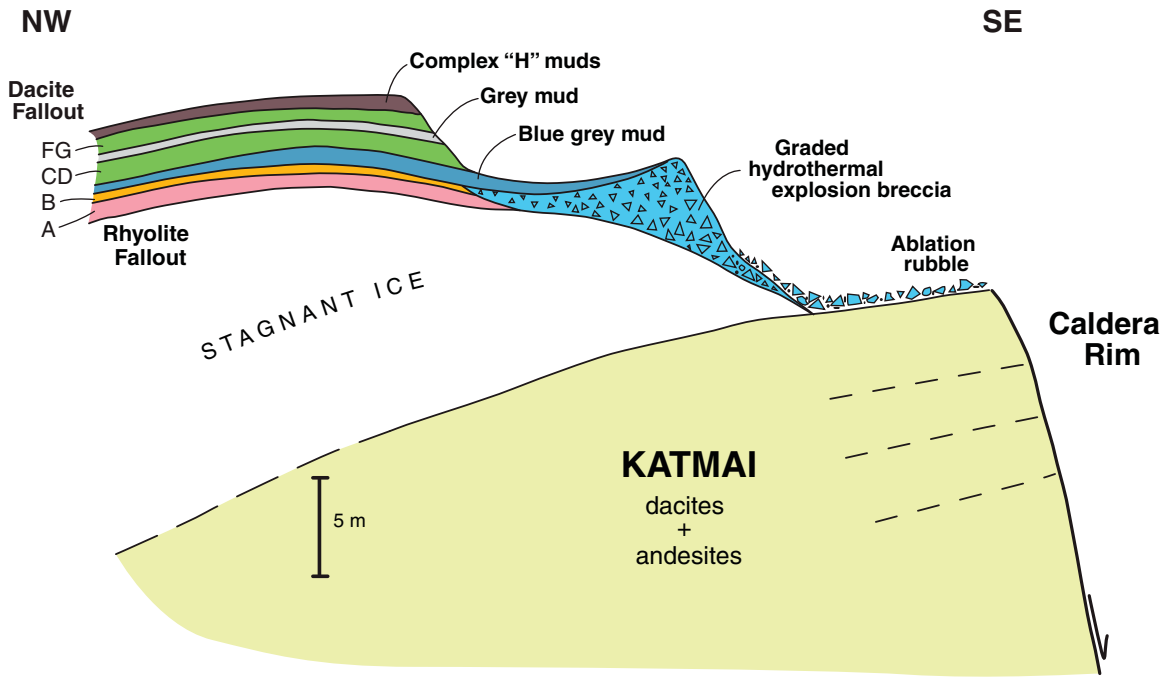

Figure 26. Sketch of stratigraphic relations near northwest rim of Katmai caldera, showing breccia and mud layers expelled during caldera collapse and intercalated within the regional pumice-fall sequence from Novarupta. Deposited upon a glacier that was beheaded by collapse, section has been widely disrupted by a century of ablation of subjacent ice, margin of which has locally receded as much as 500 m from rim.

it was at least twice as extensive. It debouched from a single steep gorge fed from Metrokin Glacier (Fig. 3), which mantles the south and southwest slopes of the Katmai edifice all the way to the caldera rim (Hildreth and Fierstein, 2003). The deposit overlies a nearly complete section of Layers A through G, although G is partly scoured in places. Fine ash-fall Layer H is widely preserved atop the primary uneroded surface of the debris-flow deposit, indicating that the flow was emplaced right after the explosive plinian sequence ended. Field pumice counts yield a 7:3 ratio of dacite to rhyolite lapilli, similar to that of the bulk fallout mantling Mount Katmai and unlike that of any 1912 ignimbrite package (Hildreth, 1983; Fierstein and Wilson, 2005). The deposit contains uncharred branches and twigs as well as rooted

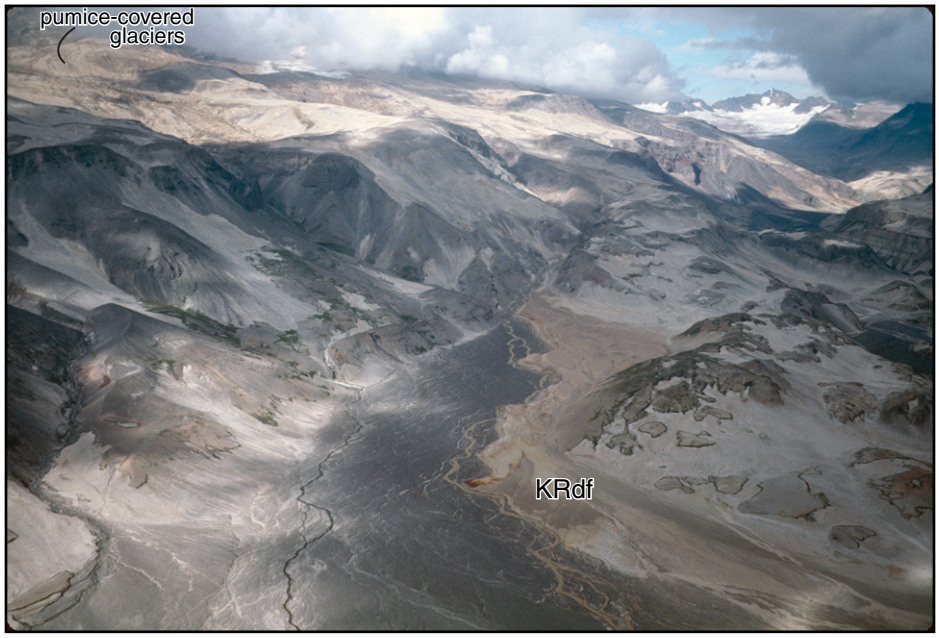

Figure 27. Katmai River pumiceous debris-flow deposit, pink sheet at lower center (KRdf), which emerged from gorge fed by Metrokin Glacier (Fig. 3) on south slope of Mount Katmai (summit in cloud). Remnant, much eroded in a century, is ~2.5 km long and as thick as 18 m. Repeatedly mistaken for a pyroclastic-density-current deposit, which it resembles, it contains uncharred wood and consists of Novarupta fall deposits that were remobilized from snow-clad slope of Mount Katmai and emplaced as a cold debris flow sandwiched between 1912 fall Layers A–G, below, and Layer H, above. For close-up views, see Hildreth (1983) or Hildreth and Fierstein (2012). At left and center, thick Katmai andesitic lavas (as in Fig. 17); in right distance, Katmai River Canyon. Pale gray pumice-fall deposits of 1912 still mantle all but steepest slopes and active alluvial plains.

bushes that are bent over downhill and retain intact bark (Hildreth and Fierstein, 2012). The source area was a snow-mantled glacier ~4 km^2 in area that sloped 11°–14° southward and was blanketed by at least 5 m of pumiceous fallout. Such supraglacial fall deposits, representing at least 0.02 km^3 of material, would be nearly double that originally constituting the debris-flow deposit (Hildreth, 1983). Beneath the main dacite-rhyolite debris flow, an all-rhyolite pumiceous debris flow left a deposit 0.5–1 m thick (Hildreth, 1991) that is intercalated within the pumice-fall section at the level of Layer B_2.

Many lesser pumice-rich debris-flow deposits emplaced syneruptively are preserved along Noisy River and upper Knife Creek, downstream from glaciers on Mount Katmai, as described by Hildreth and Fierstein (2012). The timing of each ashy debris flow can usually be inferred from its pumice compositions and thus related via the pumice-fall stratigraphy and seismicity to the main pulses of caldera collapse (Fig. 23).

Intracaldera Lake Behavior, Water Chemistry, Temperature Decline, and New Glaciers

Caldera collapse left steep walls and a jagged rim, which was initially capped by ice cliffs of the beheaded glaciers in four sectors, 90°–150°, 190°–260°, 290°–360°, and 5°–10°, thus fringing ~60% of the caldera margin (photos on p. 175 and 178 of Griggs, 1922). Because much of the ice had been fed from higher on the vanished summits, the ice cliffs wasted over an interval of decades, thinning and receding 50–800 m from the rim, and leaving rubbly ablation debris—consisting largely of what had been 1912 supraglacial ejecta. On the southwest side, however, peak 6200, which stands 275 m higher than the rim, has continued to sustain an ice shelf (Fig. 5). Much of the shelf has receded from the rim, but a narrow ice tongue has extended from its north end into a rim scallop and down the west wall toward the lake (Figs. 5, 12, and 22).

Complex collapse left kilometer-wide slump blocks that rose to inward-sloping benches 300–400 m above the caldera floor at its north and southwest margins. The benches had accumulated snow patches by 1917 (p. 172 of Griggs, 1922) and still only modest snowfields by 1923 (figs. 12 and 17 of Fenner, 1930). By Hubbard's first trip to the rim (1929), the snowfields had turned to ice and he reported a bergschrund (Hubbard, 1932), but the earliest record of extensively crevassed glaciers on the benches is a set of 1951 aerial photographs. As observed in 1953–1954 by Muller and Coulter (1957), the southwest intracaldera glacier terminated in ice cliffs 50–80 m above the lakeshore, the north glacier mantled only the upper half of its bench, and the narrow ice tongue on the west wall reached halfway down to the lake. In 1976, the western edge of the southwest glacier had barely reached the lake but later wasted back. Although all three intracaldera glaciers have long calved icebergs into the lake, a set of 1987 aerial photographs shows all of them terminating on steep rocky slopes just shy of entering the lake. By 1999, however, small tongues of both slump-block glaciers had reached the lakeshore (Figs. 6, 9, and 15). The steep western ice tongue had surged in 1976 and did so again in 2001, twice temporarily reaching the lakeshore but subsequently wasting back upslope. Snow that accumulates directly on the benches is clearly augmented by drift and avalanching from the rim.

The lake itself has a complex century-long filling history. Although a turquoise lake was 10–15 m deep during the expeditions of 1916–1919 (Griggs, 1922), it had disappeared by 1923 when Fenner and Yori descended to a caldera-floor mudflat (Fenner, 1930). Fenner described numerous steam columns rising from the floor and the fringing talus; fumarolic incrustations and the odor of H_2S; boiling mud pots as wide as 8 m that produced gigantic bursting mud bubbles; and a mud geyser that erupted at short intervals in jets as high as 60 m with loud detonations. He also showed that the Horseshoe Island was a dome of platy to blocky dacite lava ~350 m in diameter with ~20 m of visible relief. It had a steep-walled central lagoon, ~75 m wide, >20 m deep, and open to the northwest (figs. 15 and 16 of Fenner, 1930), that had been explosively reamed through the dome; Fenner described stratified deposits dipping radially from the dome that may have been related to such an event. He suggested but could not confirm that Jurassic sedimentary rocks cropped out near the base of the caldera wall. While this is not unreasonable in view of the elevations and extracaldera distribution of Naknek Formation exposures (Riehle et al., 1993), such rocks have not been identified in the breccias deposited explosively on the caldera rim. The question remains unresolved because the base of the wall is now obscured by at least 200 m of lake water.

By 1929, Horseshoe Island was fully concealed by the rising lake (Hubbard, 1932), implying a filling rate of at least 3–4 m/yr after 1923. When it was 10–15 m deep in 1917, lake level was surveyed at ~1003 m asl (Griggs, 1922), but by 1951 it was ~1188 m (Motyka, 1977), yielding an average filling rate of 5.4 m/yr for 34 years. For the short interval 1951–1953, Muller and Coulter (1957) also estimated a change of ≥5 m/yr. In 1974, Motyka (1977) surveyed lake level at 1235 m (and 1.2 m higher in 1975), giving a reduced rate of ~2 m/yr (47 m in 23 years) for the interval 1951–1974. Returning in 1977, however, Motyka (1978) found the level to have risen to 1242 m, implying an increase to ~3 m/yr for 1975–1977. We are not aware of any precise measurements since 1977, but our own observations on many trips to the caldera rim (1976–2001) suggest that additional deepening of ~10 m had taken place by 2001.

From an inflatable boat carried to the lake in 1977, Motyka (1978) measured a depth no greater than 200 m, an apparent discrepancy of ~50 m with the 1917 survey: [(1242–1003 m) + (10–15 m) = 249–254 m depth by 1977]. The discrepancy could reflect large uncertainties in one or both surveys or up to 50 m of lake-floor sedimentation in 60 years. Whether adequate to account for the discrepancy or not, sediment accumulation is still substantial in the 21st century, as shown by continuing rock fall from unstable walls, several muddy melt-water waterfalls, and aeolian and sheet-wash transport of 1912 ejecta and glacial ablation debris across the rim.

According to pilots quoted by Muller and Coulter (1957), the lake had not frozen over in winter as late as 1953. Motyka (1977) reported that it did freeze in 1967 but not in 1975, suggesting variations in heat flux through the lake floor. Winter and spring freezing has become common in recent decades, however. Since 1953, summer observers have witnessed calved icebergs circulating around the lake and melting within hours. A yellow-green upwelling in the northeastern part of the lake has been observed intermittently for decades, roughly over the site of the mud geyser photographed in 1923 by Fenner (1930). In 1975, Motyka (1977, 1978) paddled through the upwelling, reporting a flux of small sulfur particles, bubbles, and the odor of H_2S. In 1977, he measured a lake-bottom temperature of 20.5°C, which declined to 12°C only 10 m above the floor, then remained nearly constant at 8.8°C at depths between 150 m and 10 m. Motyka noted that this represented a substantial temperature increase from the 5.5°C recordings he had made at depths of 10–60 m only two years earlier.

Two water samples taken at a depth of 60 m in 1975 and analyzed at the U.S. Geological Survey (USGS) in Menlo Park contained (in mg/L) 1350–1750 Cl, 1200–1250 SO_4, 590–760 Na, 120–140 SiO_2, and 12–14 B; their pH was 2.5–3.0 as measured in the field or 2.05 as calculated in the lab (Motyka, 1977). Another sample taken in the summer of 1989 had a similar composition (Cameron and Larson, 1992). The acidity suggests dissolution of gaseous CO_2 in the lake water and little or no bicarbonate ion. Such chloride-sulfate waters are typical

of volcanic crater lakes and are consistent with meteoric melt water mixed with a substantial input of fluids from drowned fumaroles.

Extracaldera Glacier Behavior Since 1912

Behavior of glaciers on Mount Katmai involves the complication that some (not all) were partly beheaded by caldera collapse (Fig. 3). Nonetheless, all of the dozen radial extracaldera glaciers around Mount Katmai were blanketed with several meters of Novarupta fall deposits. Knife Creek Glacier #3, although still partly fed from peak 6128, lost at least half its catchment area to collapse of the summit (Fig. 3). The glacier has since thinned and disrupted its thick ejecta blanket, but its upper reach remains active and crevassed; although its lower half looks hummocky and stagnant, its terminus actually advanced ~225 m between 1951 and 1987. Knife Creek Glacier #4 is fed from the extensive North Katmai Icefield, which was partly beheaded but remains robust, not shrinking. The vigorously lobate terminus of Glacier #4 advanced ~150 m between 1951 and 1987, and a National Geographic Society photograph taken in 1919 (Hildreth and Fierstein, 2012) shows that Glacier #4 had already advanced 500 m before 1951, for a total of 650 m since 1919. Knife Creek Glacier #5 is supplied from an isolated cirque 2.5 km northeast of the caldera rim and was thus not affected by caldera formation. Between 1919 and 1951, its terminus advanced ~1300 m, but since 1951 its distal 700-m reach has thinned and stagnated, although its terminal position has changed little.

Two substantial glaciers west and south of the caldera exhibit inconsistent behavior. The Wishbone Glacier, fed from the Katmai-Trident saddle, divides into two tongues that extend several kilometers southward into narrow gorges. The southeast tongue advanced 200 m between 1951 and 1989, while the southwest tongue thinned and receded slightly, although it has a small western lateral lobe that advanced 110 m (Hildreth et al., 2003a). Due south of the caldera rim, Metrokin Glacier was partly beheaded but continues being supplied by the west-rim ice shelf below peaks 6128 and 6200 (Fig. 3). Its canyon-confined terminus retreated ~600 m between 1951 and 1989 and another 400 m between 1989 and 2001. This is the glacier that shed the Katmai River pumiceous debris flow; so its insulating blanket of fallout was substantially less than that on other glaciers of Mount Katmai.

The steep southeast slope of Mount Katmai supports three small glaciers, all beheaded by collapse and today respectively 1.8, 2.1, and 1.2 km long (Fig. 3). The northern one fills the valley below the East Notch of the caldera rim. Termini of all three have retreated >1 km since 1951.

The East Katmai Icefield (Fig. 3) is largely fed by three ice tongues on the steep east slope of the mafic cone (peak 6715). Only its upper parts have been cleared of 1912 ejecta, but the whole ice field is actively crevassed. It contributes northward to Ikagluik Glacier, the terminus of which has moved little since 1951, and contributes southward to Noisy Glacier, which advanced ~150 m since 1951.

The North Katmai Icefield (Fig. 3) is also robustly active, feeding icefalls that descend toward Glacier #4 and toward Ikagluik Creek. The ice field is partly supplied by a series of small cirque glaciers on the steep north rim of the caldera. Although these were deprived of contributions from higher on the foundered edifice, each remains actively crevassed and shrinkage is limited to the notches on the caldera rim.

The lower halves of all five Knife Creek Glaciers remain heavily mantled with 1912 fallout, which is as thick as 10 m atop their low-relief distal lobes. Owing to firn accumulation and a century of surface flow, their upper surfaces are now generally tephra-free except for areas of stagnant ice near the caldera rim. Much of the fallout mantle has been disrupted by ice movement and wasting, but complete sections (Layers A–H) are locally intact. Intercalated within some supraglacial fall sections are (1) layers and pods of pyrite-bearing hydrothermal mud ejected from Mount Katmai during caldera collapse (Hildreth, 1991) and (2) meter-thick deposits of pumiceous debris flows that were remobilized down snow-clad slopes during the eruptive sequence. Evidence for interaction of 1912 pyroclastic flows with the Knife Creek Glaciers, including ice-marginal phreatic craters, is summarized by Hildreth and Fierstein (2012).

Since 1912, Knife Creek Glaciers #1, #2, #3, and #4 have all advanced over the margins of the Valley of Ten Thousand Smokes ignimbrite sheet. Post-1912 behavior of glaciers on all the neighboring volcanoes of the Katmai cluster were described by Hildreth et al. (2000, 2001, 2002, 2003a). All 12 radial glaciers on Mount Mageik, which lies just upwind of the principal 1912 fallout sector, have retreated, which is probably typical of the integrated climatic influence on ice budgets in the Katmai region during the late 20th century. Nearby, however, from Trident to Snowy Mountain, glaciers have retreated, stagnated, or advanced, roughly in proportion to the thickness and retention of 1912 fallout blankets upon them. It seems clear that the buff pumice mantle retards ablation.

COMPOSITION OF ERUPTIVE PRODUCTS

Major and Trace Elements

Products erupted at Mount Katmai represent a typical medium-K arc suite (Figs. 28 and 29), calcic by the criterion of Peacock (1931) and both tholeiitic and calcalkaline by the criterion of Miyashiro (1974). Some 35 samples from NE Katmai range continuously from 52.5 to 66.2% SiO_2, and 117 samples from SW Katmai define an array that fully overlaps the former and extends continuously from 51.6 to 72.3% SiO_2. As typical of arc suites, Ti and Zr contents are modest. TiO_2 ranges from 1.11% to 0.57% and as low as 0.40% in rhyolites. Zr concentration is 52–190 ppm in the basalt-to-dacite arrays and as high as 220 ppm in rhyodacites. Samples of relatively mafic, phenocryst-poor magmatic enclaves, common in dacite and rhyodacite hosts, range from 52.5 to 59.3% SiO_2. No products of Mount Katmai are primitive, as even the most mafic samples contain <50 ppm Ni, and only eight of the 152 samples analyzed have >5% MgO, only one of which has >6%. A comparative analysis of rear-arc versus volcanic-front centers in the Katmai region (including Mount Katmai) concluded that mafic magmas at all centers issued from normal mid-ocean ridge basalt (NMORB) source mantle fluxed by slab contributions that are most effective beneath the arc front and diminish behind it (Hildreth et al., 2004).

Phenocryst Mineralogy

Most products of Mount Katmai are plagioclase-rich, two-pyroxene andesites and dacites (Hildreth and Fierstein, 2012). Sparse olivine is present in basaltic lava flows of NE Katmai, in mafic lithic blocks expelled in 1912, and in some enclaves. Fe-Ti oxide microphenocrysts are ubiquitous and abundant, except generally absent in the basalts, in which plagioclase, olivine, and clinopyroxene tend to be small (0.2–1 mm) and sparse. Clinopyroxene typically exceeds orthopyroxene in andesites, whereas orthopyroxene is the more abundant pyroxene in dacites and rhyodacites. Plagioclase-pyroxene-oxide clots, typically 1–3 mm across and enclosing interstitial glass, are common in most Mount Katmai andesites and dacites. Several generations of plagioclase are present in most of the andesites and dacites, as identified by varied internal sieve patterns, intergrown composite crystals, and coexisting crystals having either sieved rims or clean overgrowths. No hornblende was observed except sparsely in the 22.8-ka pumice fall

and ignimbrite (unit **krp**) and in some pumice clasts of 1912 dacite. Rhyolite pumice ejected in both of these large pyroclastic eruptions contains trace amounts of zircon, uniquely for Mount Katmai, as reflected in the Zr deficiency of the rhyolites relative to the andesite-dacite compositional arrays (Fig. 29).

Sr Isotopes

Thirteen lava samples from Mount Katmai gave $^{87}Sr/^{86}Sr$ ratios that range from 0.70335 to 0.70366, while the 22.8-ka plinian pumice fall (unit **krp**) gave 0.70370 and 0.70372, slightly more radiogenic than the south-rim rhyolite lava flow (unit **krh**; 0.70365). The west-rim dacite agglutinate (unit **kwa**) and dacite pumice from the Lethe Assemblage (unit **kla**) in the lower Valley of Ten Thousand Smokes gave virtually identical values of 0.70360. For the stratigraphically continuous zoned scoria fall on the south rim (unit **kzs**), ratios for dacite and andesite pumice, respectively 0.703576 and 0.703459, differ substantially.

It was shown that $^{87}Sr/^{86}Sr$ ratios for ~55 samples from the arc-front centers in the Katmai cluster (Martin, Mageik, Trident, Katmai, and Snowy) exhibit a general trend toward more radiogenic values in more evolved rocks (fig. 9 of Hildreth et al., 2004), specifically with decreasing Sr and increasing SiO_2. Plots of $^{87}Sr/^{86}Sr$ versus ratios such as Ba/La, Ba/Ta, and Th/Yb, conventionally interpreted (where positively correlative) to reflect slab-derived contributions, are scattered. Because the arc-front $^{87}Sr/^{86}Sr$ values correlate with fractionation indices, we infer that intracrustal contributions govern the Sr budget to a greater degree than does the subduction component (Hildreth et al., 2004).

Figure 30 presents $^{87}Sr/^{86}Sr$ data for Mount Katmai, Trident, and the 1912 eruption, plotted against such a fractionation index (1/Sr). Also shown are data for a rhyolite sill and a tonalitic porphyry stock, both of Pliocene age, that crop out adjacent to the Valley of Ten Thousand Smokes. The diagram suggests that comparable Tertiary intrusive rocks are more likely than the shallowly exposed Jurassic sedimentary rocks (**Jn**) to have provided assimilants that raised $^{87}Sr/^{86}Sr$ values during evolution of the mafic to andesitic arrays, from which dacites and rhyolites subsequently fractionated.

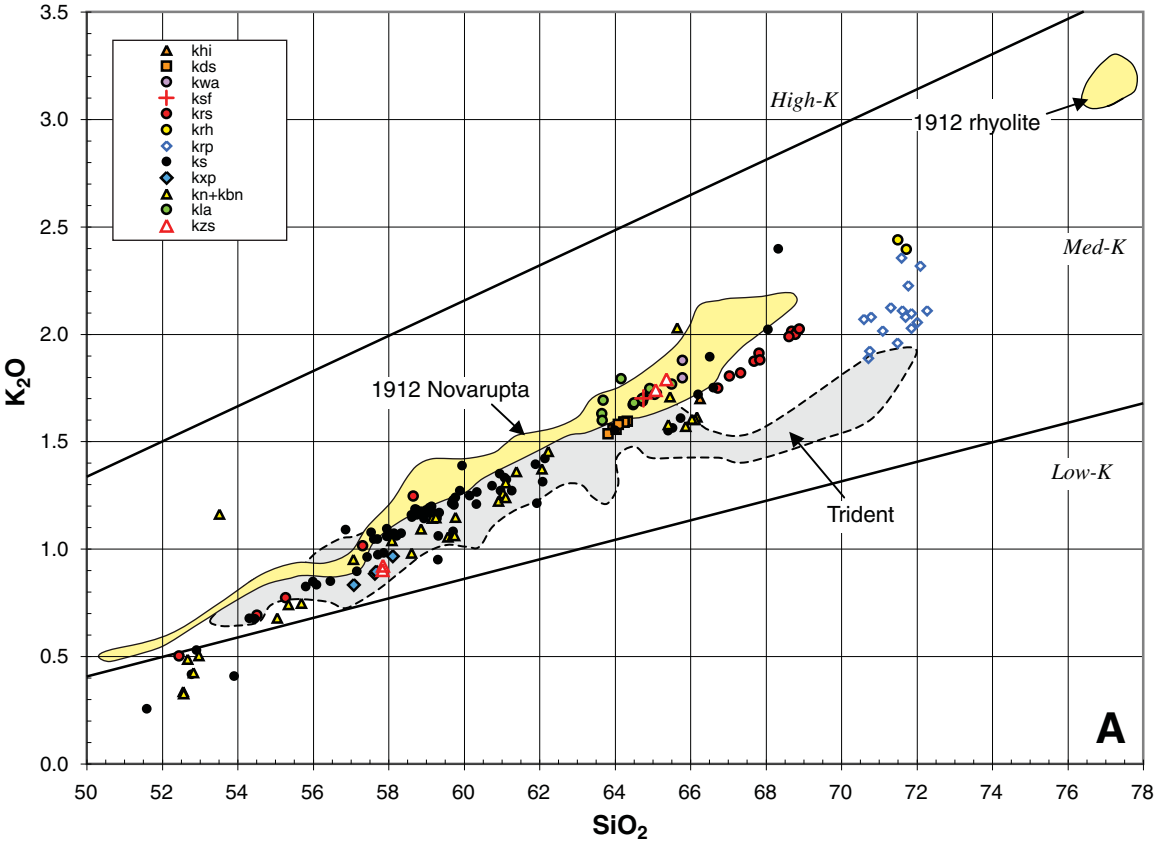

Figure 28 (*Continued on following page*). Compositional variations versus SiO_2 content (all in wt%) for ~160 samples from Mount Katmai, subdivided as in inset and keyed to list of map units of Figure 3. Shaded fields enclose ~265 samples of 1912 Novarupta pumice and dome lava and ~105 samples from Trident Volcano. 1912 data are tabulated by Hildreth and Fierstein (2012) and Trident data by Hildreth et al. (2003a). Five andesitic samples of unit krs are chilled phenocryst-poor enclaves in rhyodacite host lavas. (A) K_2O versus SiO_2. (B) Total alkalies versus SiO_2. Alkaline/subalkaline boundary and named fields follow LeBas et al. (1986). (C) FeO*/MgO ratio versus SiO_2. Tholeiitic/calcalkaline (TH/CA) boundary after Miyashiro (1974). FeO* is total iron calculated as FeO. Most map units are calcalkaline. Unit kxp and andesitic enclaves in unit krs are tholeiitic. Major edifice-building assemblages ks, kn, and kbn each include numerous lava flows in both fields.

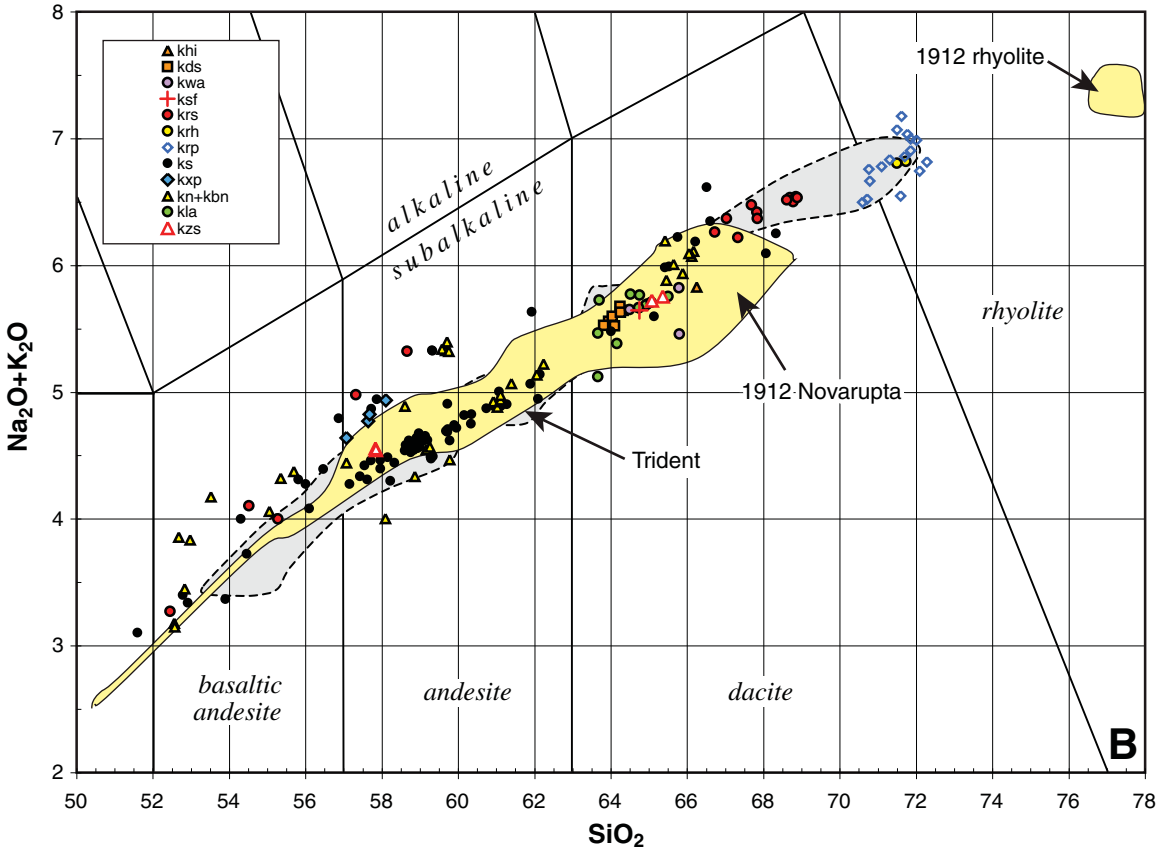

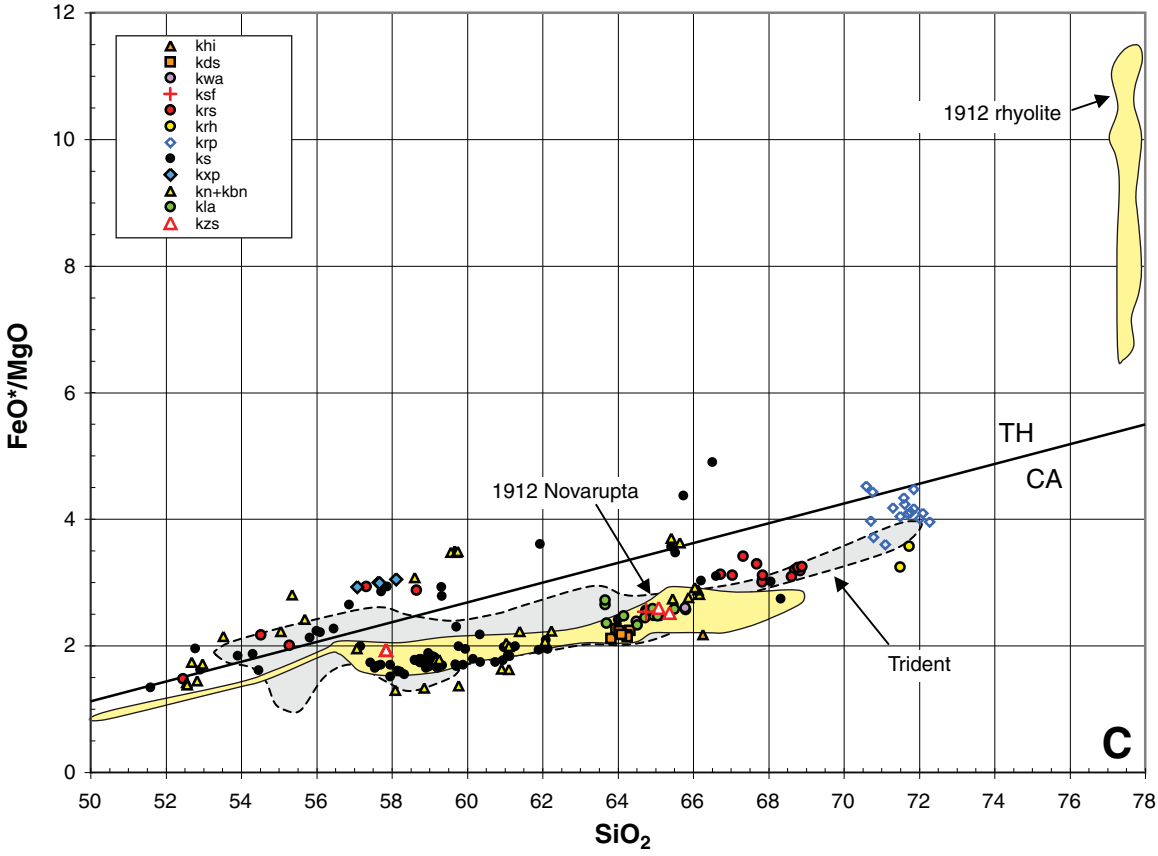

Figure 28 (*Continued*).

Affinity of 1912 Ejecta with Products of Mount Katmai

It was shown by Hildreth and Fierstein (2000) that the andesite-dacite array erupted at Novarupta in 1912 is compositionally similar to products of Mount Katmai and mostly distinguishable from pre-1912 products of the adjacent Trident cluster (see especially Figs. 29A, 29B, and 29C). Not present in the 1912 array, rhyodacites and low-silica rhyolites (68%–72% SiO_2) have been identified nowhere in the region except among the youngest eruptive products at Mount Katmai. In contrast, andesitic-dacitic Trident Volcano has never produced rhyolite during its 140-kyr eruptive history; its edifice was undisturbed in 1912, and no evidence for rhyolitic contamination is observed in products of its 1953–1974 eruptions (Hildreth et al., 2003). An independent rhyolitic magma body beneath Novarupta itself in 1912 is likewise unlikely because of the rapid decline in temperature and magmatic gases in vent-area fumaroles and the absence of uplift, deformation, or even minor eruptive activity subsequent to emplacement of the rhyolitic plug dome. Although clear that the intermediate magma was withdrawn 10 km laterally from beneath Katmai caldera, the evidence that the 1912 rhyolite had also been stored there remains inferential.

MAGMA STORAGE IN 1912

We previously elaborated evidence favoring joint pre-eruptive storage of the continuously zoned 1912 andesite-dacite magma and the coerupted 1912 high-silica rhyolite magma (Hildreth and Fierstein, 2000, 2012). There are two considerations, however, that induce speculation that the rhyolite could have been stored elsewhere than beneath Mount Katmai (Eichelberger and Izbekov, 2000): (1) The andesite-dacite continuum (58%–68% SiO_2; 5.5 km^3 of magma) and the rhyolite (~77% SiO_2; 8 km^3 of magma) are separated by a compositional gap of >8% SiO_2; and (2) the volume of andesite-dacite magma erupted in 1912 is similar to the volume of Katmai caldera (~5.5 km^3). The volumetric mismatch need not be critical because magma chambers and plutons are commonly more areally extensive than ring-fault zones of associated calderas.

Discontinuities in bulk composition and phenocryst content are common in caldera-forming pyroclastic eruptions, large and small (Hildreth, 1981). The compositional gaps between dacitic and rhyolitic magmas released together in large pyroclastic eruptions have elicited various models exploring whether such gaps originate by secular crystal settling, by separation of rhyolitic melt from underlying crystal-rich andesite-dacite mush, by partial melting of wall-rock

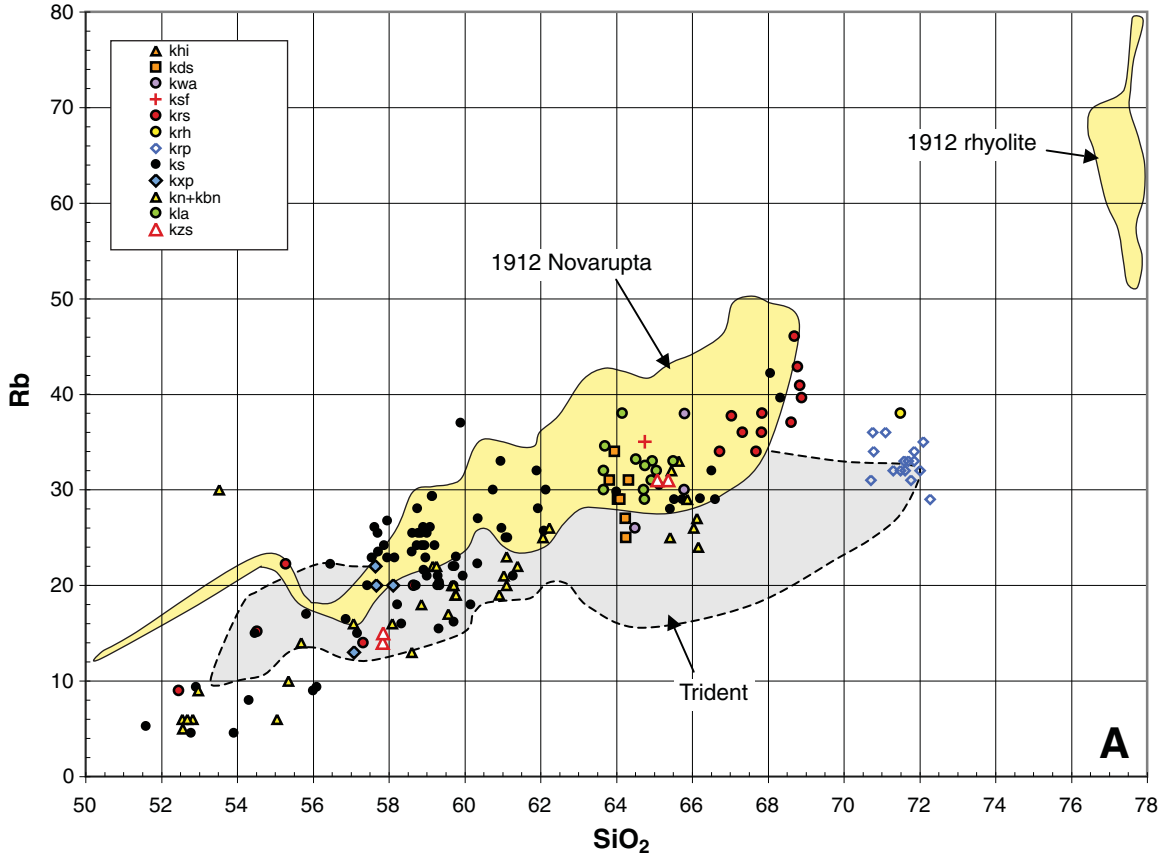

Figure 29 (*Continued on following page*). Variation of Rb, Sr, and Zr (in ppm) versus wt% SiO_2 for ~160 samples from Mount Katmai, subdivided as indicated in inset, which is keyed to list of map units of Figure 3. Shaded enclosures are fields for ~105 samples from Trident Volcano and ~265 samples of 1912 Novarupta pumice and dome lava. Data tabulated as stated in Figure 28. Trace elements indicate closer affinity of 1912 suite for Mount Katmai than for Trident. Note relative Zr enrichment of unit kds and pronounced effect of zircon fractionation on Zr content of rhyolites.

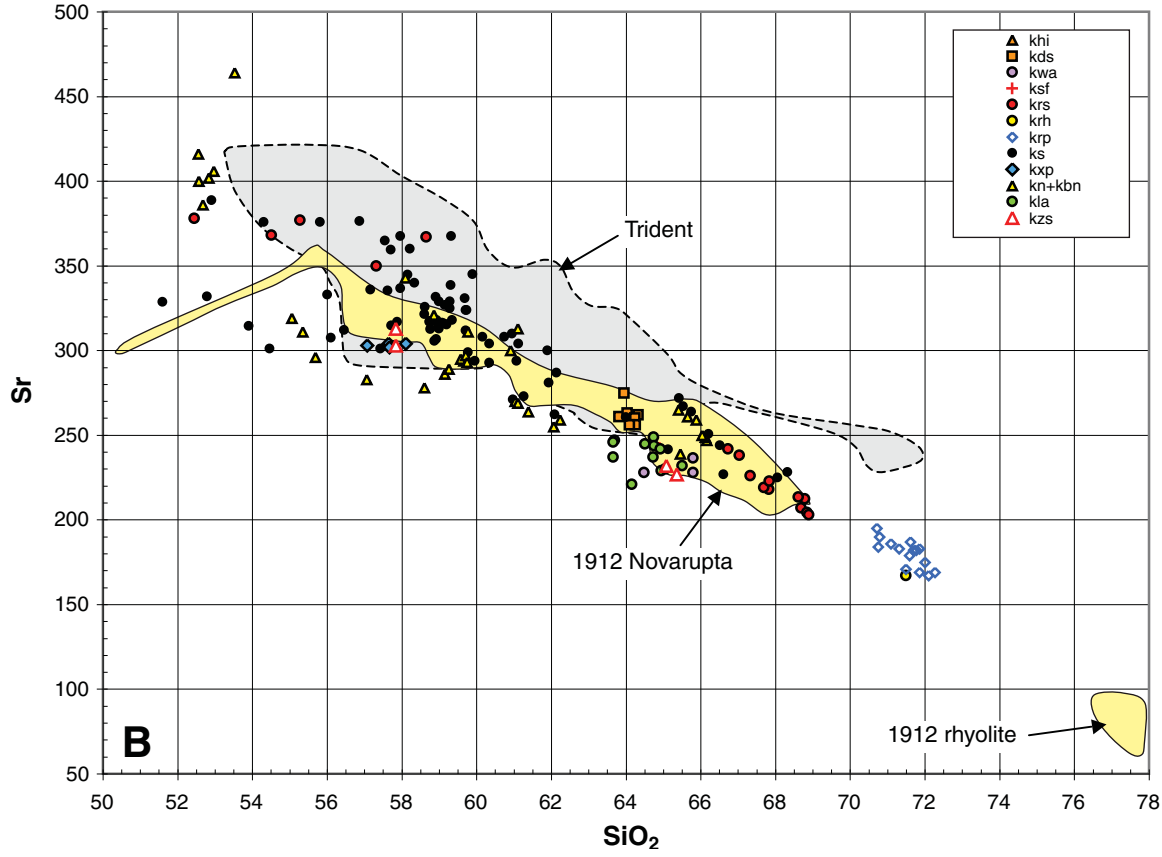

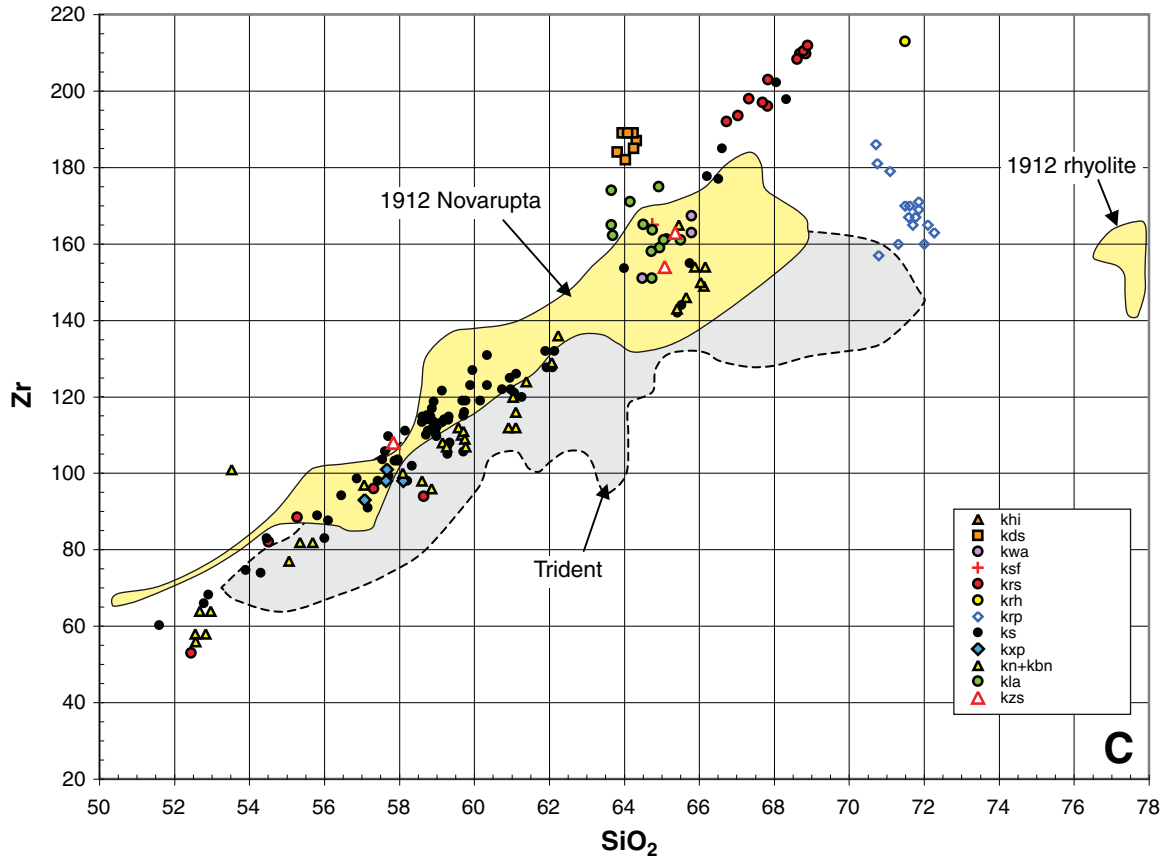

Figure 29 (*Continued*).

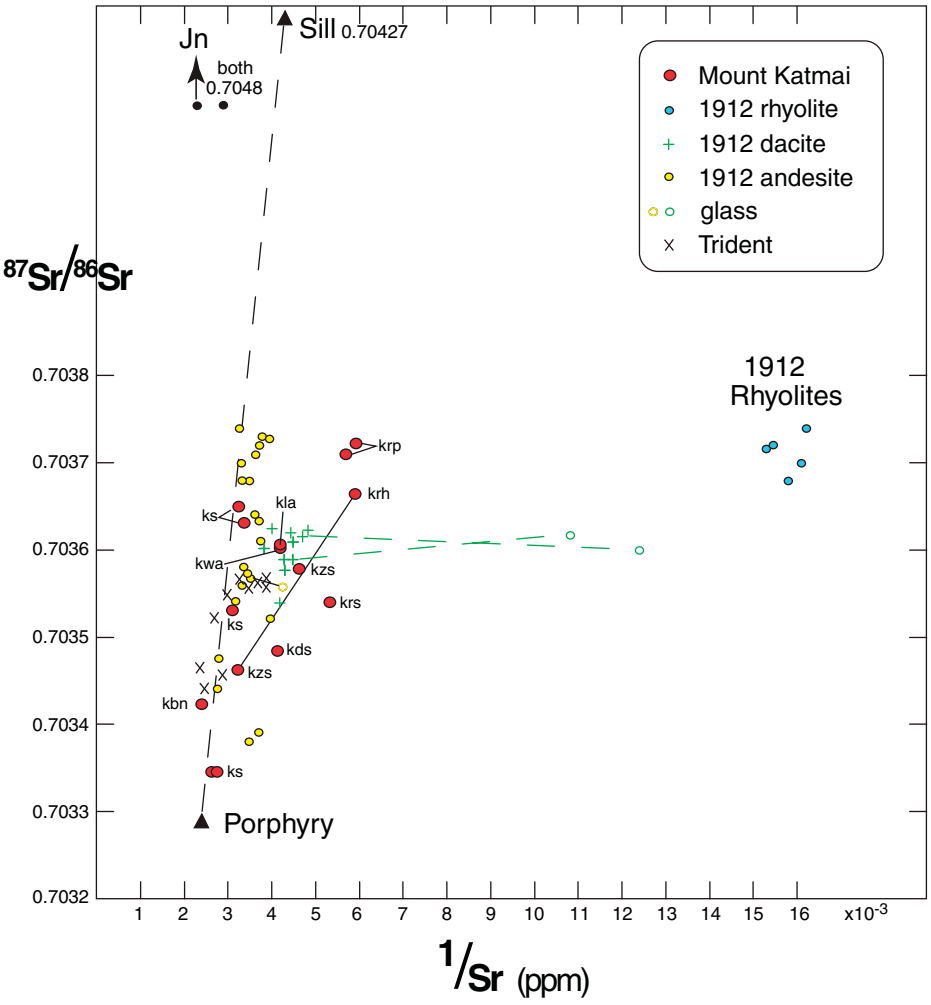

Figure 30. Sr-isotope ratios plotted against reciprocal of Sr concentration (in ppm), a convention that transforms a mixing hyperbola into a straight line. Line connects data (▲) for Pinnacle Porphyry (63%–65% SiO_2) and high-silica rhyolite sill (77% SiO_2), both near Mount Mageik and both ~3.1 Ma (Lowenstern and Mahood, 1991; Hildreth and Fierstein, 2003). It is not implied that these particular Pliocene intrusions provided assimilants to 1912, Trident, or Katmai magmas, but, instead, that comparable Tertiary intrusive rocks are more likely candidates than the shallowly exposed Naknek Formation (Jn). Symbols are identified in inset for 38 samples of 1912 ejecta, 10 samples for Trident group, and 15 samples for Mount Katmai. Note that 1912 andesite ejecta alone span $^{87}Sr/^{86}Sr$ range for entire 1912 suite. Tie-lines connect data for three 1912 whole-pumice samples and their matrix glasses, illustrating fractionation trend from andesite-dacite continuum toward 1912 rhyolites. Katmai samples are identified by map labels, as in Figure 3. Least radiogenic Katmai samples are among most mafic. Most radiogenic Katmai samples are most silicic: South-rim rhyolite lava (krh) is slightly less radiogenic than (roughly contemporaneous) plinian pumice fall (krp) at Windy and Mageik Creeks. Dacite pumice from west-rim agglutinate (kwa) is isotopically and chemically identical to pumice in Lethe Assemblage (kla) 23 km northwest. Andesite and dacite components of zoned scoria fall (kzs) are isotopically different, but they plot on a mixing line with the stratigraphically subjacent rhyolite (krh).

granitoids, or by some independent source of the rhyolite.

For the 1912 suite, many lines of evidence favor contiguity of all the 1912 magmas prior to eruption. About 3 km^3 of rhyolite magma erupted before being joined by any coerupting andesite and dacite, indicating that the conduit that fed the Novarupta vent tapped the rhyolitic part of the reservoir first. It took 3–4 h before the first andesite-dacite arrived at the vent, and for the rest of Episode I, all three were intimately commingled, culminating in the onset of caldera collapse in the 11th hour. Despite the bulk compositional gap, Fe-Ti-oxide thermobarometry demonstrates continuity in both magma temperature and oxygen fugacity (Hildreth, 1983) between the nearly aphyric rhyolite (800°–857°C) and the extensively crystallized dacite (848°–950°C)-to-andesite (952°–990°C) continuum. Thermal and redox continuity suggests physical contiguity, supporting the inference that the andesite-dacite mush was the proximate heat source that kept the rhyolite nearly aphyric. The phenocryst-rich intermediate magma may have graded down into a cumulate substrate that served not only as thermal buffer but, by compaction and upward percolation of its evolved interstitial melt, as a contributor of rhyolitic liquid (see Bacon and Druitt, 1988; Sisson and Bacon, 1999).

The rhyolitic and intermediate magmas all appear to have assimilated melt from crustal rocks that had only modest Sr-isotopic influence (Fig. 30) and negligible Nd and O isotopic effects (Hildreth, 1987; Hildreth and Fierstein, 2012). Oxygen-isotope data for 1912 ejecta suggest a normal magmatic fractional-crystallization progression from andesite through dacite to rhyolite, with no detectable contribution from sedimentary or hydrothermally altered rocks. Likewise, for both matrix glass and whole-rock samples, parallelism of rare-earth patterns, with increasing REE abundance (and Eu deficiency) from andesite to dacite to rhyolite (Hildreth and Fierstein, 2012) suggests a simple fractionation sequence with insufficient extraneous contributions to the rhyolite to be chemically identifiable. Although the Sr-isotope data (Fig. 30) indicate small crustal contributions to most Trident, Katmai, and 1912 magmas, the combined Nd, Sr, and O isotope results show that the rhyolite magma was not substantially a partial melt of the Mesozoic and older stratified rocks constituting the Alaska Peninsula basement. Taken altogether, the isotope data favor fresh arc-intrusive rocks as the most likely source of minor partial-melt contributions.

The glass (melt) phase within the crystal-rich 1912 dacite is itself high-silica rhyolite only slightly less evolved than the nearly aphyric

1912 rhyolite, and concentrations of most elements overlap (Hildreth and Fierstein, 2012). If most of the melt constituting the rhyolite had once been interstitial liquid that escaped upward from a compacting (and gas-saturated) volume of intermediate crystal mush, slight compositional differences could have resulted from (1) limited subsequent crystal fractionation of the rhyolite, (2) additions of small wall-rock partial-melt increments to both, as inferred from the Sr-isotope data (Fig. 30), (3) internal crystal-liquid re-equilibration of the melt-depleted dacite mush, and (4) contamination of the dacite mush by melt and crystals from the contiguous andesite. By such a mechanism, glass in the dacite pumice would represent the melt phase left behind in the dacite mush after escape of the melt fraction that became the rhyolite.

Studies of melt inclusions in quartz crystals from 1912 rhyolite indicate entrapment of vapor-saturated melt at pressures of 100–130 MPa (Lowenstern, 1993; Wallace, 2005), implying chamber depth of 3–6 km, as likewise indicated by phase-equilibrium experiments on both the rhyolite (Coombs and Gardner, 2001) and the andesite-dacite compositional continuum (Hammer et al., 2002). Figure 31 presents our updated magma storage model for 1912, reflecting the constraints just summarized. The high-silica rhyolite that dominated the 1912 eruption remains a regional rarity of unproven origin. Its chemical and isotopic similarity to the melt (glass) phase of the coerupted dacite,

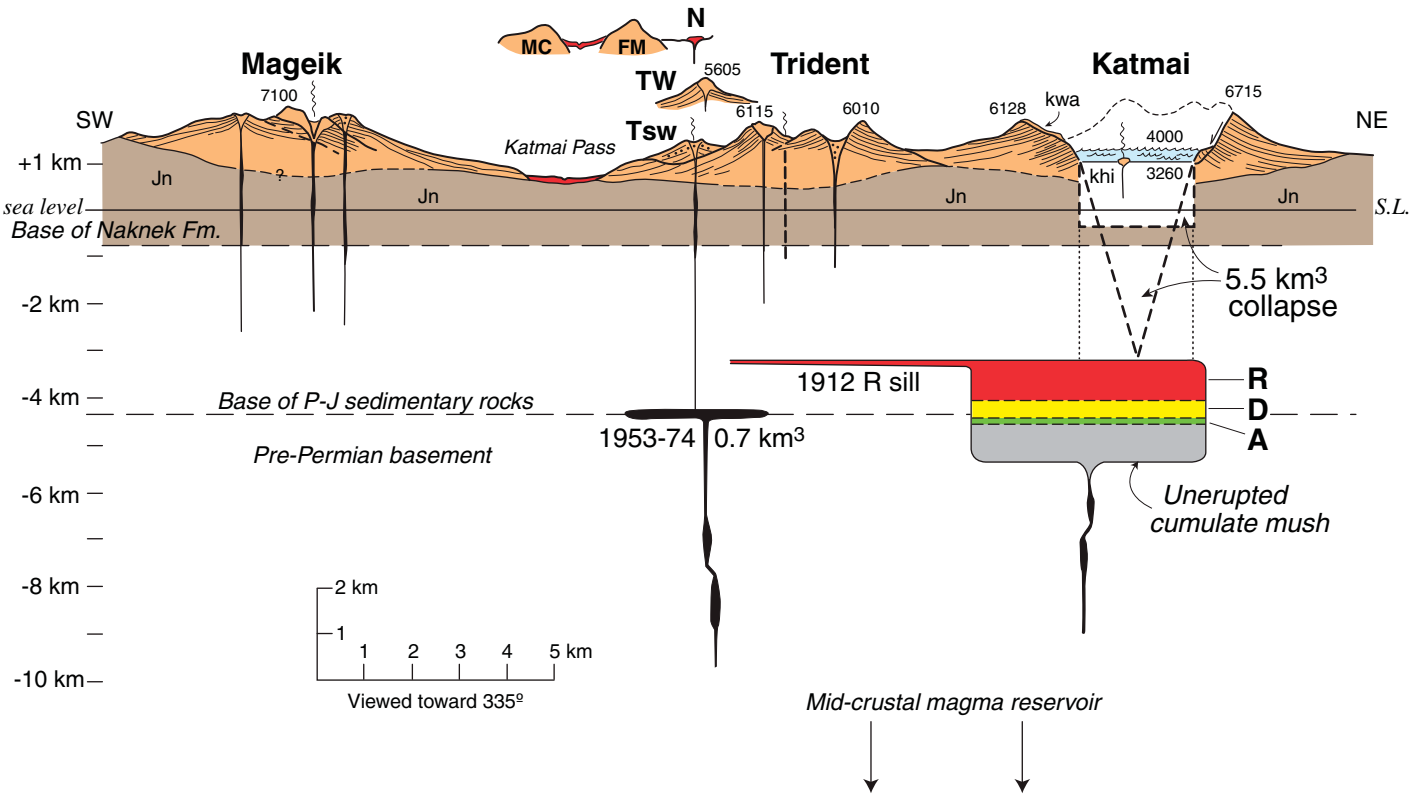

Figure 31. Katmai volcanic cluster magmatic plumbing system; schematic illustration drawn to scale along N65°E volcanic axis, looking N25°W with no vertical exaggeration. Jn—marine sedimentary rocks of Jurassic Naknek Formation, underlain by Permian to Jurassic (P–J) marine formations, here all close to horizontal. Novarupta (N), Falling Mountain (FM), Mount Cerberus (MC), and West Trident (TW) are not actually along section, but their relative positions (see Fig. 2) are indicated above profile, respectively 4.5 km, 4 km, 4 km, and 1.5 km northwest of line of section. Pre-collapse profile of Mount Katmai is adapted from Figure 4; volume displaced in 1912 was ~5.5 km^3 and surface subsidence was 1.3 ± 0.1 km vertically. Displaced volume is modeled alternatively as conical funnel and cylindroid, each having top surface area (4 km^2) equal to that of caldera floor. Unit khi, Horseshoe Island dacite dome; unit kwa, remnant of pre-1912 agglutinated dacite fallout that mantles west rim and peak 6128 and thickens into a pre-1912 crater (Figs. 5, 12, and 21). Magma reservoir of 1912 is depicted (just before eruption) as a unitary chamber zoned from andesite (A) to dacite (D) to rhyolite (R) in the proportions (1:4.5:8) erupted. Because magma volume erupted (13.5 km^3) was 2.3 times greater than volume collapsed, the magma erupted is depicted as elongate along the volcanic axis, 1.3 km thick, 2 km across axis (into the profile), and 5 km along axis, thus extending well beyond caldera footprint (as common for exhumed calderas and their source plutons). Rhyolite sill is depicted penetrating subhorizontal Mesozoic sedimentary strata and extending 6 km toward Novarupta or Trident, whence the magma presumably diked its way toward surface. Advancing from thermally zoned reservoir 10 km to Novarupta through cold wall rocks, nearly aphyric rhyolite should have crystallized more unless its propagation were rapid. Chamber would have been larger to extent that additional magma failed to erupt. Depth of reservoir is constrained by experimental work to 3–6 km and is here represented arbitrarily at an upper-crustal discontinuity, beneath but (for clarity) clear of the caldera-collapse models. The 0.7 km^3 of magma that erupted at Southwest Trident (T_{SW}) in 1953–1974 is shown stored as a circular sill 100 m thick; as a vertical dike, it could presumably have had an aspect ratio much thinner. Elevations of summits on profile are in feet (1 m = 3.28 feet). Wavy vertical lines indicate present-day fumarolic emissions.

its thermal and redox continuity with the dacite, and the similar storage depths inferred experimentally are all consistent with a comagmatic zoned system. If the rhyolite originated elsewhere, the string of coincidences is remarkable. If the phenocryst-poor 1912 rhyolite had not been contiguous with the 1912 dacite magma reservoir, then, for the thermal, redox, isotopic, and chemical reasons elaborated, it should have been derived from another just like it.

ACKNOWLEDGMENTS

Important contributions to our fieldwork on the Mount Katmai edifice were made by Maura Hanning and Bruce Houghton. Helicopter pilots Bill Springer, Jim Sink, and Sam Egli set us down in some breathtaking places that we were unlikely ever to have reached on foot. Many seasons backpacking on foot were supported by the Geothermal Research and Volcano Hazards Programs of the USGS, and several later seasons with helicopter support by Alaska Volcano Observatory under the leadership of Terry Keith and Tom Murray. Helpful reviews were provided by Raffaello Cioni, Bruce Houghton, and William E. Scott.

REFERENCES CITED

Abe, K., 1992, Seismicity of the caldera-making eruption of Mount Katmai, Alaska, in 1912: Bulletin of the Seismological Society of America, v. 82, p. 175–191.

Bacon, C.R., and Druitt, T.H., 1988, Compositional evolution of the zoned calcalkaline magma chamber of Mount Mazama, Crater Lake, Oregon: Contributions to Mineralogy and Petrology, v. 98, p. 224–256, doi:10.1007/BF00402114.

Bacon, C.R., Vazquez, J.A., and Wooden, J.L., 2012, Peninsular terrane basement ages recorded by Paleozoic and Paleoproterozoic zircon in gabbro xenoliths and andesite from Redoubt Volcano, Alaska: Geological Society of America Bulletin, v. 124, p. 24–34, doi:10.1130/B30439.1.

Cameron, W.A., and Larson, G.L., 1992, Baseline inventory of the aquatic resources of Aniakchak National Monument, Alaska: Technical Report NPS/PNROSU/NRTR-92/03, National Park Service, Seattle, 215 p.

Coombs, M.L., and Gardner, J.E., 2001, Shallow-storage conditions for the rhyolite of the 1912 eruption at Novarupta, Alaska: Geology, v. 29, p. 775–778, doi:10.1130/0091-7613(2001)029<0775:SSCFTR>2.0.CO;2.

Curtis, G.H., 1968, The stratigraphy of the ejecta from the 1912 eruption of Mount Katmai and Novarupta, Alaska, *in* Coats, R.R., Hay, R.L., and Anderson, C.A., eds., Studies in Volcanology: Geological Society of America Memoir 116, p. 153–210.

Detterman, R.L., Case, J.E., Miller, J.W., Wilson, F.H., and Yount, M.E., 1996, Stratigraphic framework of the Alaska Peninsula: U.S. Geological Survey Bulletin 1969-A, 74 p.

Eichelberger, J.C., and Izbekov, P.E., 2000, Eruption of andesite triggered by dyke injection: Contrasting cases of Karymsky Volcano, Kamchatka, and Mount Katmai, Alaska: Philosophical Transactions of the Royal Society of London, series A, v. 358, p. 1465–1485.

Fenner, C.N., 1923, The origin and mode of emplacement of the great tuff deposit of the Valley of Ten Thousand Smokes: National Geographic Society, Contributed Technical Papers, Katmai Series, No.1, p. 1–74.

Fenner, C.N., 1925, Earth movements accompanying the Katmai eruption: Journal of Geology, v. 33, p. 116–139 and 193–223.

Fenner, C.N., 1930, Mount Katmai and Mount Mageik: Zeitschrift für Vulkanologie, v. 13, p. 1–24.

Fenner, C.N., 1950, The chemical kinetics of the Katmai eruption: American Journal of Science, v. 248, p. 593–627 and 697–725.

Fierstein, J., 2007, Explosive eruptive record in the Katmai region, Alaska Peninsula: An overview: Bulletin of Volcanology, v. 69, p. 469–509, doi:10.1007/s00445-006-0097-y.

Fierstein, J., and Hildreth, W., 1992, The plinian eruptions of 1912 at Novarupta, Katmai National Park, Alaska: Bulletin of Volcanology, v. 54, p. 646–684, doi:10.1007/BF00430778.

Fierstein, J., and Wilson, C.J.N., 2005, Assembling an ignimbrite: Compositionally defined eruptive packages in the 1912 Valley of Ten Thousand Smokes ignimbrite, Alaska: Geological Society of America Bulletin, v. 117, p. 1094–1107, doi:10.1130/B25621.1.

Fierstein, J., Houghton, B.F., Wilson, C.J.N., and Hildreth, W., 1997, Complexities of plinian fall deposition at vent: An example from the 1912 Novarupta eruption: Journal of Volcanology and Geothermal Research, v. 76, p. 215–227, doi:10.1016/S0377-0273(96)00081-9.

Filson, J., Simkin, T., and Leu, L., 1973, Seismicity of a caldera collapse: Galápagos Islands 1968: Journal of Geophysical Research, v. 78, p. 8591–8622, doi:10.1029/JB078i035p08591.

Fliedner, M.M., and Klemperer, S.L., 2000, Crustal structure transition from oceanic arc to continental arc, eastern Aleutian Islands and Alaska Peninsula: Earth and Planetary Science Letters, v. 179, p. 567–579, doi:10.1016/S0012-821X(00)00142-4.

Griggs, R.F., 1920, The great Mageik landslide: The Ohio Journal of Science, v. 20, p. 325–354.

Griggs, R.F., 1922, The Valley of Ten Thousand Smokes: Washington, D.C., National Geographic Society, 340 p.

Hammer, J.E., Rutherford, M.J., and Hildreth, W., 2002, Magma storage prior to the 1912 eruption at Novarupta, Alaska: Contributions to Mineralogy and Petrology, v. 144, p. 144–162, doi:10.1007/s00410-002-0393-2.

Hildreth, W., 1981, Gradients in silicic magma chambers—Implications for lithospheric magmatism: Journal of Geophysical Research, v. 86, p. 10153–10192, doi:10.1029/JB086iB11p10153.

Hildreth, W., 1983, The compositionally zoned eruption of 1912 in the Valley of Ten Thousand Smokes, Katmai National Park, Alaska: Journal of Volcanology and Geothermal Research, v. 18, p. 1–56, doi:10.1016/0377-0273(83)90003-3.

Hildreth, W., 1987, New Perspectives on the eruption of 1912 in the Valley of Ten Thousand Smokes, Katmai National Park, Alaska: Bulletin of Volcanology, v. 49, p. 680–693, doi:10.1007/BF01080359.

Hildreth, W., 1991, The timing of caldera collapse at Mount Katmai in response to magma withdrawal toward Novarupta: Geophysical Research Letters, v. 18, p. 1541–1544, doi:10.1029/91GL01083.

Hildreth, W., and Fierstein, J., 2000, Katmai volcanic cluster and the great eruption of 1912: Geological Society of America Bulletin, v. 112, p. 1594–1620, doi:10.1130/0016-7606(2000)112<1594:KVCATG>2.0.CO;2.

Hildreth, W., and Fierstein, J., 2003, Geologic map of the Katmai Volcanic Cluster, Katmai National Park, Alaska: U.S. Geological Survey Map I-2778, scale 1:63,360.

Hildreth, W., and Fierstein, J., 2012, The Novarupta-Katmai Eruption of 1912: Largest Eruption of the Twentieth Century: Centennial Perspectives: U.S. Geological Survey Professional Paper 1791, 259 p.

Hildreth, W., Fierstein, J., Lanphere, M.A., and Siems, D.F., 1999, Alagogshak volcano: A Pleistocene andesite-dacite stratovolcano in Katmai National Park: Geologic Studies in Alaska by the U.S. Geological Survey 1997: U.S. Geological Survey Professional Paper 1614, p. 105–113.

Hildreth, W., Fierstein, J., Lanphere, M.A., and Siems, D.F., 2000, Mount Mageik, a compound stratovolcano in Katmai National Park. Geologic Studies in Alaska by the U.S. Geological Survey 1998: U.S. Geological Survey Professional Paper 1615, p. 23–34.

Hildreth, W., Fierstein, J., Lanphere, M.A., and Siems, D.F., 2001, Snowy Mountain: A pair of small andesite-dacite stratovolcanoes in Katmai National Park: Geologic Studies in Alaska by the U.S. Geological Survey 1999: U.S. Geological Survey Professional Paper 1633, p. 13–34.

Hildreth, W., Fierstein, J., Lanphere, M.A., and Siems, D.F., 2002, Mount Griggs: A compositionally distinctive Quaternary stratovolcano behind the main volcanic line in Katmai National Park: Studies by the U.S. Geological Survey in Alaska, 2000: U.S. Geological Survey Professional Paper 1662, p. 87–112.

Hildreth, W., Fierstein, J., Lanphere, M.A., and Siems, D.F., 2003a, Trident Volcano: Four contiguous stratocones adjacent to Katmai Pass, Alaska Peninsula: Studies by the U.S. Geological Survey in Alaska, 2001: U.S. Geological Survey Professional Paper 1678, p. 1–28.

Hildreth, W., Lanphere, M.A., and Fierstein, J., 2003b, Geochronology and eruptive history of the Katmai Volcanic Cluster, Alaska Peninsula: Earth and Planetary Science Letters, v. 214, p. 93–114, doi:10.1016/S0012-821X(03)00321-2.

Hildreth, W., Fierstein, J., Siems, D.F., Budahn, J.R., and Ruíz, J., 2004, Rear-arc vs. arc-front volcanoes in the Katmai reach of the Alaska Peninsula: A critical appraisal of across-arc compositional variation: Contributions to Mineralogy and Petrology, v. 147, p. 243–275, doi:10.1007/s00410-004-0558-2.

Hildreth, W., Fierstein, J., and Calvert, A.T., 2007, Blue Mountain and the Gas Rocks: Rear-arc dome clusters on the Alaska Peninsula: U.S. Geological Survey Professional Paper 1739-A, p. 1–27.

Houghton, B.F., Wilson, C.J.N., Fierstein, J., and Hildreth, W., 2004, Complex proximal deposition during the plinian eruptions of 1912 at Novarupta, Alaska: Bulletin of Volcanology, v. 66, p. 95–133, doi:10.1007/s00445-003-0297-7.

Hubbard, B.R., 1932, Mush You Malemutes!: New York, The America Press, 179 p.

Jolly, A.D., and McNutt, S.R., 1999, Seismicity at the volcanoes of Katmai National Park, Alaska, July 1995–December 1997: Journal of Volcanology and Geothermal Research, v. 93, p. 173–190, doi:10.1016/S0377-0273(99)00115-8.

Jolly, A.D., Moran, S.C., McNutt, S.R., and Stone, D.B., 2007, Three-dimensional P-wave velocity structure derived from local earthquakes at the Katmai group of volcanoes, Alaska: Journal of Volcanology and Geothermal Research, v. 159, p. 326–342, doi:10.1016/j.jvolgeores.2006.06.022.

Kienle, J., Swanson, S.E., and Pulpan, H., 1983, Magmatism and subduction in the eastern Aleutian Arc, *in* Shimozuru, D., and Yokoyama, I., eds., Arc Volcanism: Physics and Tectonics: Tokyo, Terra Scientific Publishing Co., p. 191–224.

LeBas, M.J., LeMaitre, R.W., Streckeisen, A., and Zanettin, B., 1986, A chemical classification of volcanic rocks based on the total alkali–silica diagram: Journal of Petrology, v. 27, p. 745–750.

Lowenstern, J.B., 1993, Evidence for a copper-bearing fluid in magma erupted at the Valley of Ten Thousand Smokes, Alaska: Contributions to Mineralogy and Petrology, v. 114, p. 409–421, doi:10.1007/BF01046542.

Lowenstern, J.B., and Mahood, G.A., 1991, Petrogenesis of high-silica rhyolite on the Alaska Peninsula: Geophysical Research Letters, v. 18, p. 1565–1568, doi:10.1029/91GL01554.

Martin, G.C., 1913, The recent eruption of Katmai volcano in Alaska: National Geographic, v. 24, p. 131–181.

Miller, T.P., McGimsey, R.G., Richter, D.H., Riehle, J.R., Nye, C.J., Yount, M.E., and Dumoulin, J.A., 1998, Catalog of the historically active volcanoes of Alaska: U.S. Geological Survey Open-File Report 98-582, 104 p.

Miyashiro, A., 1974, Volcanic rock series in island arcs and active continental margins: American Journal of Science, v. 274, p. 321–355, doi:10.2475/ajs.274.4.321.

Moore, J.C., et al., 1991, EDGE deep seismic reflection transect of the eastern Aleutian arc-trench layered lower crust reveals underplating and continental growth: Geology, v. 19, p. 420–424, doi:10.1130/0091-7613(1991)019<0420:EDSRTO>2.3.CO;2.

Moran, S.C., 2003, Multiple seismogenic processes for high-frequency earthquakes at Katmai National Park, Alaska: Evidence from stress tensor inversions of fault-plane solutions: Bulletin of the Seismological Society of America, v. 93, p. 94–108, doi:10.1785/0120020113.

Mori, J., White, R.A., Harlow, D.H., Okubo, P., Hoblitt, R.P., Laguerta, E.P., Lanuza, A., and Bautista, B.C., 1996,

Volcanic earthquakes following the 1991 climactic eruption of Mount Pinatubo: Strong seismicity during a waning eruption, *in* Newhall, C.G., and Punongbayan, R.S., eds., Fire and Mud: Eruptions and Lahars of Mount Pinatubo, Philippines: Seattle, University of Washington Press, p. 339–350.

Motyka, R.J., 1977, Katmai caldera: Glacier growth, lake rise, and geothermal activity: Short Notes on Alaskan Geology—1977: Alaska Division of Geological and Geophysical Surveys, Geologic Report 55, p. 17–21.

Motyka, R.J., 1978, Surveillance of Katmai caldera and crater lake, Alaska: 1977: Final report on U.S. National Park Service purchase order PX 9100-7-1009: Geophysical Institute, University of Alaska, Fairbanks, 19 p.

Muller, E.H., and Coulter, H.W., 1957, Incipient glacier development within Katmai caldera, Alaska: Journal of Glaciology, v. 3, p. 13–17.

Murphy, R.A., Thurber, C.H., and Prejean, S.G., 2010, Initial results from a temporary seismic array in Katmai National Park, Alaska: Velocity and attenuation models: Seismological Research Letters, v. 81, no. 2, p. 352.

Newhall, C.G., and Punongbayan, R.S., eds., 1996, Fire and Mud: Eruptions and Lahars of Mount Pinatubo, Philippines: Seattle, University of Washington Press, 1126 p.

Newhall, C.G., Daag, A.S., Delfin, F.G., Jr., Hoblitt, R.P., McGeehin, J., Pallister, J.S., Regalado, M.T.M., Rubin, M., Tubianosa, B.S., Tamayo, R.A., Jr., and Umbal, J.V., 1996, Eruptive history of Mount Pinatubo, *in* Newhall, C.G., and Punongbayan, R.S., eds., Fire and Mud: Eruptions and Lahars of Mount Pinatubo, Philippines: Seattle, University of Washington Press, p. 165–195.

Peacock, M.A., 1931, Classification of igneous rock series: The Journal of Geology, v. 39, p. 54–67, doi:10.1086/623788.

Pinney, D.S., and Beget, J.E., 1991, Late Pleistocene volcanic deposits near the Valley of Ten Thousand Smokes, Katmai National Park, Alaska, *in* Reger, R.D., ed., Short Notes on Alaskan Geology 1991: Alaska Division of Geological and Geophysical Surveys Professional Report 111, p. 45–53.

Plafker, G., Moore, J.C., and Winkler, G.R., 1994, Geology of the southern Alaska margin, *in* Plafker, G., and Berg, H.C., eds., The Geology of Alaska: Chapter 12 of The Geology of North America, volume G-1, Geological Society of America, p. 389–449.

Prejean, S., Haney, M., Pesicek, J., and Thurber, C., 2008, Seismicity and structure of the Katmai volcanic cluster, Alaska, revealed: American Geophysical Union, Fall Meeting, abstract V54A-07.

Riehle, J.R., Detterman, R.L., Yount, M.E., and Miller, J.W., 1993, Geologic map of the Mount Katmai quadrangle and adjacent parts of the Naknek and Afognak quadrangles, Alaska: U.S. Geological Survey Map I-2204; scale 1:250,000.

Shew, N., and Lanphere, M.A., 1992, Map showing potassium-argon ages from the Mount Katmai and adjacent parts of the Naknek and Afognak quadrangles, Alaska Peninsula, Alaska: U.S. Geological Survey Map MF-2021-E, scale 1:250,000.

Simkin, T., and Howard, K.A., 1970, Caldera collapse in the Galápagos Islands, 1968: Science, v. 169, p. 429–437, doi:10.1126/science.169.3944.429.

Sisson, T.W., and Bacon, C.R., 1999, Gas-driven filter pressing in magmas: Geology, v. 27, p. 613–616, doi:10.1130/0091-7613(1999)027<0613:GDFPIM>2.3.CO;2.

Wallace, P.J., 2005, Volatiles in subduction zone magmas: Concentrations and fluxes based on melt inclusion and volcanic gas data: Journal of Volcanology and Geothermal Research, v. 140, p. 217–240, doi:10.1016/j.jvolgeores.2004.07.023.

Wilson, F.H., 1985, The Meshik arc—An Eocene to earliest Miocene magmatic arc on the Alaska Peninsula: Alaska Division of Geological and Geophysical Surveys, Professional Report 88, 14 p.

Wood, C.A., and Kienle, J., eds., 1990, Volcanoes of North America: Cambridge University Press, 354 p.